

2016

## Virus Particles Provide Nanotopographical Cues For Osteogenic Differentiation Of Mesenchymal Stem Cells

Kamolrat Metavarayuth  
*University of South Carolina*

Follow this and additional works at: <https://scholarcommons.sc.edu/etd>



Part of the [Chemistry Commons](#)

---

### Recommended Citation

Metavarayuth, K.(2016). *Virus Particles Provide Nanotopographical Cues For Osteogenic Differentiation Of Mesenchymal Stem Cells*. (Doctoral dissertation). Retrieved from <https://scholarcommons.sc.edu/etd/3750>

This Open Access Dissertation is brought to you by Scholar Commons. It has been accepted for inclusion in Theses and Dissertations by an authorized administrator of Scholar Commons. For more information, please contact [digres@mailbox.sc.edu](mailto:digres@mailbox.sc.edu).

VIRUS PARTICLES PROVIDE NANOTOPOGRAPHICAL CUES FOR OSTEOGENIC  
DIFFERENTIATION OF MESENCHYMAL STEM CELLS

by

Kamolrat Metavarayuth

Bachelor of Science in Pharmacy  
Chulalongkorn University, 2008

Master of Science  
University of Florida, 2012

---

Submitted in Partial Fulfillment of the Requirements

For the Degree of Doctor of Philosophy in

Chemistry

College of Arts and Sciences

University of South Carolina

2016

Accepted by:

Qian Wang, Major Professor

Chuanbing Tang, Chair, Examining Committee

Thomas M. Makris, Committee Member

Maria Marjorette Pena, Committee Member

Lacy Ford, Senior Vice Provost and Dean of Graduate Studies

© Copyright by Kamolrat Metavarayuth, 2016  
All Rights Reserved.

## ACKNOWLEDGEMENTS

I first would like to express my sincere gratitude to my advisor Prof. Qian Wang. As a mentor, he motivated and supported me through my graduate study. Dr. Wang provided me sincere guidance and has always been confidence in my abilities, allowing me to pursue my research goals and successful results. He has given me the opportunity to work in an interdisciplinary field, which expose me to various new techniques. Not only he is my mentor, but also he is my friend who supported me and guided me through my hard time. He gave me invaluable suggestions which really helped me overcome many obstacles. When I first started here, two senior graduate students taught me new laboratory techniques, Pongkwan Sitasuwan, Ph.D. and Jittima Luckanagul, Ph.D. I would like to also extend my gratitude to them. Through their experienced lessons, they always give me helpful suggestions which facilitated me in problem solving and effective troubleshooting.

I would like to thank former and current fellow laboratory members for creating a supportive and fun working environment, especially Xiaolei Chang, Ph.D., Hong Guan, Ph.D., and Lin Lv. I have enjoyed my four years working and spending time with all of you.

I would like to thank all my friends here, Gresi Bonomo Irdam, Panita Maturavongsadit, Preecha Kittikhunnatham and in Thailand, Woraporn Jiewjaroen, Sathita Sukwattanajaron, and Usanee Hiranyawech for always be there for me and let me reach out to you anytime no matter how busy you are.

Thank you my beloved family members, my parents, my little sister and brother, for their unconditional love and support. Their encouragement and understanding has provided me the greatest comfort and strength.

## ABSTRACT

One key aspect of tissue engineering is to develop biomimetic scaffolding materials that can modulate the proliferation, self-renewal and differentiation of multipotent stem cells into different lineages. Bone marrow derived mesenchymal stem cells (BMSCs) can differentiate into several target cells such as osteoblasts, chondrocytes, adipocytes, and smooth muscle cells. BMSCs are commonly used for *in vitro* osteogenesis studies in bone tissue engineering field. However the mechanisms and signaling pathways that these cells use to recognize and response to biomaterial surface are still unclear. This dissertation focuses on investigating the effect of chemical and physical cues introduced by virus nanoparticles on the promotion of osteogenic differentiation of BMSCs by virus coated two dimensional substrates.

Introduction to surface nanotopography influences on cell behaviors is highlighted in chapter 1. In this chapter, background and reports on the impact of different nanotopographies on stem cell behaviors are described.

Then we investigated effects of particle shapes, nanoscale features, and surface chemistry on osteogenesis of BMSCs by utilizing substrates fabricated from five different plant viruses nanoparticles in chapter 2. Three shapes of virus nanoparticles (rod, fiber, and spherical) were used to investigate the effect of particle morphology. In each group of the same shape virus, different type of viruses were also included to examine whether surface nanoscale feature and different in amino acid sequence of coat protein can affect the differentiation.

On the other hand, the ordered arrangement of coat proteins on virus nanoparticles has been well documented to exhibit astonishing effect on immune system stimulation. Likewise, we sought to examine this effect by comparing arranged and random organization of coat proteins on nanoparticles in chapter 3. For this study, the randomly coated TMV coat proteins on gold nanorods (TMV-GNRs) was assembled and used to represent nanoparticles with random TMV coat protein organization.

Chapter 4 focuses on mechanical pathway of virus substrates mediated osteogenesis of BMSCs through a centralized modulator, bone morphogenetic protein 2 (BMP2) which is believed to be responsible for accelerated osteogenesis. The possible pathways associated with virus substrates induced BMP2 upregulation is further explored in this chapter. It was discovered that expression level of BMP2 and many genes involved in cell motility had significant alteration early after osteoinduction on TMV substrate. These results suggest stress-induced osteogenesis as the underlying mechanisms of virus substrates stimulated osteoblastic differentiation.

Collectively, the research presented in this dissertation investigates the underlying mechanism of virus substrates mediate osteogenic differentiation of BMSCs in order to gain insights into the design of functional biomaterials for tissue engineering and regenerative medicine applications.

## TABLE OF CONTENTS

ACKNOWLEDGEMENTS.....	iii
ABSTRACT .....	v
LIST OF FIGURES .....	ix
LIST OF TABLES .....	xi
CHAPTER 1 INTRODUCTION: THE INFLUENCE OF SURFACE TOPOGRAPHICAL CUES ON THE DIFFERENTIATION OF MESENCHYMAL STEM CELLS.....	1
1.1 Stem cell fate and microenvironment.....	1
1.2 Topological cues from the substrates .....	2
1.3 Plant virus provides topographical cues for cell culturing.....	10
1.4 Possible mechanism of topographical cues induced stem cell differentiation ...	16
1.5 Summary .....	19
1.6 References .....	21
CHAPTER 2 VIRUS NANOPARTICLES MEDIATED OSTEOGENIC DIFFERENTIATION OF BONE DERIVED MESENCHYMAL STEM CELLS ...	34
2.1 Introduction .....	34
2.2 Results and discussion.....	36
2.3 Conclusions .....	53
2.4 Experimental section .....	56
2.5 References .....	62
CHAPTER 3 NANOTOPOGRAPHICAL CUES MEDIATE OSTEOGENESIS OF STEM CELLS ON VIRUS SUBSTRATES THROUGH BMP-2 INTERMEDIATE.....	71

3.1 Introduction .....	71
3.2 Results and discussion.....	74
3.3 Conclusions .....	83
3.4 Experimental section.....	83
3.5 References .....	90
CHAPTER 4 POSSIBLE SIGNALING PATHWAY INVOLVED IN VIRUS SUBSTRATE-MEDIATED BONE DIFFERENTIATION OF MESENCHYMAL STEM CELLS .....	
4.1 Introduction .....	95
4.2 Results and discussion.....	98
4.3 Conclusions .....	105
4.4 Experimental section.....	106
4.5 References .....	111
APPENDIX A – REPRINT PERMISSION FOR CHAPTER 1 .....	122
APPENDIX B – REPRINT PERMISSION FOR CHAPTER 2.....	123

## LIST OF FIGURES

Figure 1.1 Schematic illustration of different factors affecting surface topography: Roughness, Anisotropic pattern, and Isotropic pattern.....	3
Figure 1.2 Examples of surface roughness influences cell behaviors .....	5
Figure 1.3 Examples of isotropic pattern influences cellular responses.....	9
Figure 1.4 Electrospun nanofibres induce stem cell differentiation .....	11
Figure 1.5 Genetically engineered TMV-RGD enhances cell adhesion on fibrous substrates.....	13
Figure 1.6 TMV-induced osteogenic differentiation in BMSCs <i>in vitro</i> .....	15
Figure 1.7 Schematic diagram depicts interrelation of common intracellular signaling events triggered by changes in substrate topography and predicting sequential events for TMV-induced BMP-2 upregulation, leading to accelerated osteogenesis.....	18
Figure 2.1 Molecular models shows surface topography of plant viruses used in this study.....	37
Figure 2.2 Representative AFM micrographs showing the coverage of PDL coated substrate with different virus nanoparticles indicate the viral particles.....	41
Figure 2.3 RT-qPCR analysis showed significant BMP2 upregulation in cells grown on TMV, TVCV, PVX, and TYMV coated substrates .....	43
Figure 2.4 The expression of osteogenic marker in BMSCs cultured on PDL and different virus nanoparticles coated substrates under osteogenic conditions .....	44
Figure 2.5 BMP2 immunohistochemical staining suggests the protein expressions are localized to the cell aggregates; most are found on TMV, TVCV, PVX, and TYMV substrates.....	46
Figure 2.6 Nearest neighbor analysis of BMSCs cultured on PDL virus substrates .....	47
Figure 2.7 Cytochemical analysis of the bone differentiation process of BMSCs on PDL and viruses coated substrates at 4 and 7 days after osteogenic induction.....	49

Figure 2.8 Immunochemical staining showing the difference in vinculin size of cells on PDL or virus coated substrates for 24 hours .....	52
Figure 2.9 Representative actin (top panel) and vinculin (bottom panel) immunofluorescent heat maps of cells culture on PDL and virus coated substrates .....	54
Figure 3.1 Schematic shows TMV coat protein coated gold nanorod (TMV-GNRs) preparation and structural comparison of align and random TMV coat protein (TMV-CP) coated nanorod structure .....	75
Figure 3.2 CTAB-GNRs characterization. <b>(a-c)</b> TEM image of <b>(a)</b> wild type TMV <b>(b-c)</b> CTAB-GNRs <b>(d)</b> height profile AFM image of CTAB-GNRs shows diameter measurement of the gold nanorod .....	76
Figure 3.3 Transmission electron microscopy image shows layer by layer coating of CTAB-GNRs with PAA and PAH .....	78
Figure 3.4 Characterization of nanoparticles coated substrates for stem cell cultures .....	79
Figure 3.5 TEM image shows intact nanorod structure of TMV-GNRs after assembly process .....	80
Figure 3.6 Osteogenesis of mesenchymal stem cells .....	82
Figure 4.1 BMP2 inhibitor (Noggin) inhibits TMV induced osteogenesis of stem cells ..	99
Figure 4.2 RhoA/ROCK pathway involves in TMV substrates mediated osteogenesis of stem cells .....	101
Figure 4.3 Proposed signaling cascade of virus substrates mediated osteogenesis of MSCs .....	104

## LIST OF TABLES

Table 2.1 Summary of advantages and drawbacks of each virus coating procedure .....	39
Table 2.2 Primers used for RT-qPCR to measure gene expression levels. BGLAP: bone-gamma-carboxyglutamate protein; BMP2: bone morphogenetic protein 2; SPP1: secreted phosphoprotein 1.....	59
Table 3.1 Primers used for RT-qPCR to measure gene expression levels. BGLAP: bone-gamma-carboxyglutamate protein; BMP2: bone morphogenetic protein 2.....	89
Table 4.1 Primers used for RT-qPCR to measure gene expression levels. BGLAP: bone-gamma-carboxyglutamate protein; BMP2: bone morphogenetic protein 2.....	109

## CHAPTER 1

# INTRODUCTION: THE INFLUENCE OF SURFACE TOPOGRAPHICAL CUES ON THE DIFFERENTIATION OF MESENCHYMAL STEM CELLS<sup>1</sup>

### 1.1 STEM CELL FATE AND MICROENVIRONMENT

One key aspect of tissue engineering is to develop biomimetic scaffolding materials that can modulate the proliferation, self-renewal and differentiation of multipotent stem cells into different lineages. *In vivo*, stem cells exist in a complex and active environment, a key component of which is the extracellular matrix (ECM).[1] The ECM provides physical and chemical supports for the cell and contains supramolecular assemblies of proteins and glycosaminoglycans, which play a vital role in the cell behavior. In order to undergo fundamental biological processes, the cells must adhere to the underlying ECM. As a result, many novel biomaterials, which are purposely created to improve or replace biological functions, have been designed to resemble the ECM. To engineer a biomimetic scaffold resembling native ECM, and ultimately, to enable the tissue regeneration, an extensive study on the interactions between stem cells and implanted materials is necessary.

During recent years, there is extensive research emphasizing on the chemical (i.e. functional groups, surface charge, surface energy, hydrophobicity, and protein composition) and physical (i.e. overall architecture, porosity, surface topography, and elastic modulus) properties of ECM which influence stem cell fate.[2] The study of each

<sup>1</sup>Metavarayuth K, Sitasuwan P, Zhao X, Lin Y, Wang Q. 2015. *ACS. Biomater. Sci. Eng.* 2: 142-51. Reprinted here with permission of publisher (Appendix A).

of these properties is crucial to develop biomaterials that guide stem cells for proper tissue regeneration. In this chapter, we focus our discussion on the surface topography of 2D scaffold, especially, with an emphasis on the virus-based materials.

## 1.2 TOPOLOGICAL CUES FROM THE SUBSTRATES

It was first demonstrated in 1911 that cell behaviors can be controlled by topological cues from the underlying substrates.[3] Later, the term contact guidance was coined by Paul Weiss in 1945.[4] Contact guidance refers to the phenomenon that cells adjust their orientation and align along the patterns that they are cultured on. Cells can respond to topographical features as small as 5 nm [5] so it is important to achieve surface patterns at a nanometer-scale resolution. Current nano- and micro-fabrication methods include electron beam- or photo-lithography, self-assembling systems, microcontact printing, particle synthesis, replica casting or molding, chemical etching, sandblasting and electrospinning.[5, 6] These techniques enable the recapitulation of topographical cues in the cell niche in a controllable and reproducible fashion. In general, factors affecting substrate surface topography include (1) roughness of the underlying surface, and (2) patterns on the surface (Figure 1.1).[7, 8]

The most studied aspect of topography is surface roughness which relates to the texture of the uppermost layer of a material and is quantified by measuring the protrusions or depressions at the surface. Numerous experiments have reported that surface roughness can influence cell behaviors like adhesion, migration, proliferation and differentiation. [9-14] In general, the optimal microscale surface roughness that induces osteogenic differentiation of mesenchymal stem cells is the surface that has average

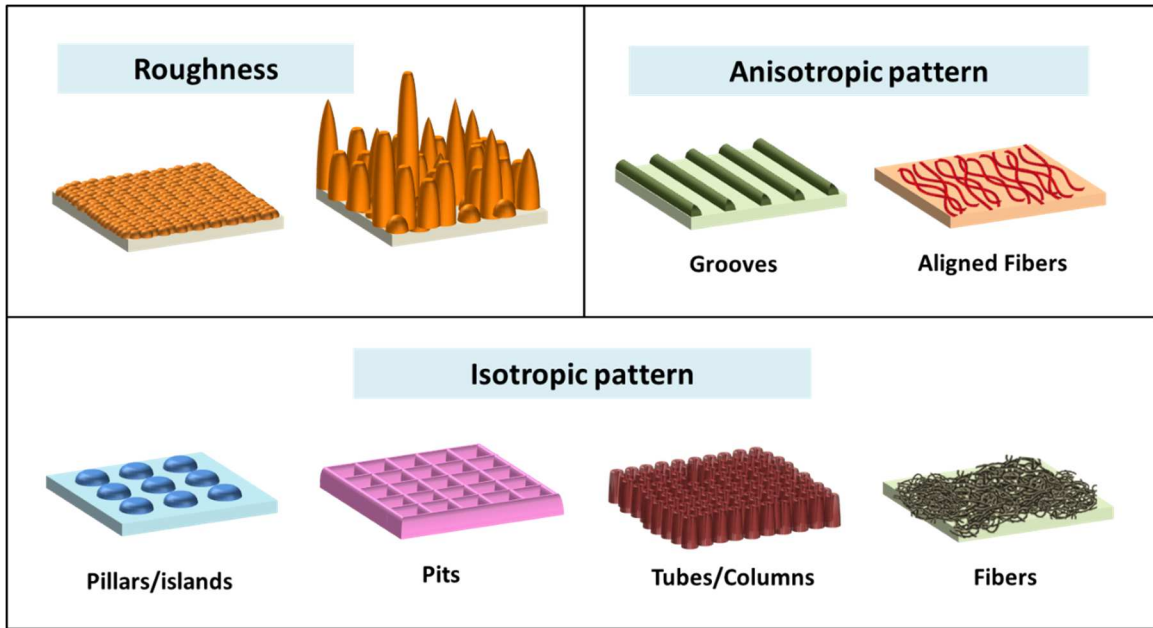


Figure 1.1 Schematic illustration of different factors affecting surface topography: Roughness, Anisotropic pattern, and Isotropic pattern.

roughness (Ra) closed to 1  $\mu\text{m}$ . [9-14] For example, Yang *et al.* investigated the enhancement of osteogenic differentiation by surface roughness introduced to hydroxyapatite (HA) discs. The discs have Ra of surface topography ranging from 0.2 to 1.65  $\mu\text{m}$ , and human bone-marrow mesenchymal stem cells (hBMSCs) were cultured in osteogenic medium ( $\alpha$ -MEM supplemented with 10% fetal bovine serum, 50 mg/mL ascorbic acid, 10 mM glycerophosphate, 100 nM dexamethasone and 100 U/mL penicillin and 100 mg/L streptomycin) on these discs. The optimal osteogenic differentiation was observed on discs with surface topography characterized by Ra ranging from 0.7 to 1.0  $\mu\text{m}$  (Figure 1.2a,b). [9] Recent study by Faia-Torres *et al.* applied polycaprolactone (PCL) gradient substrate to study effect of surface roughness on osteogenesis of MSCs in basal growth media without soluble osteogenic inducers. They demonstrated that the expression of osteogenic markers (alkaline phosphatase (ALP) and collagen type I proteins) and mineralization are related to the surface roughness. [10] More specifically, their results show that peak expression of normalized ALP was found in the area that has substrate gradient at position 5 mm that corresponded to Ra~0.93  $\mu\text{m}$ . This trend is also consistent with a systemic review by Wennerberg and Albrektsson which concluded that moderately rough surface (Ra~1-2  $\mu\text{m}$ ) showed strongest bone responses. [8] In addition, various experiments have shown that nanoscale surface-roughness can also influence cell behavior. Although the optimal nano-roughness scale for osteogenic differentiation cannot be specified, introduction of nanoscale roughness to substrate surface by acid etching usually is reported to have a positive influence on osteogenic activity. For example, the study shown by Takeuchi *et al.*, who demonstrated

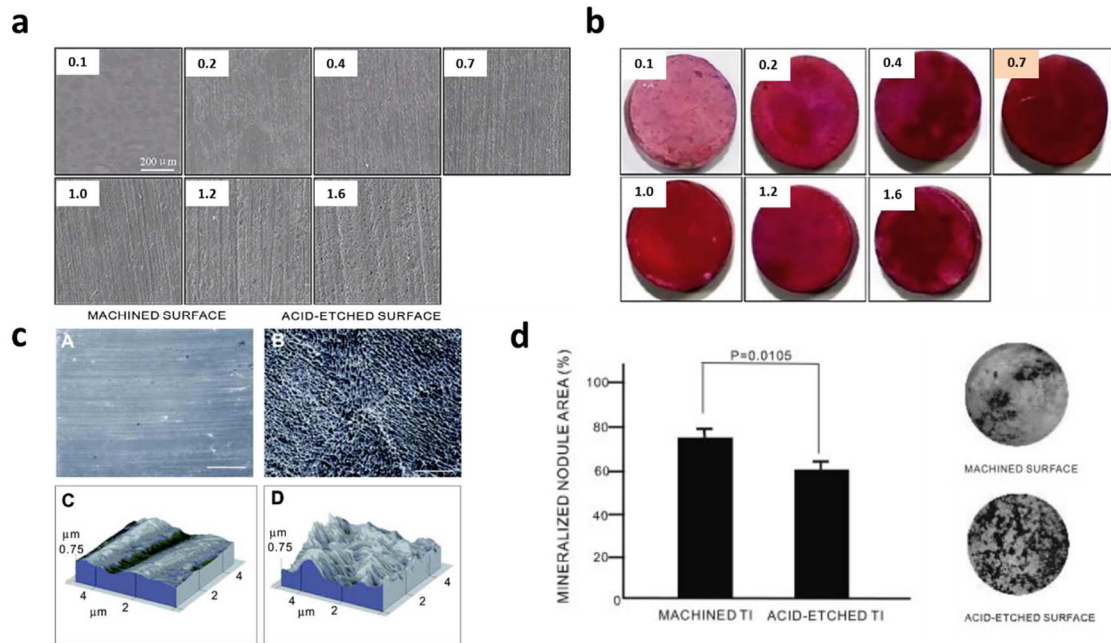


Figure 1.2 Examples of surface roughness influences cell behaviors **(a)** Scanning electron microscopic (SEM) images of the surface morphology of hydroxyapatite (HA) discs. Scale bar is 200  $\mu\text{m}$ . **(b)** Alizarin Red staining of differentiating hBMSCs in osteogenic medium. Note darkest red staining at Ra 0.7  $\mu\text{m}$ . Reproduced with permission from ref 8a. Copyright 2015 Elsevier B.V. **(c)** Surface morphology of titanium discs for osteoblastic cell culture. SEM images of machined titanium (A) and acid-etched titanium (B). Bar = 20  $\mu\text{m}$ . AFM images of the machined titanium (C) and the acid-etched titanium (D). **(d)** Mineralized nodule area. The percentage of the mineralized nodule area relative to the culture area was measured on the day-28 mineralized tissue using a digital image analyzer. Right: Representative images of the mineralized cultures from the triplicate experiments. Data are shown as the mean  $\pm$  SD ( $n = 3$ ). Reproduced with permission from ref 9. Copyright 2005 Wiley Online Library.

that when cultured on dual acid-etched titanium surface with a Ra of 110 nm rat bone-marrow derived osteoblast differentiation increased compared to Ra = 49 nm.[15] Similar observations have been noted by de Oliveira *et al.*[16, 17] Contrary to this, rat periosteal cell-differentiation into osteoblasts, which could be seen on machined titanium disk surfaces (Ra = 49 nm), was inhibited on acid etched surfaces (Ra = 183 nm), while chondrocyte specific genes were activated when cultured in an osteochondral-defined culture medium containing both osteogenic and chondrogenic differentiation factors.[18]

In explaining cell responses to surface pattern, we will use a classification based on the orientation of topography (isotropic or anisotropic). An anisotropic surface has a clear orientation such as ridges and grooves surfaces. On the other hand, an isotropic surface is a surface with no orientation, such as evenly or randomly distributed pits, protrusions, pillars, channels, or etc. Techniques developed to engineer these surface orientations are not the focus of this mini review and they have been reviewed in detailed elsewhere.[19, 20]

Cell orientation and migration along the anisotropic direction of ridges and grooves have long been observed in microscale.[21-25] Multiple studies revealed that MSCs committed to adipogenic [26] and myogenic [27] phenotypes when microscale grooves are introduced to substrate surface, especially with the groove scale less than 500 nm. Conversely, osteogenic differentiation is negatively affected by this particular anisotropic pattern.[28, 29] Periodicity can also modulate differential function of cells. In particular, if MSCs are cultured on grooves with a short distance pitch and become highly aligned, osteogenesis can be reduced. However, increasing the pitch to around 50  $\mu\text{m}$  can improve osteogenesis with great efficiency.[30] With the development of lithographic

techniques, recent studies have focused on whether cells align on nanoscale ridges and grooves and can still be induced by contact guidance.[31-38] In a study by Zhu *et al.*, stem cell derived osteoblasts were cultured on polystyrene (PS) nanogrooves (300-nm pitch, 60- to 70-nm depth) substrates in dexamethasone, ascorbic acid and  $\beta$ -glycerophosphate supplemented media, which were found to exhibit anisotropic orientation in both cellular actin and mineralized matrix.[38] In addition, elongation of stem cells plays an important role in neuronal differentiation of stem cells. In fact, nanogroove topography is widely studied for neuron tissue engineering, [39-42] For example, Yim *et al.* have shown that hMSCs could differentiate and proliferate on the nanogratings of 350 nm width. In addition, alignment of cytoskeleton and nuclei of elongated hMSCs were observed along the nanogratings, and gene profiling and immunostaining showed significant up-regulation of neuronal markers such as microtubule-associated protein 2 (MAP2) compared to unpatterned and micropatterned controls.[39]

In summary, anisotropic topographies induce dramatic morphological changes (via contact guidance) in cellular, cytoskeletal, and focal adhesions regardless of micro- or nanoscale, which subsequently could lead to changes in gene expression and modulate stem cell differentiation into specific lineages.

As comparison, isotropic patterns cannot influence the cell alignment, Instead, it has been shown to enable the control of more-collective cell functions. Cell response to isotropic pattern is often inconsistent and difficult for in-depth analysis due to the variation in cell types, cell culture condition, properties of materials, etc. Common

isotropic topographies that will be reviewed here are distributed pillars, pit, nanotubes, and random nanofibers.

Random distributed pillars or islands on a supporting surface has been demonstrated to influence osteogenesis of stem cells. There are many factors that can be varied in a pillared surface substrate, for example, height, shape and diameter of island, and distance between two islands. The complexity of pillared surface makes it inappropriate to compare the results from each study. Nevertheless, there is a general trend of cell behaviors attributed to surface isotropic topographies. The introduction of pillars or islands to substrate surface usually enhances osteogenic differentiation [43-46] but particular dimension of the island that induces the highest differentiation cannot be nailed down. Besides dimension of topographical cues, the distribution of topographical feature may also have significant influences on stem cell behaviors. Dalby *et al.* reported that surfaces composed of nanopits with controlled disordered resulted in increased expression of osteogenic markers relative to surfaces consisting of either highly ordered or randomly displaced nanopits (Figure 1.3a).[47] In addition to distribution of nanopits, depth of nanopits has also been shown to affect cell responses. In general, the deeper pit tends to enhance higher osteogenesis of stem cells.[48, 49] Another feature of isotropic surface that is currently explored particularly for bone tissue engineering is nanotubes. There is an increasing number of data elucidating the benefits of using TiO<sub>2</sub> nanotubes, one of the lateral spacing topographical cues, for enhanced orthopedic implant surfaces, however, inconsistent responses have been reported from various researching groups. For instance, it has been criticized that MSCs behave differently on TiO<sub>2</sub> nanotubes (Figure 1.3b) with diameters of 15 – 100 nm.[50, 51] Three different optimal diameters of TiO<sub>2</sub>

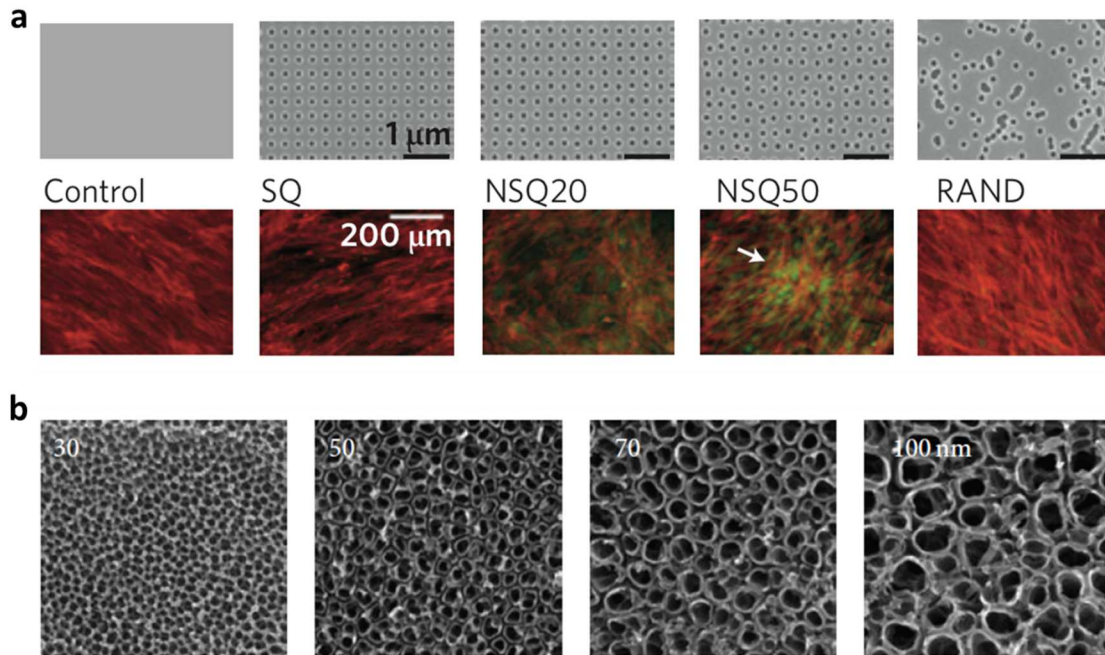


Figure 1.3 Examples of isotropic patterns that influence cellular responses. **(a)** Top row shows images of nanotopographies fabricated by electron beam lithography (EBL) on poly(methyl methacrylate) (PMMA). All present 120 nm diameter pits (100 nm deep, absolute or average 300 nm center–center spacing) with square (SQ), control disordered 20 (NSQ 20), control disordered 50 (NSQ 50,  $\pm 20$  or 50 nm from true center) and random placements (RAND). Bottom row shows osteoprogenitors cultured on the control, note the lack of positive osteopontin (OPN) stain; SQ, note reduced cell numbers compared with the control; NSQ20, note some OPN positive cells; NSQ50, note abundant OPN positive cells and bone nodule formation (arrows); RAND, note good cell populations but lack of positive OPN stain. Cells were cultured in osteoinduction media containing dexamethasone and L-ascorbic acid. Color code: actin, red; OPN, green. Reproduced with permission from ref 21. Copyright 2007 Nature publishing group. **(b)** SEM images of titanium oxide nanotube having various diameters (30, 50, 70, and 100 nm). Reproduced with permission from ref 23a. Copyright 2009 Wiley Online Library.

nanotubes scaffolds for osteogenic differentiation have been obtained from three groups of pioneers in bone tissue engineering.[50-52]

Electrospun nanofiber webs may also be evaluated within the context of topographic effect because randomly deposited nanofibers with variable nanoscale thicknesses provide nanotextures coupled with micropores.[53, 54] Electrospun fibers have been investigated as promising tissue engineering scaffolds since they mimic the nanoscale properties of native ECM. It can be aligned on substrate surface to create both anisotropic and isotropic topography which control commitment of stem cells to a specific lineage. Recent study by Yin *et al.* demonstrate that the aligned anisotropic fibrous scaffold displays promising results in tendon-like tissue regeneration at the early repair stage, while in the random fibrous scaffold group, they observed the development of bone formation at the injury site. The two topographically-different scaffolds not only support MSC adhesion and spreading, but also induce tenogenesis and osteogenesis, respectively, both *in vitro* and *in vivo* (Figure 1.4).[55]

### 1.3 PLANT VIRUS PROVIDES TOPOGRAPHICAL CUES FOR CELL CULTURING

There are two main categories of biomaterials used to study the influence of nanotopography on cellular behaviors. The first type is polymeric materials, where nanostructures could be generated by nanoimprint lithography,[56] capillary force lithography,[57] ultraviolet assisted lithography,[58] embossing, photolithography, and micromachining.[6] Another type of biomaterials is made of stiffer metallic substrates, such as stainless steel, platinum, and titanium.[6] Deep reactive ion-etching, acid etching, photolithography, sandblasting, and mechanical machining were the techniques employed to create surface nanotopography on these metallic materials.[6, 59]

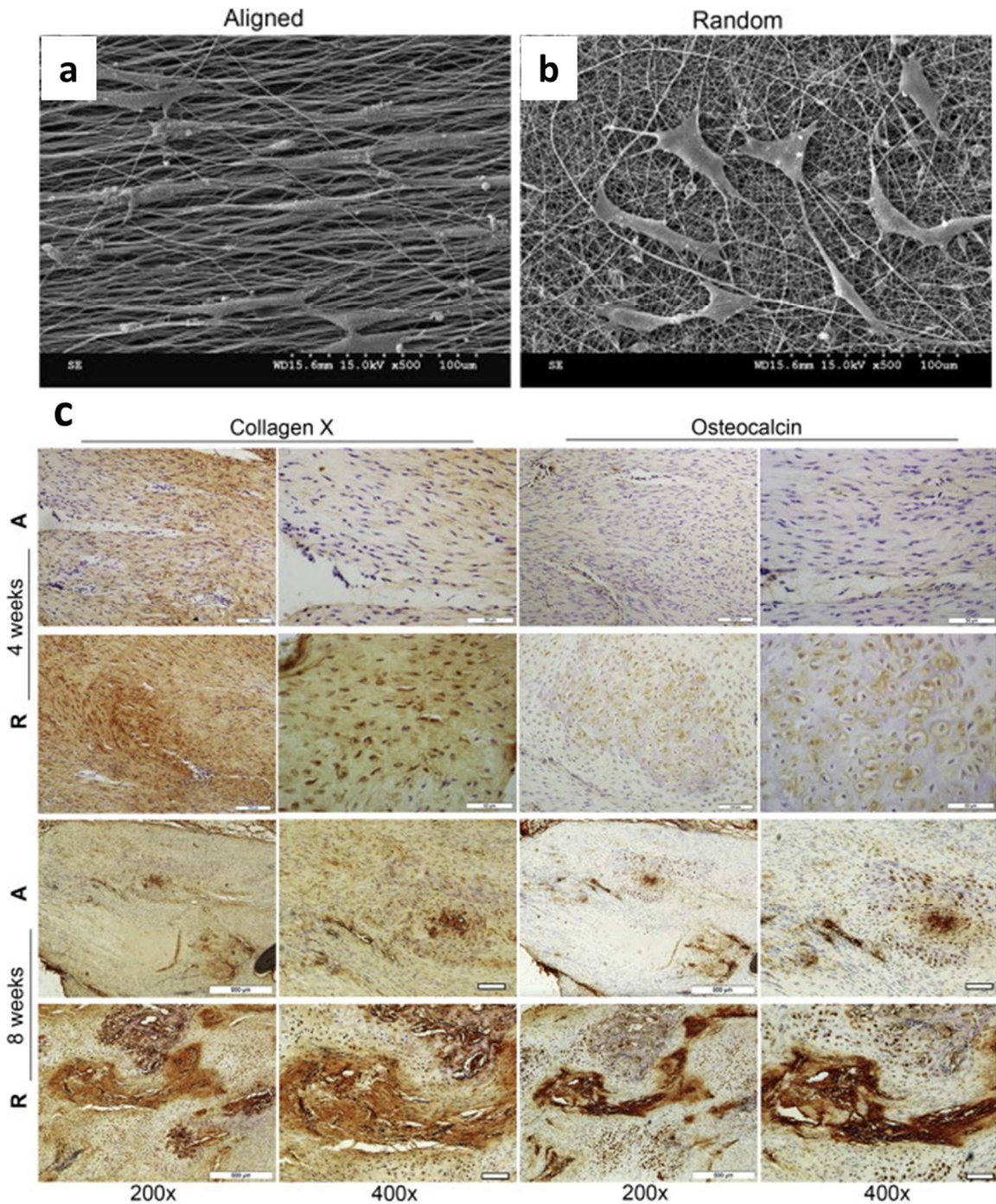


Figure 1.4 Electrospun nanofibers induce stem cell differentiation. **(a)** and **(b)** SEM images of MSCs cultured on the aligned and randomly-oriented nanofibrous scaffolds respectively. **(c)** Immunohistochemical staining of collagen type X and osteocalcin in repaired zones within sections of aligned group and randomly-oriented group after 4 weeks and 8 weeks post-surgery. Scale bars, 100  $\mu\text{m}$  (200 $\times$ ), 50  $\mu\text{m}$  (400 $\times$ ). Reproduced with permission from ref 26. Copyright 2015 Elsevier.

Further modifications to the two main types of biomaterials described above could be achieved by nanoparticle surface coating. In our laboratory, we are creating materials from plant virus nanoparticles, which can be produced in gram quantities at low cost, and the resulting particles are highly monodispersed.[60, 61] Other advantages of these bionanoparticles include the well-defined structural features, unique shapes and sizes, genetic programmability and robust chemistries.[61] For example, the cell adhesion motifs, like arginine-glycine-aspartic acid (RGD), have been incorporated into Tobacco mosaic virus (TMV) coat proteins through genetic engineering to give mutant viruses (e.g. TMV-RGD).[62] The RGD motif, predominantly found in an extracellular adhesive glycoprotein, fibronectin, and other extracellular matrix proteins, was reported to mediate cell adhesion via transmembrane integrin binding.[63] The polyvinyl alcohol (PVA) fibers incorporated with genetically engineered TMV-RGD was observed to facilitate cell adhesion and spreading with prominent actin fibers, even in the absence of serum supplement (Figure 1.5a). On the contrary, cells remained in a round shape with randomized actin structure on both PVA and PVA-TMV substrates (Figure 1.5b).[62]

Besides TMV, there are other viruses that have also been used for tissue engineering application.[64-68] One example of virus that has been widely studied is M13 bacteriophage (phage), a nanofiber-like virus that has ability of self-assembly into highly controlled periodic nanostructures when prepared in concentrated solution.[69-71] Merzlyak *et al.* have genetically engineered phage to display cell signaling motif on their coat proteins and self-assemble them into directionally organized liquid crystalline-like materials. They also demonstrated that the viral nanofiber scaffolds were able to support neural progenitor cell proliferation and differentiation as well as direct orientation of their

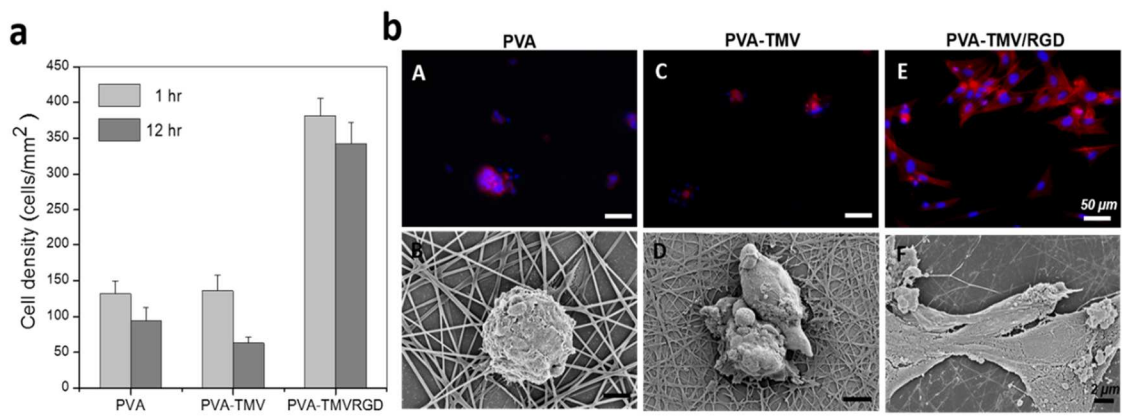


Figure 1.5 Genetically engineered TMV-RGD enhances cell adhesion on fibrous substrates.[62] (a) Baby hamster kidney (BHK) cell density analyses after 1 h and 12 h of incubation on electrospinning PVA, PVA-TMV and PVA-TMV/RGD substrates. (b) Fluorescence microscopy images stained for nuclei (blue), F-actin (red) and FESEM images of BHK cells after 1 h of incubation on substrates. Reproduced with permission from ref 32. Copyright 2011 The Royal Society of Chemistry.

growth in three dimensions.[64]

We hypothesized that the unique surface topography and polyvalent nature provided by the plant virus coat protein assembly can be harnessed to modulate stem cell responses. In particular, high-order hierarchical structure of plant virus complements investigation of the effect of ligand displayed polyvalency on cellular response as they can be genetically and/or chemically modified to display particular functional groups in a controlled spatial orientation at nanometer scale. Therefore, we have first utilized substrates randomly coated with rod-shaped TMV and spherical Turnip yellow mosaic virus (TYMV) to test osteogenic potential of bone marrow derived mesenchymal stem cells (BMSCs).[67, 72] Surprisingly, the osteogenic differentiation process was accelerated by 7 days in both cases. The underlying reasons how topography and nanopattern of virus-based materials can affect differentiation process is still not well understood. In an attempt to gain better understanding, early cellular responses to TMV coated substrate were observed within 24 hours of osteogenic induction.[73] We discovered that bone morphogenetic protein 2 (BMP-2) was upregulated endogenously during the first 24 hours with a peak expression at 8 hours (Figure 1.6a, b).

BMP-2 is one of the most potent inducers of bone differentiation in mesenchymal stem cells [74] and is highly involved in the beginning of bone repair in an animal study.[75] Recombinant human BMP-2 (rhBMP-2) is commercially available and used as therapeutic supplement for bone repair in spine fusion surgeries and tibial fracture healing.[76] However, rhBMP-2 is costly and some recent studies reported the adverse effects caused by large quantity of rhBMP-2 implant failure or leakage causing life-threatening urogenital events, retrograde ejaculation, back and leg pain, hematoma, or

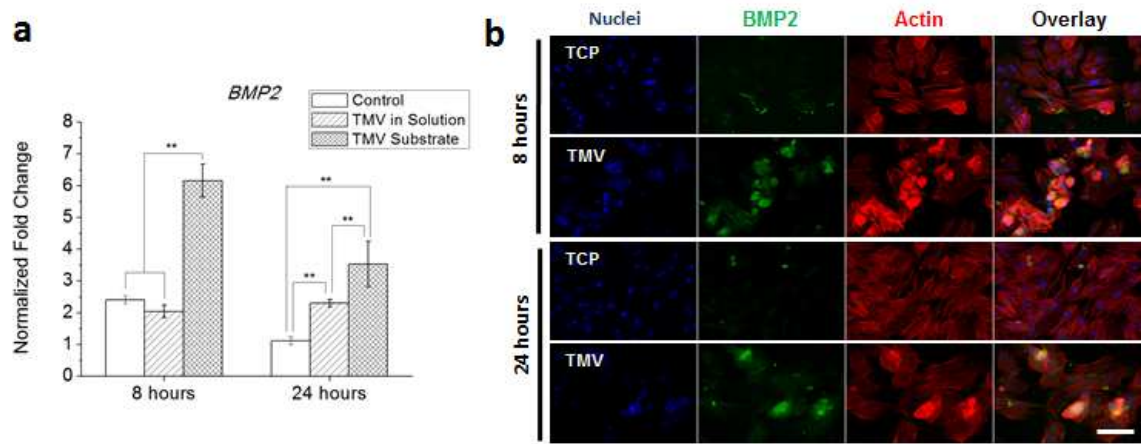


Figure 1.6 TMV-induced osteogenic differentiation in BMSCs *in vitro*. [73] (a) Gene expression profile showing an upregulation of *BMP2* mRNA level in BMSCs on TMV substrate at 8 hours after osteoinduction. (b) Immunohistochemical staining illustrating an increase in BMP2 expression at the protein level in BMSCs grown on TMV surface. Reproduced with permission from ref 37. Copyright 2012 The Royal Society of Chemistry.

breathing difficulty.[77-80] It was observed that *in vitro* osteogenic differentiation induced by supplementing BMP-2 to the cell culture was more effective when cells were grown on titanium surface with nanometer size of roughness.[81] Therefore, material-induced BMP-2 endogenous expression may provide an alternative approach to orthopedic surgeries where the morphogen is localized and the expression level is self-regulated, leading to reduce adverse effects.

#### 1.4 POSSIBLE MECHANISM OF TOPOGRAPHICAL CUES INDUCED STEM CELL DIFFERENTIATION

Initial clues of molecular mechanisms by which cells sense different topography are the differences in focal adhesion (FA) structures of cells on different substrates. Variations of FA size, strength, and composition often reflect changes in actin contractility and point to RhoA, a small GTPase whose activation enhances non-muscle myosin IIa-dependent actin contractility by stimulating the formation of stress fibers and FAs.[82] Many studies have emphasized the critical role of RhoA, Rho-associated kinase (ROCK), and its downstream effects on actomyosin contractility on the control of cell fate by cell spreading.[83-87] General concept acquired from these studies describes that MSCs differentiate along an osteogenic lineage when RhoA/ROCK pathway is activated which leads to cell spreading; whereas adipogenesis is dominated when RhoA/ROCK pathway is inhibited and cell spreading is restricted. Another key regulator of mechanotransduction is focal adhesion kinase (FAK), generally regarded as upstream of RhoA activation, is also influenced by changes in substrate nanotopography.[88] Nanotopographic substrates in the form of 14–45 nm nanopits [89] or 250 nm

nanogratings [88] also increased FAK activity. Differential activation of FAK in turn triggers downstream signaling to the mitogen-activated protein kinase (MAPK) cascade, which is an intracellular signaling cascade that delivers information about the extracellular environment to the cell nucleus.[30, 90] Ultimately, this pathway in turn influenced the transcription factor RUNX2 to control osteoblast differentiation and matrix mineralization (Figure. 1.7). Collectively, these findings suggest the participation of FAK/RhoA/ROCK/MAPK signaling pathway in substrate topography influence cell fate decisions.

Our plant virus based material provided the *in situ* endogenous BMP-2 stimulation and at the same time nanoscale surface features.[68, 73] One example of an attempt to combine BMP-2 induction with nanopatterned surface is the immobilization of BMP-2 peptides on nanoscale grooved and dot-shaped polymer surfaces, resulting in an improved osteogenesis without any other soluble inducers.[91] In this study, they discovered cytoskeleton and cell membrane stress induce RhoA/ROCK-mediated cytoskeletal tension and subsequently osteogenesis. The restrict cell morphology and stress in cell cytoskeleton observed were similar to what we observed in our plant virus scaffolds. Therefore, it is possible that nanotopographical features supplied by the virus nanoparticles influence cell spreading and introduce mechanical stress on the cell membrane leads to an early osteogenesis via the similar activation of RhoA/ROCK pathway.[92] To identify the upstream side of RhoA/ROCK signaling pathway, we started by focusing on identifying cell membrane receptors responsible for sensing the external stimuli. Our experiment showed that the size of focal adhesion complexes as identified by vinculin staining is reduced on virus-based material compared to that of

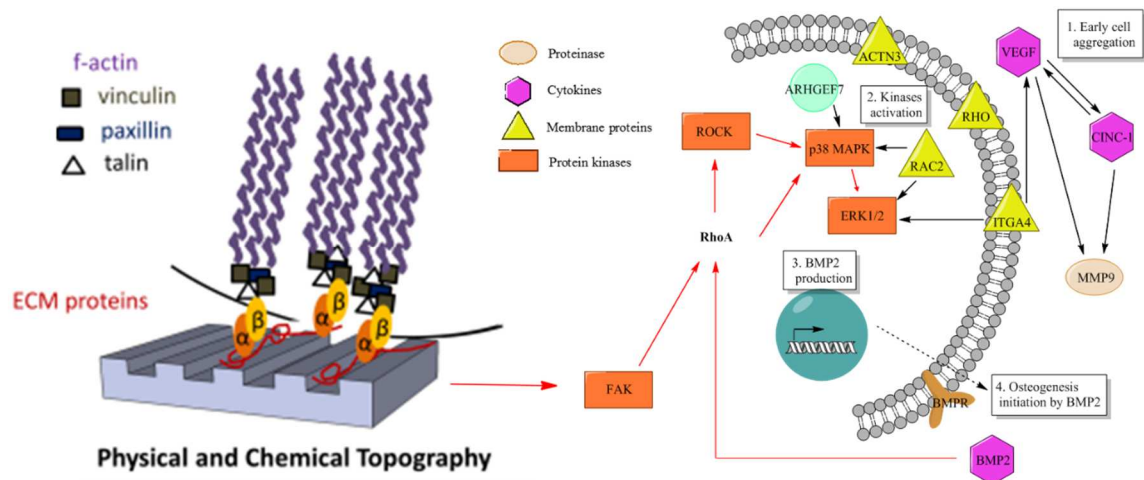


Figure 1.7 Schematic diagram depicts interrelation of common intracellular signaling events (red arrow path) triggered by changes in substrate topography and predicting sequential events for TMV-induced BMP-2 upregulation, leading to accelerated osteogenesis. Evidence in the literature suggests that key molecular players for this signaling pathway include integrins, focal adhesion-associated proteins (FAK and others), RhoA/ROCK, and MAPK. Actomyosin-driven tractional forces, which enable cells to mechanically probe their physical microenvironment, also appear to play a critical and conserved role in cells' responses to topography. Adapted with permission from ref 43. Copyright 2014 Wiley Online Library.

standard tissue culture plastics.[68, 73] Furthermore, there were a number of chemokines and small chemotactic cytokines, in addition to macrophage chemotactic protein 1 (MCP-1), produced in response to cell adhesion on TMV substrate.[93] These chemokines are not only important in the migration of immune cells during injury and infection,[94] but also the migration of stem cells during body development and maturation.[95] The production of these cytokines could be triggered as a consequence of cell membrane receptor signaling. Gene expression changes in motility genes were briefly investigated. It was discovered that actinin 3, integrin alpha 4, rhodopsin (Rho), Ras-related C3 botulinum toxin substrate 2 (Rac2), and Rho guanine nucleotide exchange factor 7 were upregulated.[93] Interestingly, Rac2, a hematopoietic-specific Rho GTPase, has been reported to play an important role in a success in long-term bone engraftment in mice.[96] These genes have been reported to be upstream of protein kinases, possibly leading to BMP-2 endogenous production which subsequently activate RhoA/ROCK-mediate cytoskeletal tension and ultimately accelerate osteogenesis (Figure 1.4c).

## 1.5 SUMMARY

Topography of implant materials plays an important role in directing stem cell fate. Microscale surface roughness has long been recognized to alter osteogenesis of stem cells. By optimizing roughness scale of material surface to  $Ra \sim 1-2 \mu m$ , bone formation can be highly induced. Anisotropic surface has been studied in term of a tool to direct cell alignment which often impacts stem cell fate. Isotropic surface is not determined to influence cell alignment, instead it is proved to be able to control cell function. Cell response to isotopic patterns is often inconsistent. For example, reported proper

dimensions of islands decorated substrate surface for osteogenesis were varied from one study to another. However, the concept that the introduction of pillars or islands to substrate surface can benefit osteogenic differentiation has been verified. In addition, the studies from Dalby *et al.* highlighted that the distribution of topographical features can significantly influence cell response. Many current studies have focused on nanotube featured materials which would also enhance bone formation; however, proper dimension of the nanotube has not been endorsed. Furthermore, fibrous materials are widely explored as promising tissue engineering scaffolds since they mimic the nanoscale properties of native ECM. It can be placed on substrate surface to create either anisotropic or isotropic surface and modulate stem cell differentiation to target phenotype.

The complex signaling cascade involved in nanotopographical cues influence cell responses is still unclear. The interaction between cells and material surface could be static or dynamic. Further study is needed to understand how a particular nano-patterning results in certain cellular response and behavior. For plant virus supplied nanotopographical cues substrates, even though the endogenous upregulation of BMP-2 was observed for BMSCs *in vitro*, we cannot be concluded that this is a universal phenomenon. Inhibiting BMP-2 by using siRNA, BMP-2 knock out, or applying BMP-2 inhibitors such as Noggin and Chordin may reaffirm the involvement of BMP-2 in the phenomenon. In addition, to investigate the participation of RhoA/ROCK pathway, Y-27632 (a selective inhibitor of ROCK), blebbistatin (an inhibitor of myosin II), and cytochalasin D (actin disrupting agent) could be employed. Despite great potential of the topographical cue guidance, there are a number of limitations for practical applications.

For example at molecular level, very limited studies have been reported to systematically elucidate the correlation between different topographical cues and cellular behaviors. It would require further investigation from many scientists in different fields, such as computational biology and molecular biology, to solve the puzzles.

## 1.6 REFERENCES

- [1] Gattazzo F, Urciuolo A, Bonaldo P. Extracellular matrix: a dynamic microenvironment for stem cell niche. *Biochim Biophys Acta*. 2014;1840:2506-19.
- [2] Kaivosoja E, Barreto G, Levon K, Virtanen S, Ainola M, Konttinen YT. Chemical and physical properties of regenerative medicine materials controlling stem cell fate. *Ann Med*. 2012;44:635-50.
- [3] Harrison RG. On the Stereotropism of Embryonic Cells. *Science*. 1911;34:279-81.
- [4] Weiss P. Experiments on cell and axon orientation in vitro; the role of colloidal exudates in tissue organization. *J Exp Zool*. 1945;100:353-86.
- [5] Curtis A, Wilkinson C. Nanotechniques and approaches in biotechnology. *Trends Biotechnol*. 2001;19:97-101.
- [6] Ross AM, Jiang Z, Bastmeyer M, Lahann J. Physical aspects of cell culture substrates: topography, roughness, and elasticity. *Small*. 2012;8:336-55.
- [7] Moore DT. *Tutorials in optics*. Washington, DC: Optical Society of America; 1992.
- [8] Wennerberg A, Albrektsson T. Effects of titanium surface topography on bone integration: a systematic review. *Clin Oral Implants Res*. 2009;20 Suppl 4:172-84.
- [9] Yang W, Han W, He W, Li J, Wang J, Feng H, et al. Surface topography of hydroxyapatite promotes osteogenic differentiation of human bone marrow mesenchymal stem cells. *Materials Science and Engineering: C*. 2016;60:45-53.

- [10] Faia-Torres AB, Charnley M, Goren T, Guimond-Lischer S, Rottmar M, Maniura-Weber K, et al. Osteogenic differentiation of human mesenchymal stem cells in the absence of osteogenic supplements: A surface-roughness gradient study. *Acta Biomater.* 2015;28:64-75.
- [11] London RM, Roberts FA, Baker DA, Rohrer MD, O'Neal RB. Histologic comparison of a thermal dual-etched implant surface to machined, TPS, and HA surfaces: bone contact in vivo in rabbits. *Int J Oral Maxillofac Implants.* 2002;17:369-76.
- [12] Grassi S, Piattelli A, de Figueiredo LC, Feres M, de Melo L, Iezzi G, et al. Histologic evaluation of early human bone response to different implant surfaces. *J Periodontol.* 2006;77:1736-43.
- [13] Park KH, Heo SJ, Koak JY, Kim SK, Lee JB, Kim SH, et al. Osseointegration of anodized titanium implants under different current voltages: a rabbit study. *J Oral Rehabil.* 2007;34:517-27.
- [14] Suzuki K, Aoki K, Ohya K. Effects of surface roughness of titanium implants on bone remodeling activity of femur in rabbits. *Bone.* 1997;21:507-14.
- [15] Takeuchi K, Saruwatari L, Nakamura HK, Yang JM, Ogawa T. Enhanced intrinsic biomechanical properties of osteoblastic mineralized tissue on roughened titanium surface. *J Biomed Mater Res A.* 2005;72:296-305.
- [16] de Oliveira PT, Nanci A. Nanotexturing of titanium-based surfaces upregulates expression of bone sialoprotein and osteopontin by cultured osteogenic cells. *Biomaterials.* 2004;25:403-13.

[17] de Oliveira PT, Zalzal SF, Beloti MM, Rosa AL, Nanci A. Enhancement of in vitro osteogenesis on titanium by chemically produced nanotopography. *J Biomed Mater Res A*. 2007;80:554-64.

[18] Kubo K, Att W, Yamada M, Ohmi K, Tsukimura N, Suzuki T, et al.

Microtopography of titanium suppresses osteoblastic differentiation but enhances chondroblastic differentiation of rat femoral periosteum-derived cells. *J Biomed Mater Res A*. 2008;87:380-91.

[19] Klymov A, Prodanov L, Lamers E, Jansen JA, Walboomers XF. Understanding the role of nano-topography on the surface of a bone-implant. *Biomaterials Science*. 2013;1:135-51.

[20] Yao X, Peng R, Ding J. Cell-material interactions revealed via material techniques of surface patterning. *Adv Mater*. 2013;25:5257-86.

[21] Wojciak-Stothard B, Madeja Z, Korohoda W, Curtis A, Wilkinson C. Activation of macrophage-like cells by multiple grooved substrata. Topographical control of cell behaviour. *Cell Biol Int*. 1995;19:485-90.

[22] Meyle J, Wolburg H, von Recum AF. Surface micromorphology and cellular interactions. *J Biomater Appl*. 1993;7:362-74.

[23] Matsuzaka K, Walboomers XF, Yoshinari M, Inoue T, Jansen JA. The attachment and growth behavior of osteoblast-like cells on microtextured surfaces. *Biomaterials*. 2003;24:2711-9.

[24] Charest JL, Bryant LE, Garcia AJ, King WP. Hot embossing for micropatterned cell substrates. *Biomaterials*. 2004;25:4767-75.

- [25] Andersson AS, Backhed F, von Euler A, Richter-Dahlfors A, Sutherland D, Kasemo B. Nanoscale features influence epithelial cell morphology and cytokine production. *Biomaterials*. 2003;24:3427-36.
- [26] Wang PY, Li WT, Yu J, Tsai WB. Modulation of osteogenic, adipogenic and myogenic differentiation of mesenchymal stem cells by submicron grooved topography. *J Mater Sci Mater Med*. 2012;23:3015-28.
- [27] Wang ZY, Lim J, Ho YS, Zhang QY, Chong MS, Tang M, et al. Biomimetic three-dimensional anisotropic geometries by uniaxial stretching of poly(epsilon-caprolactone) films: degradation and mesenchymal stem cell responses. *J Biomed Mater Res A*. 2014;102:2197-207.
- [28] Biggs MJ, Richards RG, McFarlane S, Wilkinson CD, Oreffo RO, Dalby MJ. Adhesion formation of primary human osteoblasts and the functional response of mesenchymal stem cells to 330nm deep microgrooves. *J R Soc Interface*. 2008;5:1231-42.
- [29] Watari S, Hayashi K, Wood JA, Russell P, Nealey PF, Murphy CJ, et al. Modulation of osteogenic differentiation in hMSCs cells by submicron topographically-patterned ridges and grooves. *Biomaterials*. 2012;33:128-36.
- [30] Biggs MJP, Richards RG, Gadegaard N, Wilkinson CDW, Oreffo ROC, Dalby MJ. The use of nanoscale topography to modulate the dynamics of adhesion formation in primary osteoblasts and ERK/MAPK signalling in STRO-1+ enriched skeletal stem cells. *Biomaterials*. 2009;30:5094-103.

- [31] Teixeira AI, Abrams GA, Bertics PJ, Murphy CJ, Nealey PF. Epithelial contact guidance on well-defined micro- and nanostructured substrates. *J Cell Sci.* 2003;116:1881-92.
- [32] Karuri NW, Liliensiek S, Teixeira AI, Abrams G, Campbell S, Nealey PF, et al. Biological length scale topography enhances cell-substratum adhesion of human corneal epithelial cells. *J Cell Sci.* 2004;117:3153-64.
- [33] Diehl KA, Foley JD, Nealey PF, Murphy CJ. Nanoscale topography modulates corneal epithelial cell migration. *J Biomed Mater Res A.* 2005;75:603-11.
- [34] Bunk R, Klinth J, Montelius L, Nicholls IA, Omling P, Tagerud S, et al. Actomyosin motility on nanostructured surfaces. *Biochem Biophys Res Commun.* 2003;301:783-8.
- [35] Johansson F, Carlberg P, Danielsen N, Montelius L, Kanje M. Axonal outgrowth on nano-imprinted patterns. *Biomaterials.* 2006;27:1251-8.
- [36] Barbucci R, Pasqui D, Wirsen A, Affrossman S, Curtis A, Tetta C. Micro and nano-structured surfaces. *J Mater Sci Mater Med.* 2003;14:721-5.
- [37] Hamilton DW, Riehle MO, Monaghan W, Curtis AS. Articular chondrocyte passage number: influence on adhesion, migration, cytoskeletal organisation and phenotype in response to nano- and micro-metric topography. *Cell Biol Int.* 2005;29:408-21.
- [38] Zhu B, Lu Q, Yin J, Hu J, Wang Z. Alignment of osteoblast-like cells and cell-produced collagen matrix induced by nanogrooves. *Tissue Eng.* 2005;11:825-34.
- [39] Yim EK, Pang SW, Leong KW. Synthetic nanostructures inducing differentiation of human mesenchymal stem cells into neuronal lineage. *Exp Cell Res.* 2007;313:1820-9.

- [40] Lee MR, Kwon KW, Jung H, Kim HN, Suh KY, Kim K, et al. Direct differentiation of human embryonic stem cells into selective neurons on nanoscale ridge/groove pattern arrays. *Biomaterials*. 2010;31:4360-6.
- [41] Ankam S, Suryana M, Chan LY, Moe AA, Teo BK, Law JB, et al. Substrate topography and size determine the fate of human embryonic stem cells to neuronal or glial lineage. *Acta Biomater*. 2013;9:4535-45.
- [42] Wang G, Ao Q, Gong K, Wang A, Zheng L, Gong Y, et al. The effect of topology of chitosan biomaterials on the differentiation and proliferation of neural stem cells. *Acta Biomater*. 2010;6:3630-9.
- [43] McNamara LE, Sjostrom T, Burgess KE, Kim JJ, Liu E, Gordonov S, et al. Skeletal stem cell physiology on functionally distinct titania nanotopographies. *Biomaterials*. 2011;32:7403-10.
- [44] Fiedler J, Ozdemir B, Bartholoma J, Plettl A, Brenner RE, Ziemann P. The effect of substrate surface nanotopography on the behavior of multipotent mesenchymal stromal cells and osteoblasts. *Biomaterials*. 2013;34:8851-9.
- [45] You MH, Kwak MK, Kim DH, Kim K, Levchenko A, Kim DY, et al. Synergistically enhanced osteogenic differentiation of human mesenchymal stem cells by culture on nanostructured surfaces with induction media. *Biomacromolecules*. 2010;11:1856-62.
- [46] Sjostrom T, Dalby MJ, Hart A, Tare R, Oreffo RO, Su B. Fabrication of pillar-like titania nanostructures on titanium and their interactions with human skeletal stem cells. *Acta Biomater*. 2009;5:1433-41.

- [47] Dalby MJ, Gadegaard N, Tare R, Andar A, Riehle MO, Herzyk P, et al. The control of human mesenchymal cell differentiation using nanoscale symmetry and disorder. *Nat Mater.* 2007;6:997-1003.
- [48] Wilkinson A, Hewitt RN, McNamara LE, McCloy D, Dominic Meek RM, Dalby MJ. Biomimetic microtopography to enhance osteogenesis in vitro. *Acta Biomater.* 2011;7:2919-25.
- [49] Zouani OF, Chanseau C, Brouillaud B, Bareille R, Deliane F, Foulc MP, et al. Altered nanofeature size dictates stem cell differentiation. *J Cell Sci.* 2012;125:1217-24.
- [50] Park J, Bauer S, Schlegel KA, Neukam FW, von der Mark K, Schmuki P. TiO<sub>2</sub> nanotube surfaces: 15 nm--an optimal length scale of surface topography for cell adhesion and differentiation. *Small.* 2009;5:666-71.
- [51] Park J, Bauer S, von der Mark K, Schmuki P. Nanosize and vitality: TiO<sub>2</sub> nanotube diameter directs cell fate. *Nano Lett.* 2007;7:1686-91.
- [52] Kang Y-H, Choi B, Ahn C, Oh S, Lee MS, Jin E-J. Titanium Oxide Nanotube Surface Topography and MicroRNA-488 Contribute to Modulating Osteogenesis. *Journal of Nanomaterials.* 2014;2014:8.
- [53] Badami AS, Kreke MR, Thompson MS, Riffle JS, Goldstein AS. Effect of fiber diameter on spreading, proliferation, and differentiation of osteoblastic cells on electrospun poly(lactic acid) substrates. *Biomaterials.* 2006;27:596-606.
- [54] Stevens MM, George JH. Exploring and engineering the cell surface interface. *Science.* 2005;310:1135-8.

- [55] Yin Z, Chen X, Song H-x, Hu J-j, Tang Q-m, Zhu T, et al. Electrospun scaffolds for multiple tissues regeneration in vivo through topography dependent induction of lineage specific differentiation. *Biomaterials*. 2015;44:173-85.
- [56] Huang XD, Bao L-R, Cheng X, Guo LJ, Pang SW, Yee AF. Reversal imprinting by transferring polymer from mold to substrate. *Journal of Vacuum Science & Technology B*. 2002;20:2872-6.
- [57] Suh K-Y, Park MC, Kim P. Capillary Force Lithography: A Versatile Tool for Structured Biomaterials Interface Towards Cell and Tissue Engineering. *Advanced Functional Materials*. 2009;19:2699-712.
- [58] Choi SJ, Yoo PJ, Baek SJ, Kim TW, Lee HH. An ultraviolet-curable mold for sub-100-nm lithography. *J Am Chem Soc*. 2004;126:7744-5.
- [59] Janson IA, Putnam AJ. Extracellular matrix elasticity and topography: Material-based cues that affect cell function via conserved mechanisms. *Journal of Biomedical Materials Research Part A*. 2015;103:1246-58.
- [60] Liu Z, Qiao J, Niu Z, Wang Q. Natural supramolecular building blocks: from virus coat proteins to viral nanoparticles. *Chem Soc Rev*. 2012;41:6178-94.
- [61] Liu Z, Xiao L, Xu B, Zhang Y, Mak AF, Li Y, et al. Covalently immobilized biomolecule gradient on hydrogel surface using a gradient generating microfluidic device for a quantitative mesenchymal stem cell study. *Biomicrofluidics*. 2012;6:24111-2411112.
- [62] Wu L, Zang J, Lee LA, Niu Z, Horvath GC, Braxton V, et al. Electrospinning fabrication, structural and mechanical characterization of rod-like virus-based composite nanofibers. *Journal of Materials Chemistry*. 2011;21:8550-7.

- [63] Pierschbacher M, Hayman EG, Ruoslahti E. Synthetic peptide with cell attachment activity of fibronectin. *Proc Natl Acad Sci U S A*. 1983;80:1224-7.
- [64] Merzlyak A, Indrakanti S, Lee SW. Genetically engineered nanofiber-like viruses for tissue regenerating materials. *Nano Lett*. 2009;9:846-52.
- [65] Wang J, Wang L, Li X, Mao C. Virus activated artificial ECM induces the osteoblastic differentiation of mesenchymal stem cells without osteogenic supplements. *Sci Rep*. 2013;3:1242.
- [66] Lin Y, Su Z, Niu Z, Li S, Kaur G, Lee LA, et al. Layer-by-layer assembly of viral capsid for cell adhesion. *Acta Biomater*. 2008;4:838-43.
- [67] Kaur G, Valarmathi MT, Potts JD, Jabbari E, Sabo-Attwood T, Wang Q. Regulation of osteogenic differentiation of rat bone marrow stromal cells on 2D nanorod substrates. *Biomaterials*. 2010;31:1732-41.
- [68] Metavarayuth K, Sitasuwan P, Luckanagul JA, Feng S, Wang Q. Virus Nanoparticles Mediated Osteogenic Differentiation of Bone Derived Mesenchymal Stem Cells. *Advanced Science*. 2015:n/a-n/a.
- [69] Lee S-W, Mao C, Flynn CE, Belcher AM. Ordering of Quantum Dots Using Genetically Engineered Viruses. *Science*. 2002;296:892-5.
- [70] Dogic Z, Fraden S. Smectic phase in a colloidal suspension of semiflexible virus particles. *Physical review letters*. 1997;78:2417.
- [71] Lee S-W, Wood BM, Belcher AM. Chiral Smectic C Structures of Virus-Based Films†. *Langmuir*. 2003;19:1592-8.

- [72] Kaur G, Valarmathi MT, Potts JD, Wang Q. The promotion of osteoblastic differentiation of rat bone marrow stromal cells by a polyvalent plant mosaic virus. *Biomaterials*. 2008;29:4074-81.
- [73] Sitasuwan P, Andrew Lee L, Bo P, Davis EN, Lin Y, Wang Q. A plant virus substrate induces early upregulation of BMP2 for rapid bone formation. *Integr Biol (Camb)*. 2012;4:651-60.
- [74] Cheng H, Jiang W, Phillips FM, Haydon RC, Peng Y, Zhou L, et al. Osteogenic activity of the fourteen types of human bone morphogenetic proteins (BMPs). *J Bone Joint Surg Am*. 2003;85-A:1544-52.
- [75] Ai-Aql ZS, Alagl AS, Graves DT, Gerstenfeld LC, Einhorn TA. Molecular mechanisms controlling bone formation during fracture healing and distraction osteogenesis. *J Dent Res*. 2008;87:107-18.
- [76] McKay WF, Peckham SM, Badura JM. A comprehensive clinical review of recombinant human bone morphogenetic protein-2 (INFUSE Bone Graft). *Int Orthop*. 2007;31:729-34.
- [77] Bishop GB, Einhorn TA. Current and future clinical applications of bone morphogenetic proteins in orthopaedic trauma surgery. *Int Orthop*. 2007;31:721-7.
- [78] Carragee EJ, Hurwitz EL, Weiner BK. A critical review of recombinant human bone morphogenetic protein-2 trials in spinal surgery: emerging safety concerns and lessons learned. *Spine J*. 2011;11:471-91.
- [79] Lee SH, Shin H. Matrices and scaffolds for delivery of bioactive molecules in bone and cartilage tissue engineering. *Adv Drug Deliv Rev*. 2007;59:339-59.

- [80] Shields LB, Raque GH, Glassman SD, Campbell M, Vitaz T, Harpring J, et al. Adverse effects associated with high-dose recombinant human bone morphogenetic protein-2 use in anterior cervical spine fusion. *Spine (Phila Pa 1976)*. 2006;31:542-7.
- [81] Kato RB, Roy B, De Oliveira FS, Ferraz EP, De Oliveira PT, Kemper AG, et al. Nanotopography directs mesenchymal stem cells to osteoblast lineage through regulation of microRNA-SMAD-BMP-2 circuit. *J Cell Physiol*. 2014;229:1690-6.
- [82] Hall A. Rho GTPases and the actin cytoskeleton. *Science*. 1998;279:509-14.
- [83] Yao X, Peng R, Ding J. Effects of aspect ratios of stem cells on lineage commitments with and without induction media. *Biomaterials*. 2013;34:930-9.
- [84] Bhadriraju K, Yang M, Alom Ruiz S, Pirone D, Tan J, Chen CS. Activation of ROCK by RhoA is regulated by cell adhesion, shape, and cytoskeletal tension. *Experimental Cell Research*. 2007;313:3616-23.
- [85] Wang YK, Yu X, Cohen DM, Wozniak MA, Yang MT, Gao L, et al. Bone morphogenetic protein-2-induced signaling and osteogenesis is regulated by cell shape, RhoA/ROCK, and cytoskeletal tension. *Stem Cells Dev*. 2012;21:1176-86.
- [86] McBeath R, Pirone DM, Nelson CM, Bhadriraju K, Chen CS. Cell shape, cytoskeletal tension, and RhoA regulate stem cell lineage commitment. *Dev Cell*. 2004;6:483-95.
- [87] Xu Y, Wagner DR, Bekerman E, Chiou M, James AW, Carter D, et al. Connective tissue growth factor in regulation of RhoA mediated cytoskeletal tension associated osteogenesis of mouse adipose-derived stromal cells. *PLoS One*. 2010;5:e11279.

- [88] Teo BK, Wong ST, Lim CK, Kung TY, Yap CH, Ramagopal Y, et al. Nanotopography modulates mechanotransduction of stem cells and induces differentiation through focal adhesion kinase. *ACS Nano*. 2013;7:4785-98.
- [89] Lim JY, Dreiss AD, Zhou Z, Hansen JC, Siedlecki CA, Hengstebeck RW, et al. The regulation of integrin-mediated osteoblast focal adhesion and focal adhesion kinase expression by nanoscale topography. *Biomaterials*. 2007;28:1787-97.
- [90] Khatiwala CB, Kim PD, Peyton SR, Putnam AJ. ECM compliance regulates osteogenesis by influencing MAPK signaling downstream of RhoA and ROCK. *J Bone Miner Res*. 2009;24:886-98.
- [91] Kim MJ, Lee B, Yang K, Park J, Jeon S, Um SH, et al. BMP-2 peptide-functionalized nanopatterned substrates for enhanced osteogenic differentiation of human mesenchymal stem cells. *Biomaterials*. 2013;34:7236-46.
- [92] Wang Y-K, Yu X, Cohen DM, Wozniak MA, Yang MT, Gao L, et al. Bone Morphogenetic Protein-2-Induced Signaling and Osteogenesis Is Regulated by Cell Shape, RhoA/ROCK, and Cytoskeletal Tension. *Stem Cells and Development*. 2012;21:1176-86.
- [93] Sitasuwan P. Biomaterial-Induced Osteogenesis of Mesenchymal Stem Cells by Surface Roughness and Functionalization. Columbia, SC: University of South Carolina; 2013.
- [94] Niggli V. Signaling to migration in neutrophils: importance of localized pathways. *Int J Biochem Cell Biol*. 2003;35:1619-38.
- [95] Vanden Berg-Foels WS. In situ tissue regeneration: chemoattractants for endogenous stem cell recruitment. *Tissue Eng Part B Rev*. 2014;20:28-39.

[96] Jansen M, Yang F-C, Cancelas JA, Bailey JR, Williams DA. Rac2-Deficient Hematopoietic Stem Cells Show Defective Interaction with the Hematopoietic Microenvironment and Long-Term Engraftment Failure. STEM CELLS. 2005;23:335-46.

## CHAPTER 2

### VIRUS NANOPARTICLES MEDIATED OSTEOGENIC DIFFERENTIATION OF BONE DERIVED MESENCHYMAL STEM CELLS<sup>1</sup>

#### 2.1 INTRODUCTION

It is well established that cell-material interactions regulate numerous cellular functions.[1-3] Biological processes such as adhesion, growth, differentiation and apoptosis, are controlled by cell shape and cytoskeletal organization which is directed by cell-surface interactions.[4-7] Meanwhile, the surface chemistry and topography of materials play a very crucial role in altering cell behaviors at many stages of cell growth and development.[3, 8-13] Although the dimensions of mammalian cells are on the order of a few micrometers, cellular sensing of the external environment and interaction with biomaterials occurs at the nanometer level.[14, 15] Cell interactions with nanometric surfaces often result in a specific sequence of gene and protein regulations. These series of events initiate as early as the cell begins to sense the surrounding environment. Therefore, the understanding of various topographical cues that are responsible for cellular behaviors is a key to advance tissue engineering.

In general, topographical cues can be classified as: (1) the roughness of the underlying surface (2) the ligand-display pattern and density (3) the size and shape of

<sup>1</sup>Metavarayuth K, Sitasuwan P, Luckanagul J, Feng S, Wang Q. 2015. *Adv. Sci.* 2, 1500026-33. Reprinted here with permission of publisher (Appendix B)

the contact area for cell spreading, and (4) the geometry of topological features at a nanometer scale.[16, 17] Reviewing the effect of individual cues is often complicated due to the difficulty in controlling and altering particular topographical features while preserving others. Micro/nanofabrication techniques are required to enable the recapitulation of topographical cues in the cell niche in a controllable and reproducible fashion. Examples of these technologies are mechanical roughening,[18] nano- and microindentation, and substrate-templating using a well-defined relief to impart topography with solvent-casting, electro-deposition, chemical-vapor depositions, or compression-molding processes.[19-21] These engineered micro/nanoscale topographical cues mimic the micro/nanoscale features in the physiological environment, which can be used to demonstrate how individual cues or the combination of topographical cues affect a particular cellular response. However, all these methods suffer from the laborious process, the inability of predictably generating chemistry and topography in a simultaneous fashion, the requirement for high-cost equipment, or the limited class of material can be used.[6, 22-24]

Virus particles, especially plant viruses, are uniform in size, have well organized and characterized 3D structure, and can be produced in high yield and purity.[25, 26] The symmetrical arrangement of the outer coat proteins of the viral particles makes them attractive scaffolds for polyvalent display of a variety of functional groups for various applications.[25, 27-29] In the past two decades, new materials with unique structural features have been developed for a wide range of applications, including electronics, drug delivery, imaging, gene therapy, and immunotherapy, by taking advantages of distinctive chemical and biological properties of plant viruses.[29-31] However, so far there is no

systematically investigation about how the nanoscale topographical cues of various plant virus particles coated substrates impact cell behaviors, specifically, osteogenesis of bone derived mesenchymal stem cells (BMSCs).

From our unexpected, yet significant, observation that rodlike plant virus nanoparticle, Tobacco mosaic virus (TMV) coated two dimensional substrate dramatically accelerates osteogenesis of BMSCs. The study suggested that the virus does not act as soluble inducer because supplementing cell culture media with TMV solution failed to mediate the differentiation.[32, 33] We have hypothesized that the shape of virus nanoparticle and/or nanoscale topography provided by surface structure of virus particle may be necessary for the enhanced osteogenesis. Therefore, in this study, we generate a series of plant virus nanoparticles coated substrates using a variety of viral nanoparticles with distinct morphology and nanotopography. We applied these virus based scaffolds to investigate cellular responses to different types of topographical cues (Figure 2.1). Our results show that some of these virus based scaffolds accelerate and enhance osteogenic differentiation of bone derived mesenchymal stem cells (BMSCs). This finding presented here may provide a new route for enhancing the performance of orthopedic implants by regulating stem cell differentiation with nanotopography.

## 2.2 RESULTS AND DISCUSSION

### ***2.2.1 Fabrication of virus-coated scaffolds by layer-by-layer deposition method***

We fabricated 2D virus based substrates from five plant viruses which can be categorized into three groups by morphology of the viral particles: rod shape virus, TMV and TVCV; filamentous virus, PVX, and spherical virus; TYMV and CPMV. Not only are these plant

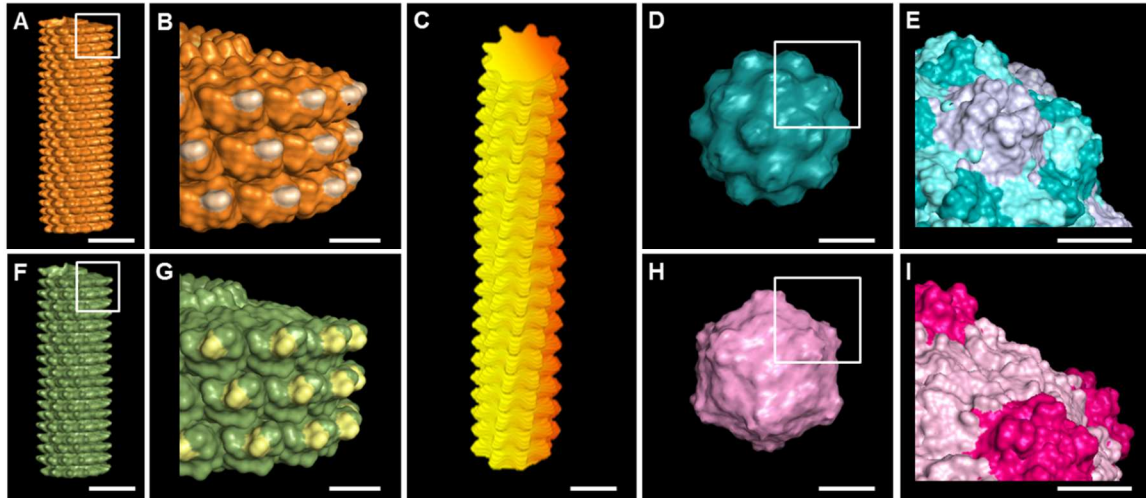


Figure 2.1 (A-I) Molecular models shows surface topography of plant viruses used in this study. (A-B) Tobacco mosaic virus (TMV); (C) Potato virus X (PVX); (D-E) Turnip yellow mosaic virus (TYMV); (F-G) Turnip vein clearing virus (TVCV); (H-I) Cowpea mosaic virus (CPMV). Scale bar indicates 10 nm in (A, C, D, F and H) and 5 nm in (B, E, G and I). The models were generated using Pymol ([www.pymol.org](http://www.pymol.org)) with co-ordinates obtained from RCSB protein data bank.

viruses morphologically different, but also they are nanotopographically dissimilar as shown in Figure 2.1

Since all these viral particles have isoelectric points (pI) less than 5.5, overall surface charges on these particles are negative in neutral pH condition. Via an electrostatic interaction, negatively charged viral particles can be strongly adsorbed onto various surfaces containing positively charged functional group. Several coating strategies and substrates were tested to screen for a high throughput method that offers uniform coating of every type of five virus particles on substrate surface. Summary of advantages and drawbacks of each coating procedure is shown in Table 2.1. Glass slide modified with organofunctional alkoxy silane molecules was first used to construct five virus coated substrates followed protocol developed by Kaur *et al.* The primary amine functional group of the organofunctional alkoxy silane can be protonated and presents positively charges under neutral condition. General coating method is dropping 0.2 mL of aqueous virus solution on the silanized glass and let the virus solution dry under sterile tissue culture hood.[34] Although, high coverage of virus nanoparticles on substrate surfaces can be achieved on this material, the coating protocol is very tedious and requires skillful personal to prepare the substrates. In addition, coffee ring effect, a pattern left by a puddle of particle-laden liquid after it evaporates is also commonly detected on the substrates prepared by this method if the virus solution is not fully covered the coating area. The higher number of virus layers could be detected around the edge and only non-uniform coatings were obtained which let to un-predictable roughness of the substrates. To avoid the coffee ring effect, 12 well plates with amine conjugated surface was tested for virus coating. With this material, the procedure for coating is easier

**Table 2.1** Summary of advantages and drawbacks of different virus coating procedures

<b>Substrates</b>	<b>Advantages</b>	<b>Drawbacks</b>
Silanized glass	<ul style="list-style-type: none"> <li>• Coating procedure was well developed</li> </ul>	<ul style="list-style-type: none"> <li>• Tedious</li> <li>• Coffee ring effect</li> <li>• Aqueous virus solution required</li> <li>• Multilayers coating</li> <li>• Time consuming</li> </ul>
Amine plate	<ul style="list-style-type: none"> <li>• Easy coating protocol</li> </ul>	<ul style="list-style-type: none"> <li>• Rough surface</li> <li>• Low coverage</li> <li>• Coffee ring effect</li> <li>• Expensive material</li> </ul>
PSS/PAH	<ul style="list-style-type: none"> <li>• Uniform coating</li> <li>• High throughput coating method</li> </ul>	<ul style="list-style-type: none"> <li>• Cell viability</li> </ul>
PAA/PAH	<ul style="list-style-type: none"> <li>• Uniform coating</li> <li>• High throughput coating method</li> </ul>	<ul style="list-style-type: none"> <li>• Cell viability</li> </ul>
PDL	<ul style="list-style-type: none"> <li>• Uniform coating</li> <li>• Biocompatible</li> <li>• High throughput coating method</li> </ul>	<ul style="list-style-type: none"> <li>• Relatively expensive reagent</li> </ul>

than silanized glass but we still could not get a consistent coating. In particular, during the drying process, more virus particles were drawn to the wall of the well and the center of each well had much less virus particle.

Since drop dry coating method failed to prepare uniform coating, we changed to a layer-by-layer (LbL) approach since it was reported by Zan *et al.* that the LbL method could create high coverage regular coating of TYMV on 2D substrate.[35] Two pairs of polyelectrolytes were tested for fabrication of the five virus particles coated substrates, polystyrene sulfonate(PSS) alternates with polyallylamine hydrochloride(PAH) and polyacrylic acid (PAA) alternates with PAH. Both of the polyelectrolytes pairs gave uniform coating with high coverage of virus particles. However, cells could not survive on the LbL substrates after a few days of culturing. To achieve a high cell viability, we employed poly-d-lysine (PDL) in our study. The interaction between positively charged amine functional group of PDL helps to retain the viral particles on the substrates by electrostatic interaction. By depositing structurally and nanotopographically distinctive viral particles on PDL coated substrate, we can readily construct an array of virus-coated scaffolds with various topographies offered by the intrinsic morphology and micro/nanotopography of each viral particle. The presence of viral particles on PDL coated surface was confirmed by atomic force microscopy (AFM) (Figure 2.2). The AFM micrographs also show a nearly complete coverage of substrates by intact viral particles. The virus particles are randomly adsorbed on 12-well plates coated with PDL, however, some area of the virus coated substrates appeared to show direction of virus particles coating under AFM. This coating pattern results from the natural irregularity of the cell culture surface of 12-well plate. To prevent the effect of plate pattern, the same lot of 12

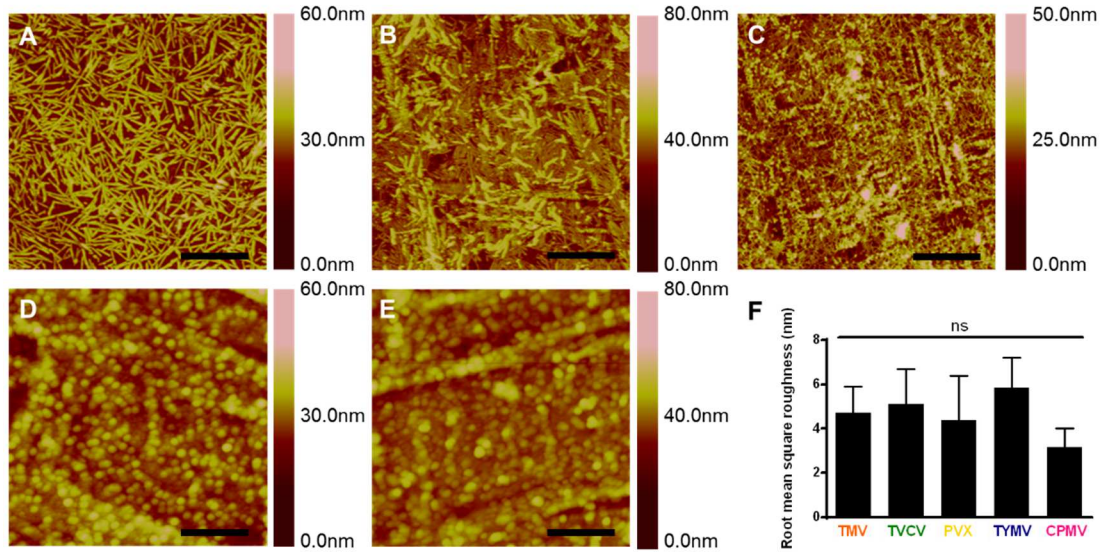


Figure 2.2 (A-E) Representative AFM micrographs showing the coverage of PDL coated substrate with different virus nanoparticles indicate the viral particles, (A) TMV; (B) TVCV; (C) PVX; (D) TYMV; and (E) CPMV, are mostly intact and fully cover the coating area. (F) Root mean square roughness of different virus nanoparticles coated substrates by AFM analysis. Scale bars indicate 1.25  $\mu\text{m}$  in (A-C) and 0.5  $\mu\text{m}$  in (D-E). The data are expressed as mean  $\pm$  s.d. (n = 4) ns indicates non-significant and  $p > 0.05$  based on ANOVA analysis.

well plates was used throughout this study. The virus substrates have been characterized in term of root mean square roughness from data collected from AFM micrographs (n = 4). There is no significant difference of microscale roughness across the virus coated substrates, created from deposition of numerous virus particles on the substrate surface, across these five virus substrates.

### ***2.2.2 Viral particles coated substrates promote Osteogenesis***

To investigate the effect of surface topography on osteogenesis, we cultured BMSCs on PDL coated substrate and the five virus-based substrates and studied the osteoblastic differentiation. BMSCs were isolated and cultured as reported in literature.[36, 37]1-3 The purity of the stem cells populations has been previously verified with several stem cells markers such as CD73 and CD90.[36, 37] The difference in the expression of bone morphogenetic protein-2 (BMP2) gene, an early osteogenic marker,[33] among BMSCs cultured on PDL and virus substrates were recorded at 6 hours after osteoinduction (Figure 2.3). Moreover, after 7 days of induction, osteocalcin (BGLAP) and osteopontin (SPP1) genes expressions were higher compare to uninduced BMSCs (Figure 2.4). These two genes are non-collagen genes actively involved during proliferation period. Osteocalcin is a specific marker for the osteoblast differentiation and mineralization, and is expressed exclusively during the post-proliferative period and reaches its maximum expression during mineralization and accumulates in the mineralized bone.[38-40] Osteopontin is known to serve as a bridge between the cells and the hydroxyapatite through the RGD and polyaspartate sequences present in it. It is one of the early markers

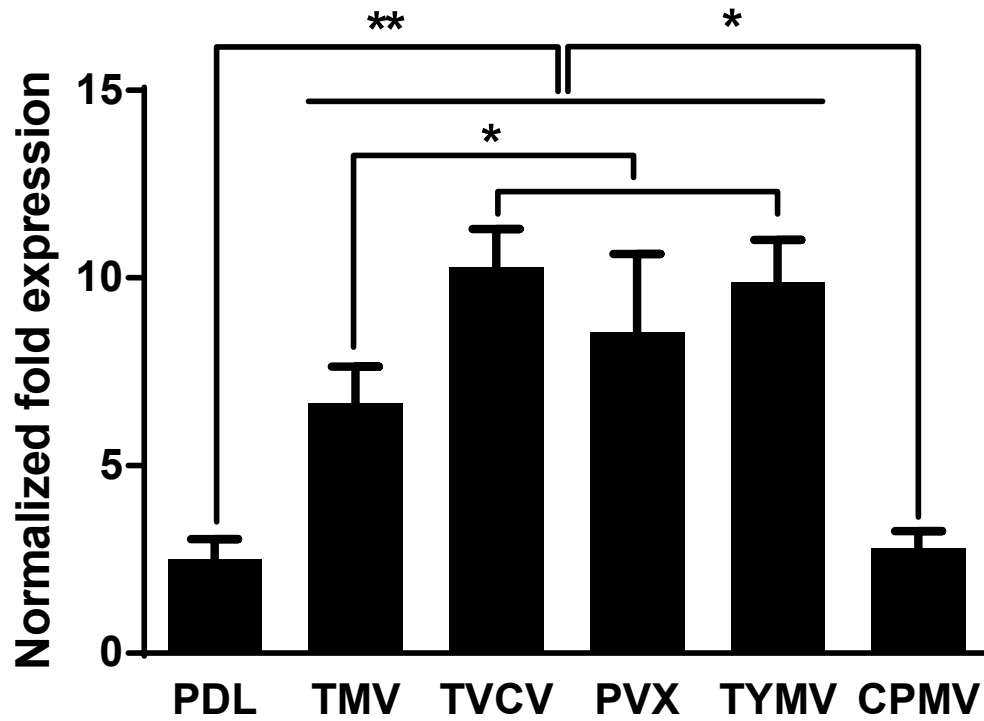


Figure 2.3 RT-qPCR analysis showed significant BMP2 upregulation in cells grown on TMV, TVCV, PVX, and TYMV (but not on CPMV) coated substrates at 6 hours after osteogenic induction. This result suggests early osteoblastic differentiation of BMSCs on the four virus coated substrates.

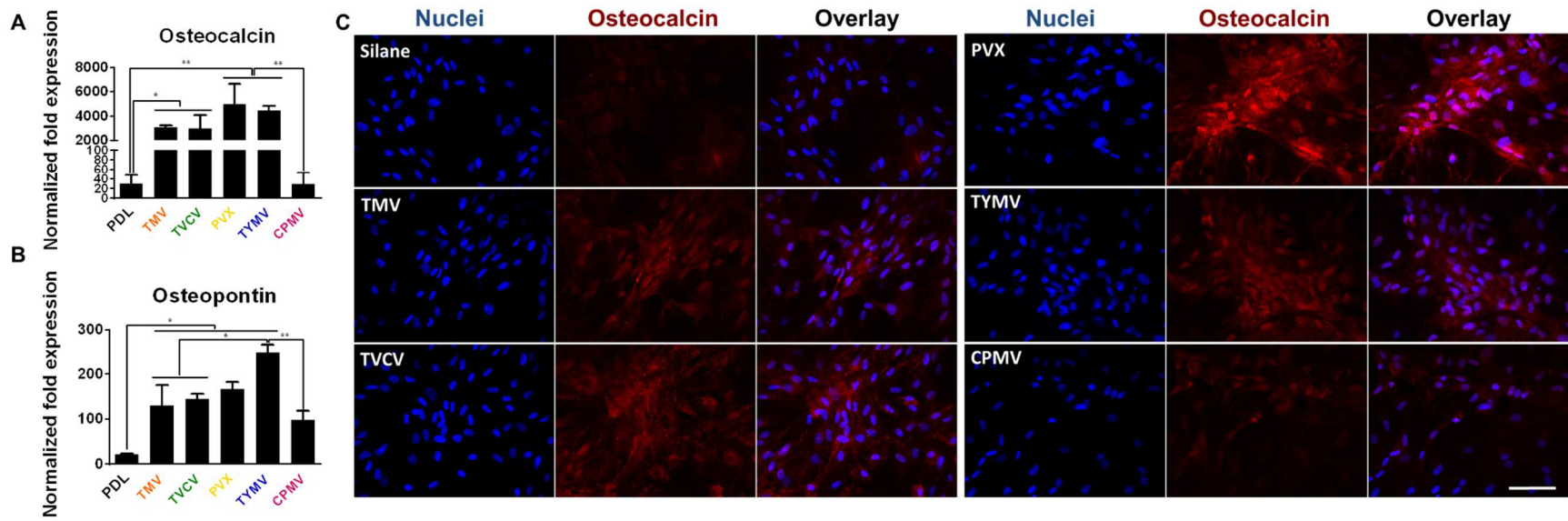


Figure 2.4 The expression of osteogenic marker in BMSCs cultured on PDL and different virus nanoparticles coated substrates under osteogenic conditions. (A-B) RT-qPCR analysis showed upregulation of osteocalcin (A) and osteopontin (B) in cells grown on TMV, TVCV, PVX, and TYMV (but not on CPMV) coated substrates at 7 days after osteogenic induction. (C) Immunohistochemical staining reveals that osteocalcin, a canonical osteogenic marker, is exclusively located in cell aggregates growing on TMV, TVCV, PVX, and TYMV substrates (not for CPMV coated substrate). Color representation: nucleus (blue), osteocalcin (red). Scale bar is 100 μm. The data were expressed as mean ± s.d. (n = 3, \* p ≤ 0.05, \*\* p ≤ 0.01 based on ANOVA)

of osteoblastic differentiation.[41] We observed significantly changes in the expression of all three osteospecific genes in cells plated on the virus based substrates, excepted CPMV coated substrate, compared to cells grew on bare PDL substrate. Interestingly, in the case of spherical-shaped viral particles, while TYMV coated substrates increased BMP2 gene expression by 4 folds and dramatically increment of BGLAP and SPP1 were observed, there was no significant difference in these gene expressions between cells plated on PDL and CPMV substrates.

Consistent with gene expression data, immunofluorescence imaging of BMP2 (Figure 2.5) and osteocalcin (Figure 2.4C) revealed that the morphogens are localized in the cell aggregates on the four virus coated substrates. BMSCs cultured on TMV, TVCV, PVX, and TYMV develop greater cell nodules, a notable feature of BMSCs undergoing osteogenesis. In order to quantify the differences in the spatial distributions of cells on each substrates, we acquired the coordination of cells and applied the nearest neighbor analysis.[42, 43] The spatial distributions of BMSCs on TMV, TVCV, PVX, and TYMV substrates were similar to the theoretical “cluster” distribution, which indicates cells tend to cluster to form the cell nodules. (Figure 2.6). On the other hand, the spatial distribution of BMSCs on PDL and CPMV were similar to the “independent” distribution and shifted towards a “regular” distribution. The data suggests that TMV, TVCV, PVX, and TYMV coated substrates are more favorable to the osteogenesis of BMSCs than PDL and CPMV substrates.

These cell clusters displayed robust positive staining for BMP2 in cell aggregates (Figure 2.6). No fluorescence signal was detected in cells grew on PDL control and CPMV substrates. Similarly, immunohistochemical staining of osteocalcin at 14 days

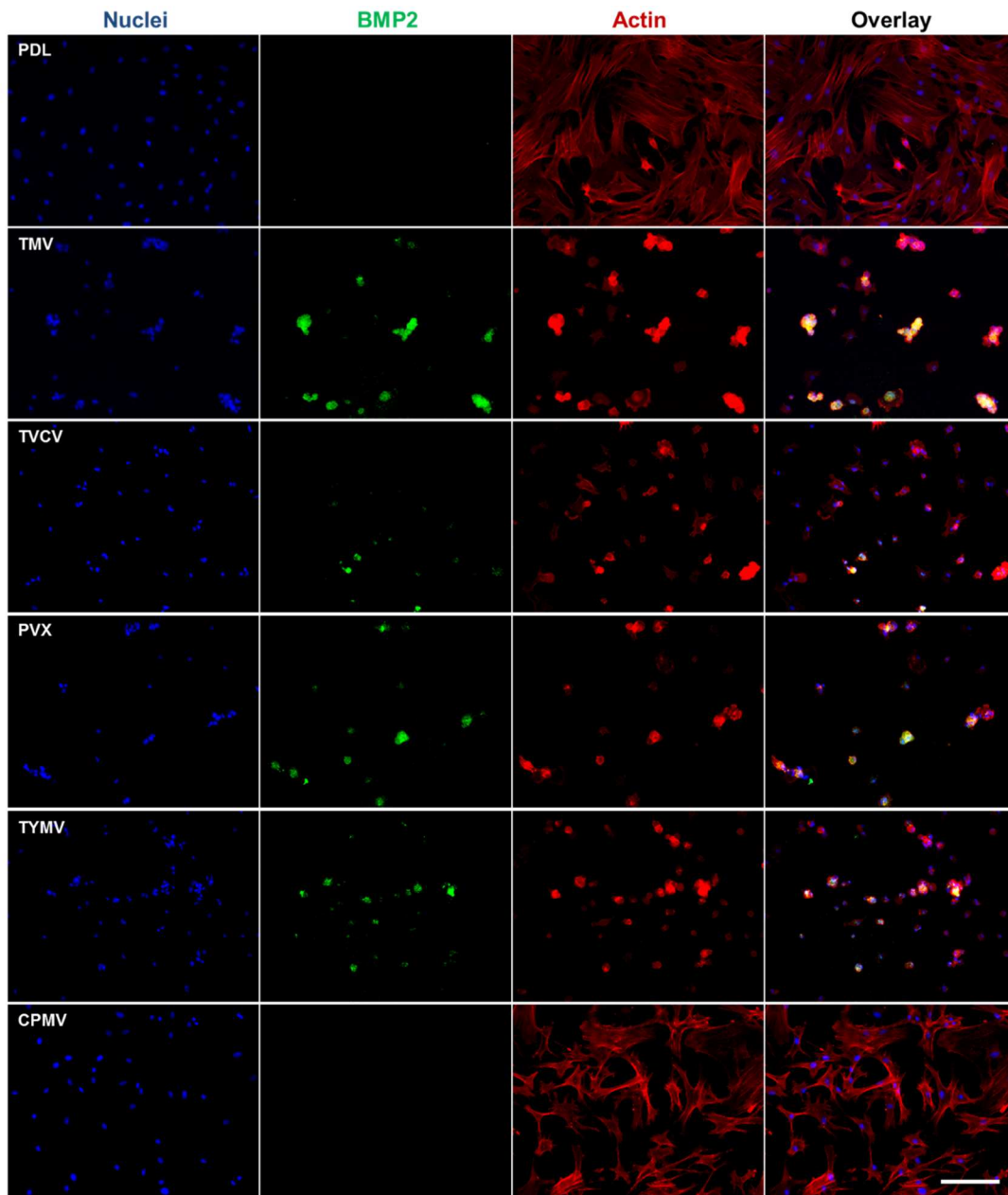


Figure 2.5 BMP2 immunohistochemical staining suggests the protein expressions are localized to the cell aggregates; most are found on TMV, TVCV, PVX, and TYMV substrates. Scale bar is 200  $\mu\text{m}$ . Color representation: nucleus (blue), BMP2 (green), actin (red).

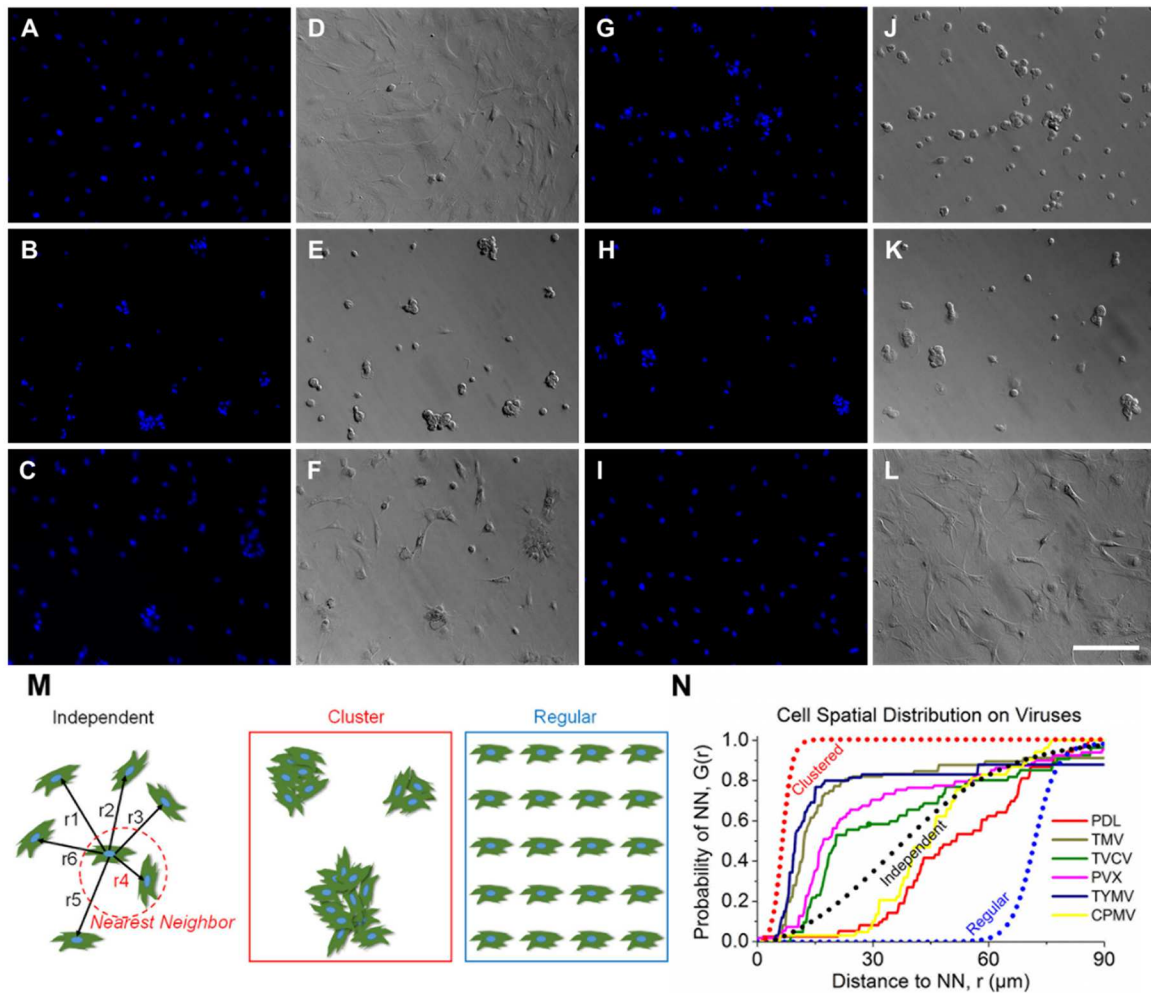


Figure 2.6 Nearest neighbor analysis of BMSCs cultured on PDL virus substrates. (A-C and G-I) DAPI immunohistochemical staining and (D-F and J-L) bright field microscopy images of BMSCs on (A, D) PDL, (B, E) TMV, (C, F) TVCV, (G, J) PVX, (H, K) TYMV, and (J, L) CPMV. (M) Schematic diagrams of the nearest neighbor analysis. In this analysis the distribution of cells can range from independent (represented by a theoretical Poisson's distribution), to clustered, or regular. (N) Plot of BMSCs spatial distribution on PDL control and virus substrates demonstrated cluster growth pattern which correlated to appearance of cells nodules on TMV, TVCV, PVX, and TYMV virus coated substrates. Scale bar is 200  $\mu\text{m}$ .

indicates that the canonical osteogenic marker was exclusively found in cells aggregates on TMV, TVCV, PVX, and TYMV substrates.

In addition to the analysis of osteo-specific markers, alkaline phosphatase (ALP) activity and calcium mineralization supported the osteogenic differentiation of cells on the four virus based scaffolds. ALP is an early marker of osteogenesis and its activity mediates matrix mineralization.[44] Cytochemical analysis of the osteogenesis process of BMSCs on PDL and virus coated substrates at day 4 and 7 after osteogenic induction suggested that cells on TMV, TVCV, PVX, and TYMV substrates had an increase in ALP activity at day 4, whereas CPMV substrates did not alter the enzyme activity when compared to PDL control. The enzyme activity drops to baseline at day 7 for cells on TMV and TVCV substrates (Figure 2.7A). It is possible that cells on these two virus substrates undergo differentiation and reach mineralization period earlier than cells on other substrates since alkaline phosphatase activity rises during cell proliferation and achieves maximum level as the culture progresses into mineralization stage. However, cellular level of ALP declines as mineralization progresses. [45] Additionally, cells on the four virus substrates at day 7 were positively stained by Alizarin red S which showed deep red color for calcium deposition in large cell nodules, whereas negatively stain was observed on PDL substrates (Figure 2.7B).

Cells on CPMV substrate only formed small nodules that were also stained with Alizarin red S. Quantification of dissolved Alizarin red S dye from cells nodules by UV-Vis absorbance indicated that the mineralization of cells on TMV substrates doubled that of PDL, and PVX and TYMV substrates increased the mineralization by 4 folds, while TVCV substrates slightly increased the mineralization of cells compared to PDL control

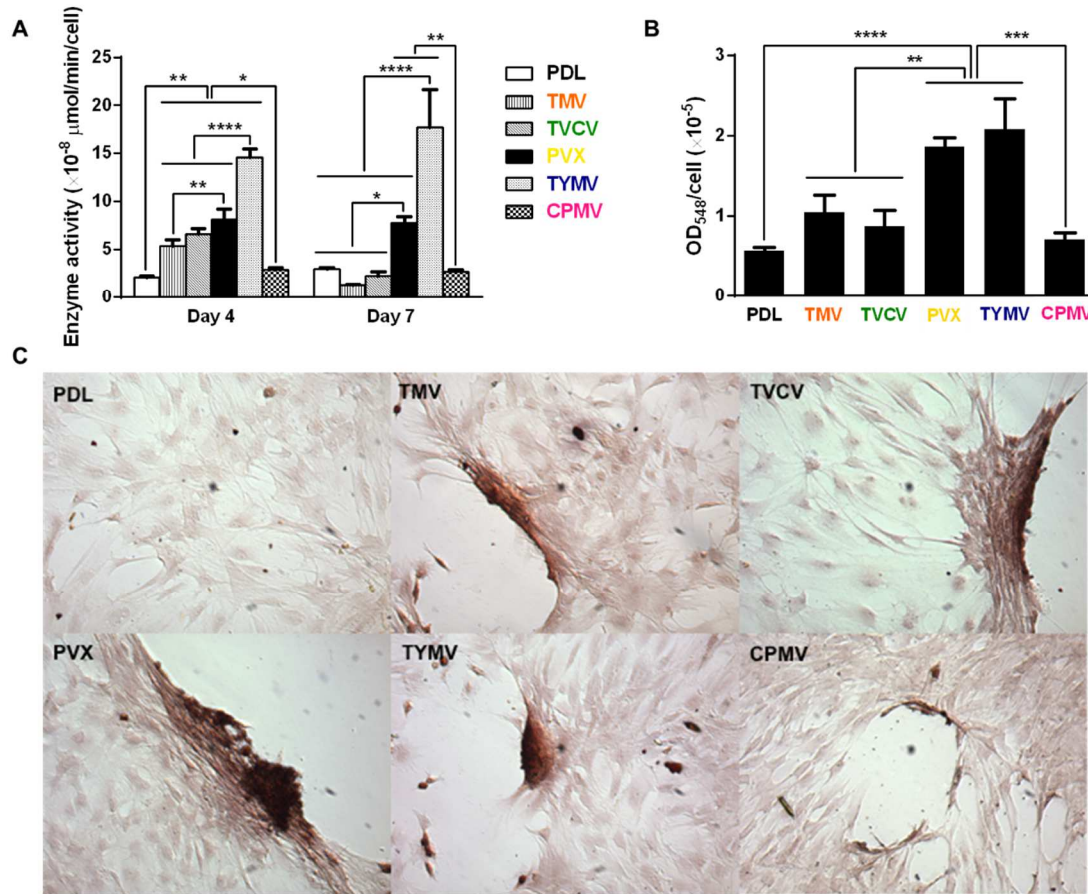


Figure 2.7 Cytochemical analysis of the bone differentiation process of BMSCs on PDL and viruses coated substrates at 4 and 7 days after osteogenic induction. (A) Alkaline phosphatase activity of cells cultured on different substrates. Cells on TMV, TVCV, PVX, and TYMV substrates have an increase in enzyme activity at day 4, while the enzyme activity of cells on CPMV substrates is not different from cells cultured on PDL control. On day 7, alkaline phosphatase activity reduces to baseline for cells on TMV and TVCV substrates. The data are expressed as mean  $\pm$  s.d. ( $n = 3$ , \*  $p \leq 0.05$ , \*\*  $p \leq 0.01$ , \*\*\*\*  $p \leq 0.0001$  based on ANOVA) (B) Absorbance at 548 nm normalized to cell number to indicate a relative amount calcium deposit at day 7 stained by alizarin red solution. The mineralization of cells on TMV substrates doubles that of PDL, while PVX and TYMV substrates increase the mineralization by 4 folds. TVCV substrates slightly increase the mineralization of cells compare to PDL control substrates. These evidences suggest an improvement in osteogenesis by virus coated substrates. The data are expressed as mean  $\pm$  s.d.. ( $n = 3$ , \*\*  $p \leq 0.01$ , \*\*\*  $p \leq 0.001$ , \*\*\*\*  $p \leq 0.0001$  based on ANOVA). (C) Alizarin red staining of each sample at day 7. Cells on virus substrates are positively stained for calcium deposition, whereas negatively stain is observed on PDL substrates.

substrates but not statistically significant (Figure 2.7C). However, as the calcium mineralization accumulates, longer incubation time of cells on these substrates could increase the difference in calcium deposition between each substrate and increase the difference of the mineralization between cells on TVCV and PDL coated substrates. Cells on CPMV substrate has comparable calcium mineralization to cells on PDL control.

The combined results from RT-qPCR, immunohistochemical staining, nearest neighbor analysis, enzyme activity and calcium mineralization unambiguously indicate that TMV, TVCV, PVX, and TYMV substrates can accelerate and enhance osteogenesis of BMSCs. The accelerated osteogenic differentiation of BMSCs on TMV and TYMV substrates has been demonstrated before in our previous studies when BMSCs were cultured on the viruses coated APTES glass coverslips.[32, 33, 46] In this study, we have confirmed that it is the topography created by deposition of virus nanoparticles on substrates, not underlying material, which mediates such differentiation.

### ***2.2.3 Nanotopography of viral based scaffolds alters cells morphology and induces differentiation***

The majority of cells cultured on the four virus substrates have noticeably smaller size at 24 hours after seeding compared to those on PDL and CPMV substrates. Previous study illustrated that cell shape and size are associated with adhesion strength of cells on a substrate.[47] Additionally, several reports showed that integrin-mediated focal adhesion is an important regulator of osteogenesis.[48, 49] It is hypothesized that too strong substrate binding may inhibit osteogenic differentiation. Mendonça et al. observed higher osteogenic differentiation of stem cells that attached looser on rough titanium disks than strongly attach cells on smooth substrate.[50] This could possibly be due to the limitation

of cells movement or migration. Strength of cell adhesion and larger focal adhesion size are correlated to an increase in localization of vinculin.[51] Therefore, we investigated cell adhesion on virus substrates by using fluorescence imaging of vinculin, a protein of focal adhesion complexes (FAC), to analyze average focal adhesion size of cells grew on PDL and virus substrates for 24 hours prior to osteoinduction. Vinculin signals were captured by fluorescence microscopy for size analysis by Slidebook™ 5 software. The data revealed the reduction in vinculin size of cells on TMV, TVCV, PVX, and TYMV but not CPMV substrates (Figure 2.8).

These results suggest that BMSCs attached to the 4 virus substrates weakly, whereas larger size of FACs dictates stronger cell-substrate adhesion in PDL and CPMV substrates.[52] The significantly smaller focal adhesion (FA) size for cells on the four virus substrates might increase cellular motility and facilitate the formation of cell aggregates within 6 hours of osteoinduction. The larger FA size observed in CPMV sample, which did not improve osteogenic differentiation, might be attributed to the expression of vimentin binding ligand on CPMV coat proteins.[53] The vimentin cytoskeleton was shown to regulate focal contact size and helps stabilize cell-matrix adhesion in endothelial cells.[54] Since major cytoskeletal component of mesenchymal cells is vimentin, the presence of vimentin binding ligand on CPMV substrate could supply additional adhesion points and consequently leads to higher adhesion strength of cells.

Several reports previously described that elongated shapes and geometries that present features of subcellular concavity at the cell perimeter increase the cytoskeletal substrates. tension in mesenchymal stem cells (MSCs), thus promoting the preference for

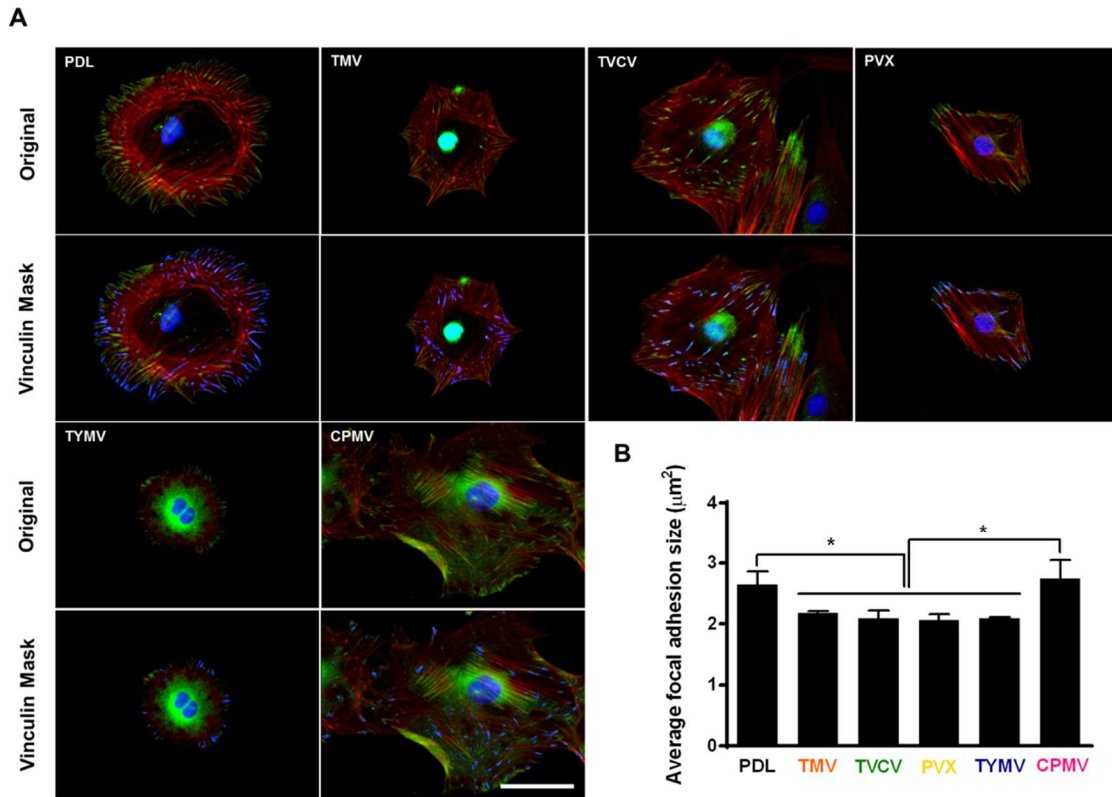


Figure 2.8 Immunochemical staining showing the difference in vinculin size of cells on PDL or virus coated substrates for 24 hours. (A) Immunofluorescence images of cells on different substrates at 24 hours prior to osteoinduction (top panel). Color representation: nucleus (blue), vinculin (green), phalloidin (red). The bottom panel demonstrates vinculin masking and selection of vinculins for size analysis. The selected vinculin spots are highlighted in blue. Scale bar is 50  $\mu\text{m}$ . (B) Average vinculin size of cells on different substrates. The data were expressed as mean  $\pm$  s.d. ( $n = 3$ , \* represents  $p \leq 0.05$  based on ANOVA).

osteogenesis.[55, 56] These similar geometries of BMSCs were also observed in our study. Representative actin and vinculin immunofluorescent heat maps of cells initially adhere on PDL and each virus coated substrates suggests that cells on TMV, TVCV, PVX, and TYMV were more elongate with higher actin stress fiber on the long axis of cells. The majority had concave features that led to high cytoskeleton tension in the region. Furthermore, vinculin of cells that grew on these four substrates were highly localized at the protrusion area which was different from those of cells on PDL and CPMV coated substrates. The majority of cells on PDL and CPMV coated substrates were rounded in shape with evenly distribute actin filaments and vinculin around cell perimeter (Figure 2.9). Moreover, overall morphology of cells on each virus substrates, which can be investigated from Figure 2.5 and 2.6, reveals that cells on CPMV have a more spread out shape compares to cells on other virus substrates. These data of morphology and immunofluorescence heatmaps along with small FA size suggests that loosely attachment of cells on unfriendly four virus, TMV, TVCV, PVX, and TYMV, coated substrates result in cytoskeleton tension, thereby enhancing osteogenic differentiation of BMSCs.

Therefore, data from this study suggest that the effect of nanoparticle morphology on differentiation is negligible. As observed from all experiments, osteogenic differentiation is comparable in cells cultured on substrates coated with different shape of virus.

## 2.3 CONCLUSIONS

A series of assorted micro-/nanoscale features possessed 2D peptide based

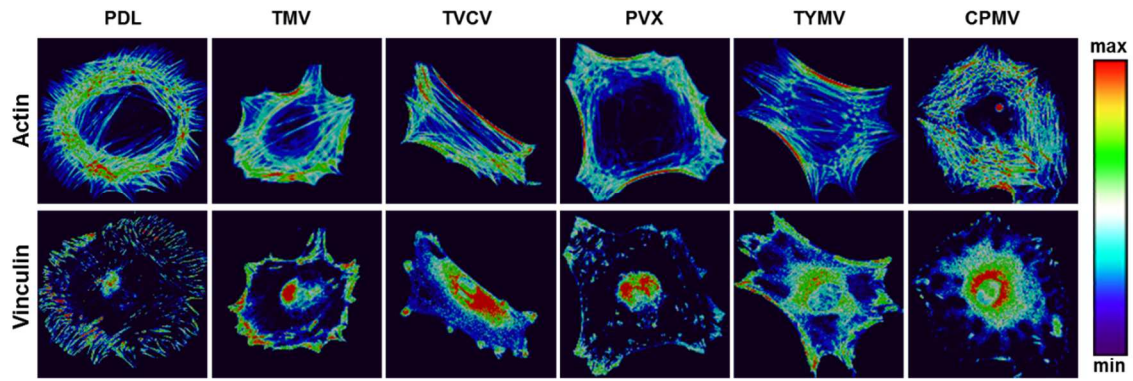


Figure 2.9 Representative actin (top panel) and vinculin (bottom panel) immunofluorescent heat maps of cells culture on PDL and virus coated substrates.

scaffolds can be simply constructed from structurally distinct viral bionanoparticles using fundamental electrostatic interaction. These virus based 2D scaffolds were used to investigate osteogenesis of BMSCs. The combined results from RT-qPCR and immunostaining of BMP2 suggest an early osteogenesis of cells on TMV, TVCV, PVX, and TYMV coated substrates as early as 6 hours after osteoinduction. Furthermore, the confirmation of the strong commitment in osteoinduction in longer term was evidenced by RT-qPCR and immunostaining of osteocalcin and osteopontin, as well as enzyme activity, and calcium mineralization. These results suggest that topographies created by TMV, TVCV, PVX, and TYMV coated substrates stimulate and enhance osteogenic differentiation. The underlying mechanisms of the observation is proposed that the stress created by the unfavorable surface from the four viral nanoparticles causes the reduction in FA size, which in turn increases cell motility and facilitates the formation of cell aggregates. The unfavorable surface may also obstruct cell spreading therefore increase cytoskeleton tension with results in high aspect ratio or subcellular concavity at the cell perimeter, thus promoting osteogenesis.

Further investigation about topography-induced differentiation is necessary for a better understanding of how surface topography provided by viral particles affect cell-material adhesion complex and facilitate the differentiation. Additionally, further studies can investigate the alignment or patterning of virus particles on the cellular responses as the unique structure or morphology of virus particles make them feasible for hierarchical structure formation in both 2D and 3D substrates.[57-61] More importantly, it will be very interesting to study if our discovery can be extended to other synthetic substrates and employed in clinic tissue engineering applications.

## 2.4 EXPERIMENTAL SECTION

***Purification of TMV, TVCV, TYMV, and CPMV:*** Infected leaves were blended with 3 volumes of 0.1 M potassium phosphate buffer pH 7.0 and 0.1%  $\beta$ -mercaptoethanol. The mixture was filtered, and the filtrate was subjected to centrifugation to remove bulk plant material. The supernatant was collected and clarified by adding an equal volume of  $\text{CHCl}_3$ /1-butanol (v/v = 1:1). The aqueous layer was then collected followed by precipitation of virus with 4% PEG 8K and 0.2 M NaCl. The pellet was centrifuged and resuspended in buffer before it was subjected to low speed centrifuge to remove PEG. The virus in supernatant was final pelleted by ultracentrifugation and resuspended in buffer.

***Purification of PVX:*** Infected leaves were blended with 2 volumes of 0.1 M potassium phosphate buffer pH 8.0 buffer, 10% ethanol and 0.1%  $\beta$ -mercaptoethanol. The mixture was filtered, and the filtrate was subjected to centrifugation to remove bulk plant material. The supernatant was collected and clarified by adding 1% Triton X-100. After centrifugation the supernatant was collected and processed by adding 4% PEG 8K and 0.2 M NaCl to precipitate virus. The pellet was centrifuged, resuspended in buffer and purified by sucrose gradient.

***Fabrication of virus based scaffolds:*** 1 mg/mL TMV, TYMV, CPMV, 10 mg/mL TVCV, and 2.67 mg/mL PVX in aqueous solution 0.7 mL were dropped into 12 well plates that were coated with Poly-d-Lysine using protocol suggested by Corning<sup>®</sup>. The virus solutions were incubated with the PDL coated plate under sterile cells culture hood for overnight. Then the bottoms of each well were rinsed briefly with 18.2 m $\Omega$  water before used for BMSCs culture.

***Surface characterization of virus based scaffolds by AFM:*** The surface morphology of virus based scaffolds was observed by AFM (Nanoscope IIIA MultiMode AFM (Veeco)). The bottoms of each 12 well plate were cut out after virus coating and rinsed with 18.2 mΩ water then dried with a stream of nitrogen gas before mounted onto AFM sample holder for imaging in the tapping mode.

***BMSC isolation and expansion:*** Primary BMSCs were isolated from the bone marrow of young adult 80 g male Wister rats (Harlan Sprague-Dawley Inc.). The procedures were performed in accordance with the guideline for animal experimentation by the Institutional Animal Care and Use committee, School of Medicine, University of South Carolina. Cells were maintained in primary media (Dullbecco's Modified Eagle's Medium (DMEM) supplemented with 10% fetal bovine serum (FBS), penicillin (100 U/mL), streptomycin (100 µg/mL), and amphotericin B (250 ng/mL)), kept at 37 °C in a CO<sub>2</sub> incubator with 95% air/5% CO<sub>2</sub> and passaged no more than seven times after isolation. To induce osteogenesis, primary media were replaced with osteogenic media consisting of DMEM supplemented with 10% FBS, penicillin (100 U/mL), streptomycin (100 µg/mL), and amphotericin B (250 ng/mL), 10 mM sodium β-glycerolphosphate, L-ascorbic acid 2-phosphate (50 µg/mL), and 10<sup>-8</sup> M dexamethasone. Media were replenished every 3-4 days.

***Quantitative real-time RT-PCR analysis (RT-qPCR):*** PDL and virus coated substrates were seeded with  $4.0 \times 10^4$  cells per well in primary media and allowed to attach overnight. The unseeded cells were used as a control to normalize the change in gene expression. The media were replaced to osteogenic media and cultured for 6 hours, 4 days, 7 days, and 14 days. The cell cultures were terminated at these time points and

total RNA was subsequently extracted using E.Z.N.A.<sup>®</sup> RNA Isolation Kit, OMEGA. At least two separate experiments were conducted with each type of sample. The purity and quantity of the extracted RNA were analyzed using Thermo Scientific Nanodrop 2000c spectrophotometer and was reverse transcribed by qScript<sup>™</sup> cDNA Supermix (Quanta Biosciences). RT-qPCR (iQ5 real-time PCR detection system Bio-Rad Laboratories) was done by the method described as: 60 cycles of PCR (95 °C for 20 s, 58 °C for 15 s, and 72 °C for 15 s), after initial denaturation step of 5 min at 95 °C, by using 12.5 µL of iQ5 SYBR Green I Supermix, 2 pmol/µL of each forward and reverse primers and 0.5 µL cDNA templates in a final reaction volume of 25 µL. Glyceraldehyde 3-phosphate dehydrogenase (GAPDH) was used as the house keeping gene. Data collection was enabled at 72 °C in each cycle and CT (threshold cycle) values were calculated using the iQ5 optical system software version 2.1. The expression levels of differentiated genes and undifferentiated genes were calculated using Pfaffl's method (M. W. Pfaffl, G. W. Horgan and L. Dempfle, Relative expression software tool) for group-wise comparison and statistical analysis of relative expression results in real-time PCR, using GAPDH as the reference gene. Quantification of gene expression was based on the CT value of each sample which was calculated as the average of at least two replicate measurements for each sample analyzed. "Pair Wise Fixed Reallocation Randomization Test" was performed on each sample and a value of  $p < 0.05$  was regarded as significant. The primers used for RT-qPCR are shown in Table 2.2. Three independent experiments were performed and analyzed for each gene expression study.

**Table 2.2** Primers used for RT-qPCR to measure gene expression levels. BGLAP: bone-gamma-carboxyglutamate protein (osteocalcin); BMP2: bone morphogenetic protein 2; SPP1: secreted phosphoprotein. 1 (osteopontin).

Gene	Sequence (5'-3')
BGLAP	Forward: AAAGCCCAGCGACTCT
	Reverse: CTAAACGGTGGTGCCATAGAT
BMP2	Forward: ACCAACCATGGGTTTGTGGTGGGAAGT
	Reverse: TCCGCTGTTTGTGTTTGGCTTGACG
GAPDH	Forward: ACTAAAGGGCATCCTGGGCTACACTGA
	Reverse: TGGGTGGTCCAGGGTTTCTTACTCCTT
SPP1	Forward: GACGGCCGAGGTGATAGCTT
	Reverse: CATGGCTGGTCTTCCCGTTGC

***Alkaline phosphatase (ALP) activity:*** After 4 and 7 days of induction in the osteogenic media, the BMSCs seeded on PDL and virus coated substrates were determined number of cells on each substrate by CellTiter Blue<sup>®</sup> assay. Then the cells were fixed with 4% paraformaldehyde for 15 min at room temperature prior to analyze ALP activity by incubating the briefly fixed cells with 1-Step p-nitrophenylphosphate solution (Thermo Scientific) for 15 min at room temperature. The solution was transferred to a new microfuge tube contained 250  $\mu$ L of 2 N NaOH and the absorbance at 405 nm was measured. The measure ALP activity from each sample was normalized to the corresponding cell number. Three independent experiments were performed and analyzed for ALP activity.

***Alizarin red staining and quantification:*** Calcium deposition on each substrate was visualized and quantified to confirm and compare osteogenic differentiation by Alizarin red staining. Fixed cell on day 7 were stained with 0.1% Alizarin red solution (Sigma-Aldrich) pH 4.1-4.5 for 30 min in the dark. The samples were washed with water (18.2 M $\Omega$ ) prior to imaging. To quantify the amount of dye on each substrate, 300  $\mu$ L of 0.1 N NaOH was added to each sample to extract the dye from the sample. The extracted dye solution was measured the absorbance at 548 nm wavelength. The measure absorbance from each sample was normalized to the corresponding cell number from CellTiter Blue<sup>®</sup> assay. Three independent experiments were performed and analyzed for Alizarin red staining and quantification.

***Immunofluorescence assays and image analysis:*** For immunofluorescence assays and image analysis, PDL or viral particles coated glass coverslips were used as substrate for BMSCs culture. The substrates were seeded with  $4.0 \times 10^5$  cells per sample.

The cultures were terminated at 24 hours after seeding to be used as vinculin immunostaining samples, 6 hours after osteoinduction for BMP2 immunostaining analysis and 14 days after osteoinduction for osteocalcin immunostaining study. After termination, cells were fixed in 4% paraformaldehyde at room temperature for 30 min. Each of the samples was then permeabilized for 20 min by 0.1% Triton-X 100 for 15 min and blocked in 1.5% bovine serum albumin (BSA, Sigma Aldrich) in PBS for 1 hour at room temperature. After the blocking, the cells were incubated overnight with mouse monoclonal antibody targeting BMP2 (R&D Systems) at 1:100 dilution in blocking buffer or Rabbit polyclonal antibody targeting osteocalcin (Santa Cruz Biotechnology) at 1:100 dilution in blocking buffer or mouse monoclonal antibody targeting vinculin (Neomarkers) at 1:200 dilution in blocking buffer. After overnight incubation, secondary goat anti-mouse antibody conjugated with fluorescein (Chemicon) was used at 1:400 dilution for 2 hours at room temperature with BMP2 and vinculin samples. Secondary goat anti-rabbit antibody conjugated with Alexa Fluor<sup>®</sup> 546 (Invitrogen) was used at 1:800 dilution for 2 hours at room temperature with osteocalcin samples. Rhodamin phalloidin (1:100 in PBS) was used to stain filamentous actin in BMP2 and vinculin samples. Fluorescein phalloidin (1:500 in PBS) was used to stain filamentous actin in osteocalcin samples. Nuclei were stained with DAPI (4,6-diamidino-2-phenylindole, 100 ng/mL). The sample were then mounted and sealed with clear nail polish before imaging. Images of the stained substrates were taken on an Olympus IX81 fluorescent microscope. SlideBook<sup>™</sup> 5 was used to select and analyze immunofluorescence images of vinculin. After setting the threshold for masks, the criteria used to select vinculin spots to be analyzed were XY shape factor larger than 1.5 and area size between 0.5-1.5  $\mu\text{m}^2$ . The

average size of vinculin for each image was calculated, followed by the calculation of average vinculin size of cells on PDL and virus substrates and the standard deviation from average values of three individual images which provide more than 500 vinculins for analysis per sample. Immunofluorescence heatmaps of actin and vinculin were generated by ImageJ software. Color histogram was generated by measuring pixel intensity across the immunofluorescence heatmaps of representative cells on each substrate.

***Spatial distribution analysis of BMSCs cultured on PDL and virus coated substrates:*** The spatial distribution of the cells on different substrates was analyzed by NIH ImageJ and R (<http://www.R-project.org>) software packages. The fluorescence images of cell nuclei were primarily processed with ImageJ to be presented as particles, and their centroid coordinates were determined. This data was then imported into R for nearest-neighbor analysis using the SpatStat module. The spatial distribution patterns of cells were identified for 70 – 90 cells on each substrate.

## 2.5 REFERENCES

- [1] Lee CH, Shin HJ, Cho IH, Kang YM, Kim IA, Park KD, et al. Nanofiber alignment and direction of mechanical strain affect the ECM production of human ACL fibroblast. *Biomaterials*. 2005;26:1261-70.
- [2] Andersson AS, Brink J, Lidberg U, Sutherland DS. Influence of systematically varied nanoscale topography on the morphology of epithelial cells. *IEEE Trans Nanobioscience*. 2003;2:49-57.

- [3] Fukushima N, Ohkawa H. Hematopoietic stem cells and microenvironment: the proliferation and differentiation of stromal cells. *Crit Rev Oncol Hematol*. 1995;20:255-70.
- [4] Bashur CA, Dahlgren LA, Goldstein AS. Effect of fiber diameter and orientation on fibroblast morphology and proliferation on electrospun poly(D,L-lactic-co-glycolic acid) meshes. *Biomaterials*. 2006;27:5681-8.
- [5] Dalby MJ, Gadegaard N, Wilkinson CD. The response of fibroblasts to hexagonal nanotopography fabricated by electron beam lithography. *J Biomed Mater Res A*. 2008;84:973-9.
- [6] Stevens MM, George JH. Exploring and engineering the cell surface interface. *Science*. 2005;310:1135-8.
- [7] Draghi L, Cigada A. Nanostructured surfaces for biomedical applications. Part I: nanotopography. *J Appl Biomater Biomech*. 2007;5:61-9.
- [8] Arnold M, Cavalcanti-Adam EA, Glass R, Blummel J, Eck W, Kantlehner M, et al. Activation of integrin function by nanopatterned adhesive interfaces. *Chemphyschem*. 2004;5:383-8.
- [9] He J, Zhou W, Zhou X, Zhong X, Zhang X, Wan P, et al. The anatase phase of nanotopography titania plays an important role on osteoblast cell morphology and proliferation. *J Mater Sci Mater Med*. 2008;19:3465-72.
- [10] Mendonca G, Mendonca DB, Aragao FJ, Cooper LF. Advancing dental implant surface technology--from micron- to nanotopography. *Biomaterials*. 2008;29:3822-35.

- [11] Yim EK, Reano RM, Pang SW, Yee AF, Chen CS, Leong KW. Nanopattern-induced changes in morphology and motility of smooth muscle cells. *Biomaterials*. 2005;26:5405-13.
- [12] Wan Y, Wang Y, Liu Z, Qu X, Han B, Bei J, et al. Adhesion and proliferation of OCT-1 osteoblast-like cells on micro- and nano-scale topography structured poly(L-lactide). *Biomaterials*. 2005;26:4453-9.
- [13] Liu Q, Cen L, Yin S, Chen L, Liu G, Chang J, et al. A comparative study of proliferation and osteogenic differentiation of adipose-derived stem cells on akermanite and beta-TCP ceramics. *Biomaterials*. 2008;29:4792-9.
- [14] Miller DC, Thapa A, Haberstroh KM, Webster TJ. Endothelial and vascular smooth muscle cell function on poly(lactic-co-glycolic acid) with nano-structured surface features. *Biomaterials*. 2004;25:53-61.
- [15] Badami AS, Kreke MR, Thompson MS, Riffle JS, Goldstein AS. Effect of fiber diameter on spreading, proliferation, and differentiation of osteoblastic cells on electrospun poly(lactic acid) substrates. *Biomaterials*. 2006;27:596-606.
- [16] Kim HN, Jiao A, Hwang NS, Kim MS, Kang do H, Kim DH, et al. Nanotopography-guided tissue engineering and regenerative medicine. *Adv Drug Deliv Rev*. 2013;65:536-58.
- [17] Bettinger CJ, Langer R, Borenstein JT. Engineering Substrate Topography at the Micro- and Nanoscale to Control Cell Function. *Angewandte Chemie International Edition*. 2009;48:5406-15.

- [18] Lampin M, Warocquier-Clérout R, Legris C, Degrange M, Sigot-Luizard MF. Correlation between substratum roughness and wettability, cell adhesion, and cell migration. *Journal of Biomedical Materials Research*. 1997;36:99-108.
- [19] Bartlett PN, Birkin PR, Ghanem MA. Electrochemical deposition of macroporous platinum, palladium and cobalt films using polystyrene latex sphere templates. *Chemical Communications*. 2000:1671-2.
- [20] Blanco A, Chomski E, Grabtchak S, Ibisate M, John S, Leonard SW, et al. Large-scale synthesis of a silicon photonic crystal with a complete three-dimensional bandgap near 1.5 micrometres. *Nature*. 2000;405:437-40.
- [21] Jiang P, Hwang KS, Mittleman DM, Bertone JF, Colvin VL. Template-Directed Preparation of Macroporous Polymers with Oriented and Crystalline Arrays of Voids. *Journal of the American Chemical Society*. 1999;121:11630-7.
- [22] Liu H, Webster TJ. Nanomedicine for implants: a review of studies and necessary experimental tools. *Biomaterials*. 2007;28:354-69.
- [23] Jager M, Zilkens C, Zanger K, Krauspe R. Significance of nano- and microtopography for cell-surface interactions in orthopaedic implants. *J Biomed Biotechnol*. 2007;2007:69036.
- [24] Dalby MJ, Pasqui D, Affrossman S. Cell response to nano-islands produced by polymer demixing: a brief review. *IEE Proc Nanobiotechnol*. 2004;151:53-61.
- [25] Destito G, Yeh R, Rae CS, Finn MG, Manchester M. Folic acid-mediated targeting of cowpea mosaic virus particles to tumor cells. *Chemistry and Biology*. 2007;14:1152-62.

- [26] Gerasopoulos K, McCarthy M, Banerjee P, Fan X, Culver JN, Ghodssi R. Biofabrication methods for the patterned assembly and synthesis of viral nanotemplates. *Nanotechnology*. 2010;21:055304.
- [27] Singh P, Gonzalez MJ, Manchester M. Viruses and their uses in nanotechnology. *Drug Development Research*. 2006;67:23-41.
- [28] Lee LA, Wang Q. Adaptations of nanoscale viruses and other protein cages for medical applications. *Nanomedicine*. 2006;2:137-49.
- [29] Mammen M, Choi S-K, Whitesides GM. Polyvalent Interactions in Biological Systems: Implications for Design and Use of Multivalent Ligands and Inhibitors. *Angewandte Chemie International Edition*. 1998;37:2754-94.
- [30] Douglas T, Young M. Viruses: making friends with old foes. *Science*. 2006;312:873-5.
- [31] Wang Q, Kaltgrad E, Lin T, Johnson JE, Finn MG. Natural supramolecular building blocks. Wild-type cowpea mosaic virus. *Chem Biol*. 2002;9:805-11.
- [32] Kaur G, Valarmathi MT, Potts JD, Jabbari E, Sabo-Attwood T, Wang Q. Regulation of osteogenic differentiation of rat bone marrow stromal cells on 2D nanorod substrates. *Biomaterials*. 2010;31:1732-41.
- [33] Sitasuwan P, Lee LA, Bo P, Davis EN, Lin Y, Wang Q. A plant virus substrate induces early upregulation of BMP2 for rapid bone formation. *Integr Biol (Camb)*. 2012;4:651-60.
- [34] Deegan RD, Bakajin O, Dupont TF, Huber G, Nagel SR, Witten TA. Capillary flow as the cause of ring stains from dried liquid drops. *Nature*. 1997;389:827-9.

- [35] Zan X, Sitasuwan P, Powell J, Dreher TW, Wang Q. Polyvalent display of RGD motifs on turnip yellow mosaic virus for enhanced stem cell adhesion and spreading. *Acta Biomater.* 2012;8:2978-85.
- [36] Valarmathi MT, Yost MJ, Goodwin RL, Potts JD. A Three-Dimensional Tubular Scaffold that Modulates the Osteogenic and Vasculogenic Differentiation of Rat Bone Marrow Stromal Cells. *Tissue Engineering Part A.* 2008;14:491-504.
- [37] Valarmathi MT, Fuseler JW, Goodwin RL, Davis JM, Potts JD. The mechanical coupling of adult marrow stromal stem cells during cardiac regeneration assessed in a 2-D co-culture model. *Biomaterials.* 2011;32:2834-50.
- [38] Gundberg CM, Hauschka PV, Lian JB, Gallop PM. Osteocalcin: isolation, characterization, and detection. *Methods Enzymol.* 1984;107:516-44.
- [39] Rodan GA, Noda M. Gene expression in osteoblastic cells. *Crit Rev Eukaryot Gene Expr.* 1991;1:85-98.
- [40] Lian JB, Stein GS. Concepts of osteoblast growth and differentiation: basis for modulation of bone cell development and tissue formation. *Crit Rev Oral Biol Med.* 1992;3:269-305.
- [41] Chen J, Singh K, Mukherjee BB, Sodek J. Developmental expression of osteopontin (OPN) mRNA in rat tissues: evidence for a role for OPN in bone formation and resorption. *Matrix.* 1993;13:113-23.
- [42] Clark PJ, Evans FC. Distance to Nearest Neighbor as a Measure of Spatial Relationships in Populations. *Ecology.* 1954;35:445-53.
- [43] Chung WJ, Merzlyak A, Yoo SY, Lee SW. Genetically engineered liquid-crystalline viral films for directing neural cell growth. *Langmuir.* 2010;26:9885-90.

- [44] Vunjak-Novakovic G. Tissue Engineering: Basic Considerations. In: Freshney RI, editor. Culture of Cells for Tissue Engineering. Hoboken, New Jersey: John Wiley & Sons, Inc.; 2006. p. 129-55.
- [45] Tohme JF, Seibel MJ, Silverberg SJ, Robins SP, Bilezikian JP. Biochemical markers of bone metabolism. *Z Rheumatol.* 1991;50:133-41.
- [46] Kaur G, Valarmathi MT, Potts JD, Wang Q. The promotion of osteoblastic differentiation of rat bone marrow stromal cells by a polyvalent plant mosaic virus. *Biomaterials.* 2008;29:4074-81.
- [47] Barnhart EL, Lee KC, Keren K, Mogilner A, Theriot JA. An adhesion-dependent switch between mechanisms that determine motile cell shape. *PLoS Biol.* 2011;9:e1001059.
- [48] Siebers MC, ter Brugge PJ, Walboomers XF, Jansen JA. Integrins as linker proteins between osteoblasts and bone replacing materials. A critical review. *Biomaterials.* 2005;26:137-46.
- [49] Garcia AJ, Reyes CD. Bio-adhesive surfaces to promote osteoblast differentiation and bone formation. *J Dent Res.* 2005;84:407-13.
- [50] Mendonca DB, Miguez PA, Mendonca G, Yamauchi M, Aragao FJ, Cooper LF. Titanium surface topography affects collagen biosynthesis of adherent cells. *Bone.* 2011;49:463-72.
- [51] Mierke CT. The role of vinculin in the regulation of the mechanical properties of cells. *Cell Biochem Biophys.* 2009;53:115-26.

- [52] Katz BZ, Zamir E, Bershadsky A, Kam Z, Yamada KM, Geiger B. Physical state of the extracellular matrix regulates the structure and molecular composition of cell-matrix adhesions. *Mol Biol Cell*. 2000;11:1047-60.
- [53] Koudelka KJ, Destito G, Plummer EM, Trauger SA, Siuzdak G, Manchester M. Endothelial targeting of cowpea mosaic virus (CPMV) via surface vimentin. *PLoS Pathog*. 2009;5:e1000417.
- [54] Tsuruta D, Jones JC. The vimentin cytoskeleton regulates focal contact size and adhesion of endothelial cells subjected to shear stress. *J Cell Sci*. 2003;116:4977-84.
- [55] Kilian KA, Bugarija B, Lahn BT, Mrksich M. Geometric cues for directing the differentiation of mesenchymal stem cells. *Proc Natl Acad Sci U S A*. 2010;107:4872-7.
- [56] Lee J, Abdeen AA, Huang TH, Kilian KA. Controlling cell geometry on substrates of variable stiffness can tune the degree of osteogenesis in human mesenchymal stem cells. *J Mech Behav Biomed Mater*. 2014.
- [57] Lin Y, Su Z, Xiao G, Balizan E, Kaur G, Niu Z, et al. Self-assembly of virus particles on flat surfaces via controlled evaporation. *Langmuir*. 2011;27:1398-402.
- [58] Peng B, Liu N, Lin Y, Wang L, Zhang W, Niu Z, et al. Self-assembly of anisotropic tobacco mosaic virus nanoparticles on gold substrate. *Science China Chemistry*. 2011;54:137-43.
- [59] He J, Niu Z, Tangirala R, Wang J-Y, Wei X, Kaur G, et al. Self-Assembly of Tobacco Mosaic Virus at Oil/Water Interfaces. *Langmuir*. 2009;25:4979-87.
- [60] Kaur G, He J, Xu J, Pingali S, Jutz G, Boker A, et al. Interfacial assembly of turnip yellow mosaic virus nanoparticles. *Langmuir*. 2009;25:5168-76.

[61] Zan X, Feng S, Balizan E, Lin Y, Wang Q. Facile method for large scale alignment of one dimensional nanoparticles and control over myoblast orientation and differentiation. ACS Nano. 2013;7:8385-96.

## CHAPTER 3

# NANOTOPOGRAPHICAL CUES MEDIATE OSTEOGENESIS OF STEM CELLS ON VIRUS SUBSTRATES THROUGH BMP-2 INTERMEDIATE

### 3.1 INTRODUCTION

Plant viruses nanoparticles have recently been utilized as multifacet nanosized building blocks for directing cell growth and differentiation.[1-5] Plant viruses can be isolated in high purity with batch to batch consistencies at low cost. The chemical and genetic modifications of virus surface to incorporate new functional groups have been extensively studied, which provides a library of viruses with diverse surface properties.[1-3, 6-8] In addition, the symmetrical arrangement of the viral proteins makes it an attractive scaffold for displaying functional groups for applications in electronics, catalysis, drug/gene delivery, imaging, and immunotherapy.

The highly structural ordered functional groups of virus nanoparticles were shown to recruit different cellular responses compared to unordered ligands. Some animal viruses display a pentameric motif integrin binding sites to promote cell internalization.[9, 10] The adhesion force associated with the clusters of integrin binding motifs can be 7-fold stronger than nonclustered ligand–receptor interactions.[11, 12] In cell signaling, RGD peptide targeted integrin receptors form dynamic clusters that are essential in cell adhesion, migration, and mechanotransduction, which can ultimately affect stem cell differentiation.[13, 14]

Previous studies from our group revealed that substrates coated with plant viruses supported mesenchymal stem cell growth and accelerated differentiation.[15-20] Bone derived mesenchymal stem cells (BMSCs) cultured on various viruses coated substrates such as wild type, phosphate modified, and genetically modified Tobacco mosaic virus (TMV), Turnip yellow mosaic virus (TYMV), Turnip vein clearing virus (TVCV), and Potato virus X (PVX) had increased alkaline phosphatase activity, calcium mineralization and had higher expression levels of genes related to bone formation, or osteogenic differentiation. More importantly, these studies have revealed a rapid upregulation of BMP2, a clinically approved therapeutic supplement for bone repair, prior to bone formation of cells on these virus substrates.

Living tissues are sophisticated systems comprised of multiple cell types surrounded in a complex, well-defined extracellular matrix (ECM). The ECM possesses topographical and adhesive features ranging from nanometers to micrometers. Many ECM proteins form large-scale structures up to several hundred micrometers in size and interact with multiple individual cells. However, recent findings emphasize that mammalian cells can respond to nanoscale features on synthetic surfaces.[21-23] The argument for this finding lies in the premise that cells contain nanoscale features whose sizes are compatible with nanoscale ECM structures, such as focal contacts/adhesions. Utilizing these nanoscale features cells can sense nanotopography of the underlying surfaces. Taking advantage of this phenomenon, scientists have fabricated biomaterials that possess unique topographies to control cell behaviors.

Bone morphogenetic protein 2 (BMP-2) is a subgroup of the bone morphogenetic proteins (BMPs) that are historically named because of their potentials to induce bone

and cartilage formation. Currently, its recombinant human form (rhBMP-2) is used clinically as therapeutic supplement for bone repair in spine fusion surgeries and tibial fracture healing.[21] Although, the supplement of rhBMP2 can accelerate bone formation for patients, rhBMP2 is costly and some recent studies reported the adverse effects caused by implant failure or leakage of high dosage rhBMP2 implants causing many complications.[24] Therefore, the possibility of using nanoscale materials to promote endogenous BMP2 production becomes an appealing route for studying the mechanisms involved in bone tissue repair.

We hypothesized that cell differentiation on plant viruses resulted from highly ordered arrangement of virus coat proteins, which provide unique nanotopographical cues to the virus substrates. Therefore we designed a systemic analysis to study two possible parameters stimulated the cellular response. First parameter we examined was the chemistry of TMV coat protein (TMV-CP) because virus coat proteins display numerous functional groups on its outer surface, therefore, chemistry of the protein may influence different cellular responses. To test this parameter poly-D-lysine (PDL) was selected to coat on the bottom of tissue culture plate to provide positive charge surface that will retain negative charged viral proteins or particles onto the substrate surface. Then we coated individual TMV-CP isolated by acetic acid catalyzed disassembly of TMV particles on the PDL substrate.[25] The second parameter is the ordered arrangement of TMV-CP in wild type virus nanoparticle. The highly ordered coat protein arrangement of many viruses was demonstrated to recruit different cellular responses.[26, 27] To study this parameter, we prepared and studied osteogenesis of cells on substrates coated with

gold nanorods that have similar dimensions to TMV but are randomly coated with TMV-CP instead of well-organized TMV-CP like wild type TMV substrate (Figure 3.1).

## 3.2 RESULTS AND DISCUSSION

### ***3.2.1 TMV-GNRs assembly and characterization***

Hybrid viral gold nanorods (TMV-GNRs) were prepared from cetrimonium bromide (CTAB) capped gold nanorods (CTAB-GNRs) that has similar dimension to wild type TMV following a protocol developed by Murphy *et al.*[28] Figure 3.2c shows length of CTAB-GNRs measured by TEM which is comparable to the size of wild type TMV (Figure 3.2a). Yield of nanorods obtained by the synthesis protocol is more than 90% as confirmed by TEM image (Figure 3.2b). Only very low percentage of other shaped gold nanoparticles is detected. In addition, the average diameter of gold nanorods was measured by the height profile of AFM image and it was calculated to be 15.7 nm (Figure 3.2d). The resultant CTAB-GNRs were used to prepare TMV-CP randomly coated GNRs. This assembly was initially attempted by inheriting electrostatic interaction between positively charged of quaternary amine functional group of CTAB and negatively charged surface of TMV-CP. However, the present of TMV-CP on surface of CTAB-GNRs was not observed after assembly. The possible explanation for this failure assembly is that hydrophobicity from long alkyl side chain of densely packed CTAB molecules on GNR surface interferes the electrostatic interaction. Therefore masking CTAB molecule on the surface could be done to prevent the hydrophobic interference.

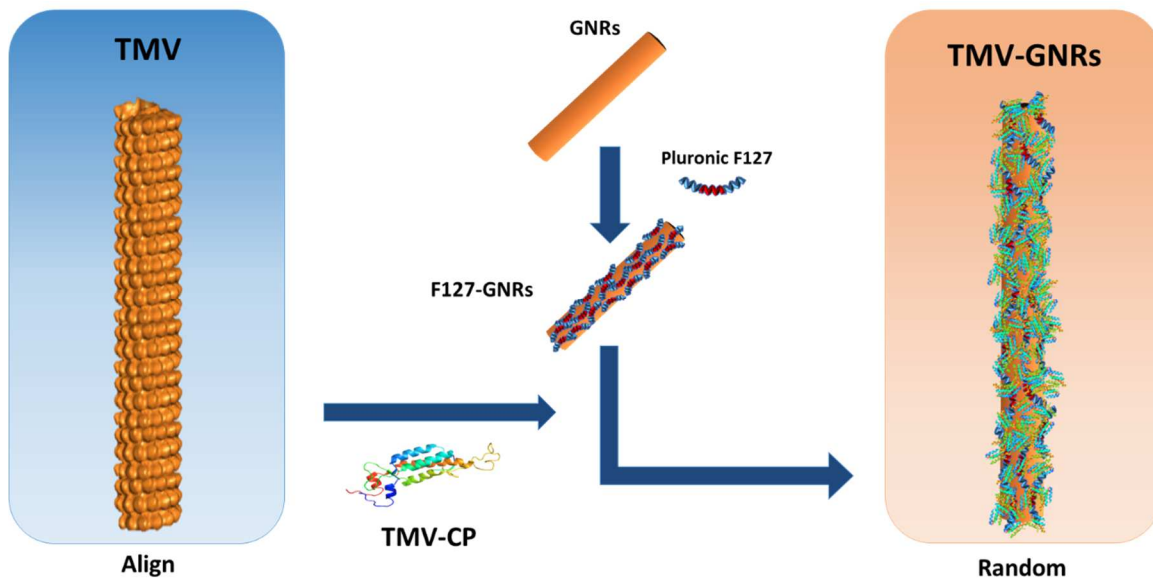


Figure 3.1 Schematic shows TMV coat protein coated gold nanorod (TMV-GNRs) preparation and structural comparison of align and random TMV coat protein (TMV-CP) coated nanorod structure. Gold nanorods (GNRs) were prepared by seed mediated growth method to have similar dimension to wild type TMV. Then TMV-CPs were randomly coated on the GNRs by using triblockcopolymer (Pluronic F127) as a binder.

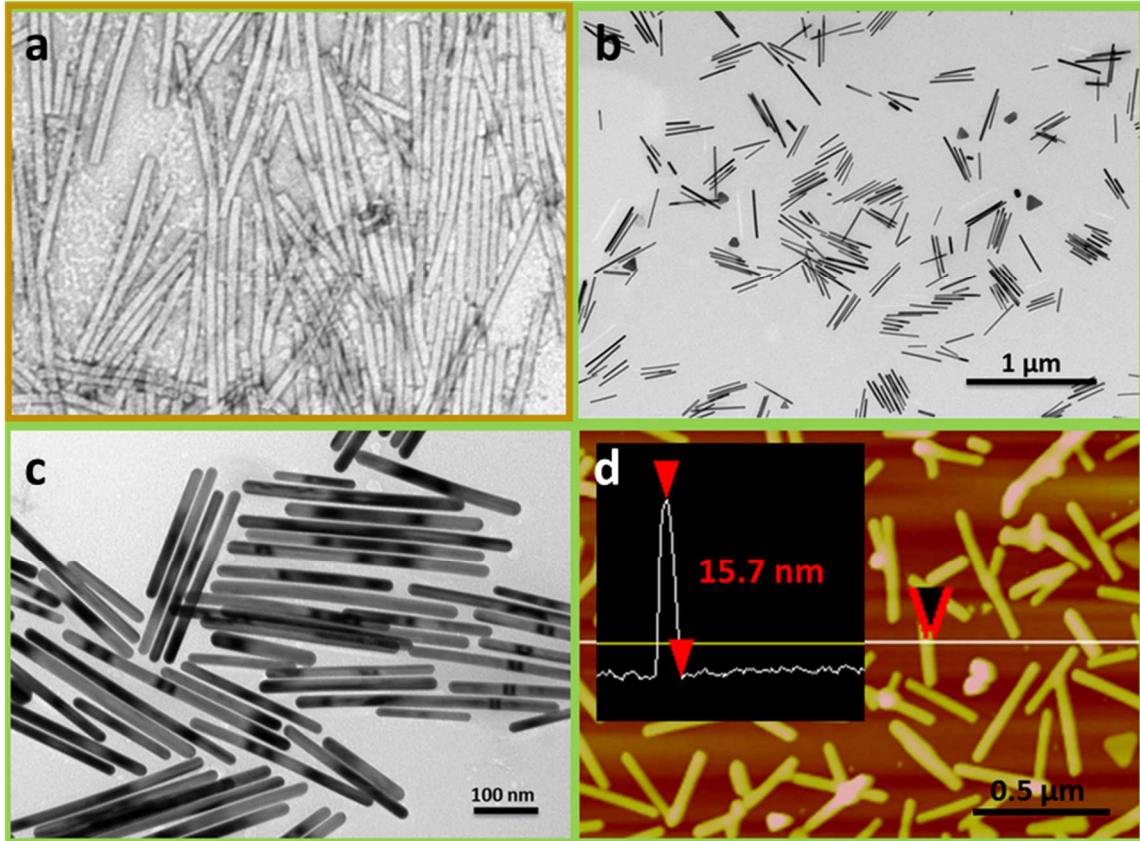


Figure 3.2 CTAB-GNRs characterization. (a-c) TEM image of (a) wild type TMV (b-c) CTAB-GNRs (d) height profile AFM image of CTAB-GNRs shows diameter measurement of the gold nanorod

LbL assembly of polyelectrolyte pair has been reported to reduce toxicity of CTAB molecule.[29] Accordingly, we covered CTAB with polyacrylic acid (PAA) and polyallylamine hydrochloride (PAH) using LbL method. Since PAH contains amine functional groups that can be protonated and display positive charges, it can interact with TMV-CP as well. The LbL coated GNRs were obtained and visualized by TEM as shown in Figure 3.3. However, aggregation of nanorod particles was observed after TMV-CP was introduced to the polymers coated GNRs. Because TMV-CP needs to be stored in high pH buffer to prevent reassembly of the coat protein, the aggregation of nanorod is attributed to the neutralization of polymer coated GNRs that deprotonates the amine functional group of PAH. In order to avoid the aggregation of nanorod, we sought for other coating strategies, which did not base on electrostatic interaction. Pluronic F127 triblockcopolymer has affinity to both CTAB-GNRs and TMV, therefore it can act as a linker in the assembly.[30, 31] The hydrophobic core of the polymer interacts with long alkyl chain of CTAB while two hydrophilic sides of Pluronic F127 are believed to form H-bond with TMV-CP.[32] The assembled structures (TMV-GNRs) were verified with TEM and zeta potential measured by dynamic light scattering (DLS) as shown in Figure 3.4. After TMV-CP had been assembled on the polymer coated GNRs, TEM image clearly shown darker and thicker stained rougher surface on rod particles which indicated a successful protein coating. The nanorod shape was still maintained after (Figure 3.5).

Another evidence of the formation of the hybridized viral-gold nanoparticle assembly is the change of the surface charge. CTAB-GNRs have positively charged

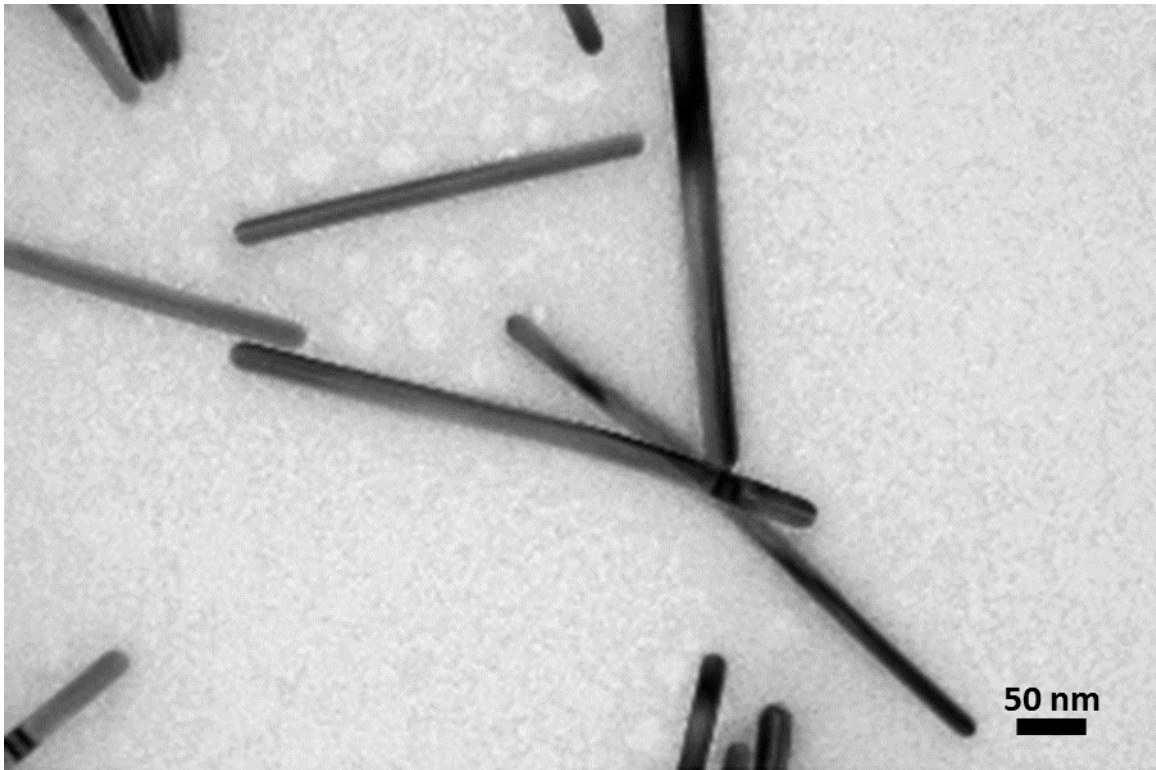


Figure 3.3 TEM image shows layer by layer coating of CTAB-GNRs with PAA and PAH. The hazy area around the surface of nanorod particles shows layers of polymers coating

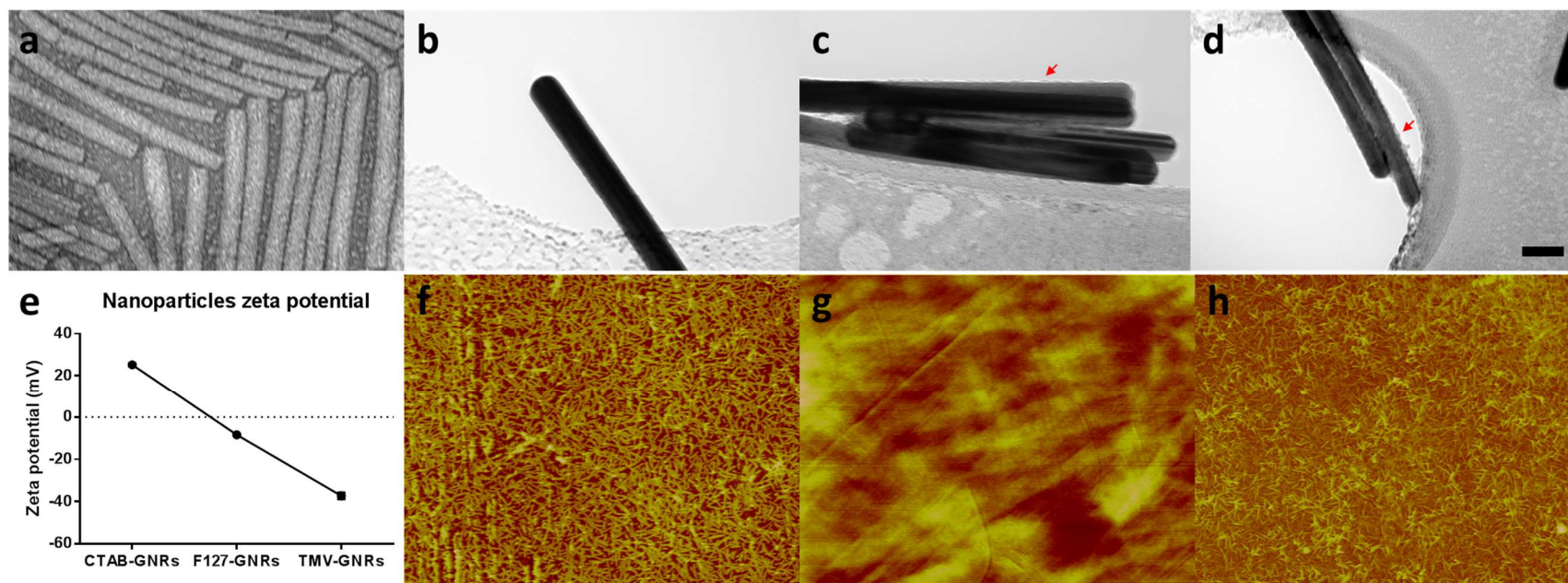


Figure 3.4 Characterization of nanoparticles coated substrates for stem cell cultures. TEM images of (a) TMV, (b) CTAB capped gold nanorods (CTAB-GNRs), (c) coated structure resulting from mixing 10 mg/mL Pluronic F127 with CTAB-GNRs (F127-GNRs), the arrow points at triblockcopolymer light stained on the nanorod surface, and (d) TMV coat protein coated gold nanorods (TMV-GNRs), the arrow designates TMV coat protein appearance on the nanorod structure. (e) Changes of zeta potentials during TMV-GNRs assemble process. CTAB-GNRs have positively charged surface from quaternary amine of CTAB, which reduced once CTAB is covered with neutral triblockcopolymer Pluronic F127. After TMV-CP is coated on the outermost layer of the nanoparticle, surface charge becomes negative as of TMV-CP. (f-h) AFM height image ( $10 \times 10 \mu\text{m}$ ) of TMV (f), TMV-CP (g), and TMV-GNRs (h), it can be noticed that the nanoparticles are mostly intact and laid flat on the surface.

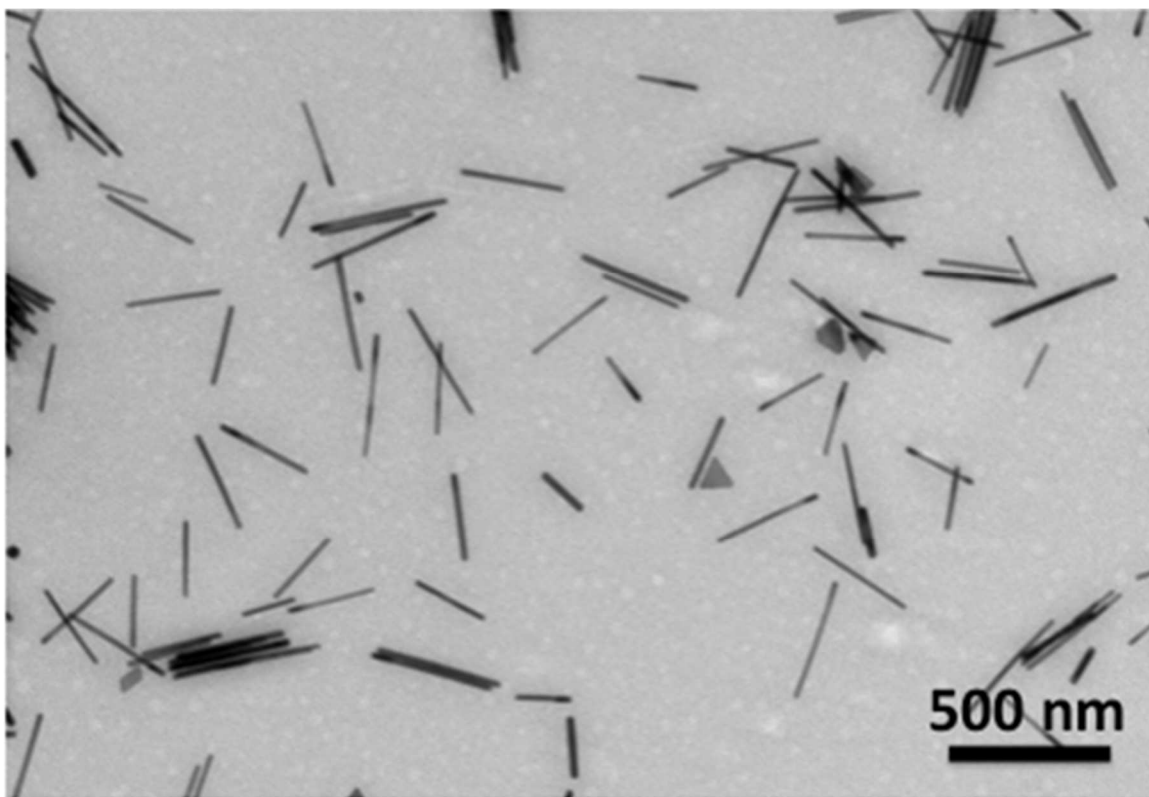


Figure 3.5 TEM image shows intact nanorod structure of TMV-GNRs upon surface coating

surface from quaternary amine of the surfactant. The positive charge is reduced once CTAB is covered with neutral triblockcopolymer, Pluronic F127. After TMV-CP is coated on the outermost layer of the nanoparticle, surface charge becomes negative as of TMV-CP. Since all the nanoparticles display negatively charged surface at neutral pH, these particles are held stably on PDL coated substrate via electrostatic interaction as shown by AFM. AFM images revealed that coating of the three nanoparticles on PDL substrates achieved almost fully coverage and nanoparticles are mostly intact and laid flat on the surface after incubation with cell culture media for 24 h.

### ***3.2.2 Effect of nanotopographical cues on osteogenesis of BMSCs***

BMSCs were cultured on these substrates in serum containing DMEM media for 24 h then osteoinduction factors (dexamethasone, ascorbic acid, and  $\beta$ -glycerophosphate) were supplemented to induce cell differentiation. For the characterization of the cells cultured on the various substrates, we probed for key osteogenic markers (BMP2, alkaline phosphatase activity and calcium sequestration). Six hours after osteoinduction BMP2 mRNA level was found to dramatically upregulate only in cells on TMV substrate (Figure 3.6a). Furthermore, 7 day afterward these cells aggregate and form cell nodules, which are positively stained by Alizarin S Red, a typical cytochemical stain for calcium in cells undergoing osteogenesis (Figure 3.6c, d). We also found at least 2-fold higher activity of alkaline phosphatase enzyme in BMSCs on TMV substrates compared to cells on other substrates (Figure 3.6b). These results highlight that nanotopographical cues provided by highly ordered arrangement of virus coat protein has dominant effect on BMSCs differentiation. Moreover, this discovery corresponds well with osteogenic

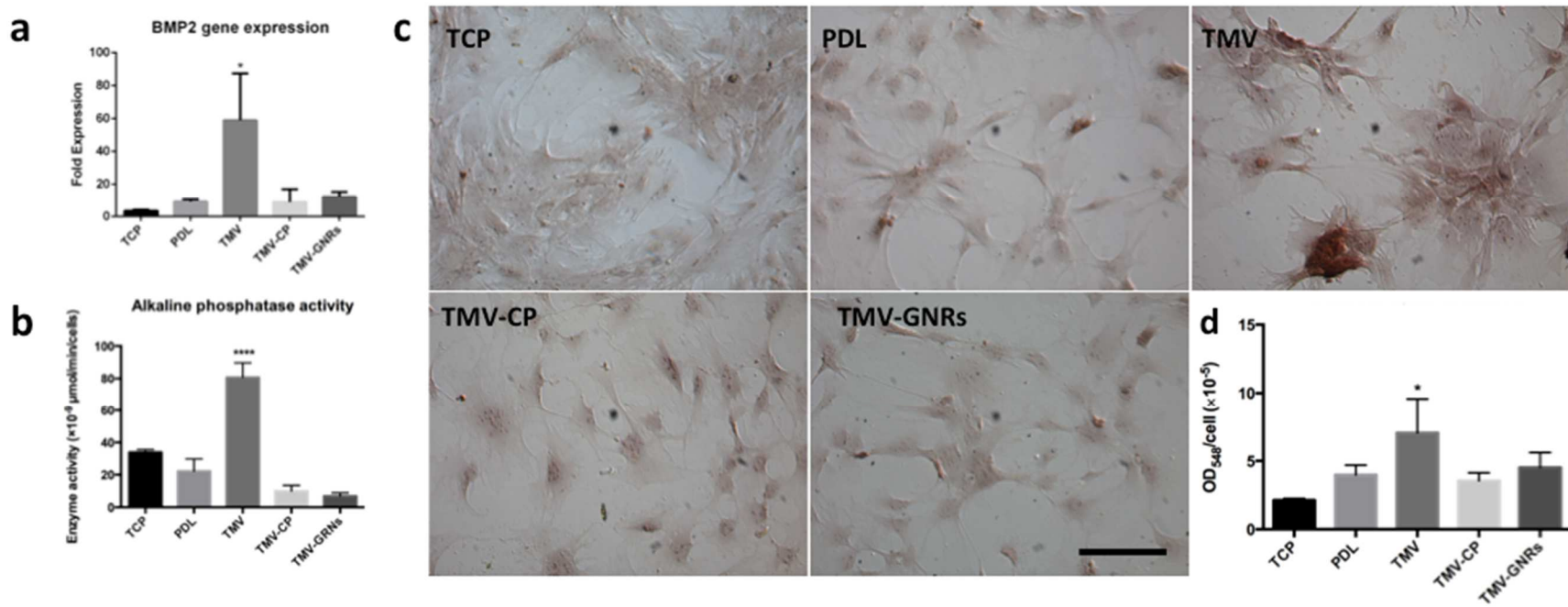


Figure 3.6 Osteogenesis of mesenchymal stem cells demonstrated by (a) At 6 hours after osteoinduction, only the cells on TMV substrate showed BMP2 gene upregulation. (b) Similarly, at day 7 after osteoinduction cells on TMV substrate have significantly higher alkaline phosphatase activity compare to TCP and PDL control. (c) The cells on TMV substrates stained positive for calcium deposition by Alizarin S Red staining and have (d) higher calcium mineralization, which quantified from solubilized dye by 0.1 N NaOH solution. The data were expressed as mean  $\pm$  s.d. ( $n = 3$ , \*  $p \leq 0.05$ , \*\*\*\*  $p \leq 0.0001$  based on ANOVA)

mediation of carbon nanotubes (CNTs), another nanoparticle that presents an arranged surface.[33] Baik *et al.* observed that CNT when coated on 2D glass substrates could mediate osteogenesis of human MSCs without osteoinduction media.

### 3.3 CONCLUSIONS

The highly ordered arrangement of virus coat proteins on viral particles has been well documented to recruit different cellular responses especially immune responses.[9, 10] The discovered osteogenic mediation properties of virus coated substrate may also base on this concept. Therefore, we prepared hybrid viral gold nanorods (TMV-GNRs) by Pluronic F127 assisted coating of TMV-CP on CTAB-GNRs and used it to prove our hypothesis. We observed stimulated stem cell differentiation on only TMV substrate but not TMV-CP or TMV-GNRs substrates. This suggests that nanotopography provided by highly ordered arrangement of TMV-CP on the native virus particles could promote the cell differentiation.

Although this study reveals that the arrangement of coat protein associates with the ability of virus substrates to stimulate osteogenesis of MSCs, additional studies involving other aligned nanoparticle structures will be necessary to eliminate other possible factors involved in virus substrates mediated osteogenesis.

### 3.4 EXPERIMENTAL SECTION

***Virus purification from infected leaves:*** Infected leaves were blended with 3 volumes of 0.1 M potassium phosphate buffer pH 7.0 and 0.1%  $\beta$ -mercaptoethanol. The mixture was filtered, and the filtrate was subjected to centrifugation to remove bulk plant

material. The supernatant was collected and clarified by adding an equal volume of  $\text{CHCl}_3$ /1-butanol (v/v = 1:1). The aqueous layer was then collected followed by precipitation of virus with 4% PEG 8K and 0.2 M NaCl. The pellet was centrifuged and resuspended in buffer before it was subjected to low speed centrifuge to remove PEG. The virus in supernatant was final pelleted by ultracentrifugation and resuspended in buffer.

***TMV coat protein (TMV-CP) purification:*** Two volumes of concentrated acetic acid were added to 1 volume of 10-30 mg/mL of TMV in 10 mM potassium phosphate buffer pH 7.4. The mixture was incubated on ice for 15 minutes and RNA was pelleted down at full speed at 4 °C for 10 min. The supernatant was further desalted into 1% acetic acid by FPLC using Sephadex G-25 (Sigma Aldrich) column. Then 1 mL aliquots of 100 mM Kphos pH 7.4 were added to the collected TMV CP fraction until the solution became cloudy. The solution was incubated at 4 °C for 1-2 hours and then TMV CP precipitate was pelleted down at 15,000 g at 4 °C for 10 minutes. TMV CP pellet was resuspended in 0.1 M potassium hydroxide with 10 mM dithiothreitol and dialyzed against 100 mM Tris-HCl pH 8.0 or water at 4 °C overnight.

***CTAB capped gold nanorods (CTAB-GNRs) synthesis:*** First, we prepared Au seeds. In a typical procedure, 0.250 mL of an aqueous 0.01 M solution of  $\text{HAuCl}_4 \cdot 3\text{H}_2\text{O}$  was added to 9.75 mL of a 0.10 M CTAB solution in a test tube (glass or plastic). The solutions were gently mixed by the inversion. The solution appeared bright brown-yellow in color. Then, 0.600 mL of an aqueous 0.01 M ice-cold  $\text{NaBH}_4$  solution was added all at once, followed by rapid inversion mixing for 2 min. Care should be taken to allow the escape of the evolved gas during mixing. The solution developed a pale brown-yellow

color. Then the test tube was kept in a water bath maintained at 25 °C for future use. This seed solution was used 5 h after its preparation. Second, we prepared Au Nanorods from Au seeds. A three-step seeding method was used. Three test tubes (labeled A, B, and C), each containing 9 mL growth solution, consisting of  $2.5 \times 10^{-4}$  M HAuCl<sub>4</sub> and 0.1 M CTAB, were mixed with 0.05 mL of 0.1 M ascorbic acid. Next, 1.0 mL of the Au seed solution was mixed with sample A. After 15 s, 1.0 mL was drawn from solution A and added to solution B, followed by thorough mixing. After 30 s, 1 mL of B was mixed with C. Then solution C was left undisturbed at 25 °C overnight.

***TMV coat protein coated gold nanoparticle (TMV-GNRs) assembly:*** aqueous solution of CTAB-GNRs was incubated with aqueous solution of 10 mg/mL Pluronic F127 1:1 ratio. After briefly mix the solution, the mixture was left undisturbed at room temperature. After 2 hours, the mixture supernatant was removed after centrifuge at 7000 rpm for 6 min. The polymer coated GNRs (F127-GNRs) was then resuspended in 10 mM potassium phosphate buffer pH 7.4. TMV-CP in 10 mM potassium phosphate buffer pH 7.4 was slowly added to a continuously stirred solution of F127-GNRs. The mixture was stirred at room temperature for 2 h. After 2 hours, the mixture supernatant was removed after centrifuge at 7000 rpm for 6 min. The TMV-CP coated GNRs (TMV-GNRs) was then resuspended in 10 mM potassium phosphate buffer pH 7.4

***Nanoparticles characterization:*** All nanoparticles were stained with 2% uranyl acetate and visualized by Philips CM-12 transmission electron microscope (TEM) at 80 kEV.  $\xi$ -potential measurements were performed on a Malvern Zetasizer ZS instrument.

***Fabrication of the scaffolds:*** 1 mg/mL TMV, TMV-CP, TMV-GNRs solutions were dropped on 18 mm. glass cover slip coated with PDL using protocol suggested by

Corning® in 12-well tissue culture plate. The nanoparticle solutions were incubated with the PDL coated cover slip under sterile cells culture hood for overnight. Then the coated cover slips were rinsed briefly with 18.2 mΩ water before used for BMSCs culture.

***Surface characterization of virus based scaffolds by AFM:*** The surface morphology of nanoparticle coated scaffolds was observed by AFM (Nanoscope IIIA MultiMode AFM (Veeco)). The bottoms of each 12 well plate were cut out after virus coating and rinsed with 18.2 mΩ water then dried with a stream of nitrogen gas before mounted onto AFM sample holder for imaging in the tapping mode.

***BMSC isolation and expansion:*** primary BMSCs were isolated from the bone marrow of young adult 80 g male Wister rats (Harlan Sprague-Dawley Inc.). The procedures were performed in accordance with the guideline for animal experimentation by the Institutional Animal Care and Use committee, School of Medicine, University of South Carolina. Cells were maintained in primary media (Dullbecco's Modified Eagle's Medium (DMEM) supplemented with 10% fetal bovine serum (FBS), penicillin (100 U/mL), streptomycin (100 µg/mL), and amphotericin B (250 ng/mL)), kept at 37 °C in a CO<sub>2</sub> incubator with 95% air/5% CO<sub>2</sub> and passaged no more than seven times after isolation. To induce osteogenesis, primary media were replaced with osteogenic media consisting of DMEM supplemented with 10% FBS, penicillin (100 U/mL), streptomycin (100 µg/mL), and amphotericin B (250 ng/mL), 10 mM sodium β-glycerolphosphate, L-ascorbic acid 2-phosphate (50 µg/mL), and 10<sup>-8</sup> M dexamethasone. Media were replenished every 3-4 days.

***Quantitative real-time RT-PCR analysis (RT-qPCR):*** PDL and virus coated substrates were seeded with  $4.0 \times 10^4$  cells per well in primary media and allowed to

attach overnight. The unseeded cells were used as a control to normalize the change in gene expression. The media were replaced to osteogenic media and cultured for 6 hours and 7 days. The cell cultures were terminated at these time points and total RNA was subsequently extracted using E.Z.N.A.<sup>®</sup> RNA Isolation Kit, OMEGA. At least three separate experiments were conducted with each type of sample. The purity and quantity of the extracted RNA were analyzed using Thermo Scientific Nanodrop 2000c spectrophotometer and was reverse transcribed by qScript<sup>™</sup> cDNA Supermix (Quanta Biosciences). RT-qPCR (iQ5 real-time PCR detection system Bio-Rad Laboratories) was done by the method described as: 60 cycles of PCR (95 °C for 20 s, 58 °C for 15 s, and 72 °C for 15 s), after initial denaturation step of 5 min at 95 °C, by using 12.5 µL of iQ5 SYBR Green I Supermix, 2 pmol/µL of each forward and reverse primers and 0.5 µL cDNA templates in a final reaction volume of 25 µL. Glyceraldehyde 3-phosphate dehydrogenase (GAPDH) was used as the house keeping gene. Data collection was enabled at 72 °C in each cycle and CT (threshold cycle) values were calculated using the iQ5 optical system software version 2.1. The expression levels of differentiated genes and undifferentiated genes were calculated using Pfaffl's method (M. W. Pfaffl, G. W. Horgan and L. Dempfle, Relative expression software tool) for group-wise comparison and statistical analysis of relative expression results in real-time PCR, using GAPDH as the reference gene. Quantification of gene expression was based on the CT value of each sample which was calculated as the average of at least two replicate measurements for each sample analyzed. "Pair Wise Fixed Reallocation Randomization Test" was performed on each sample and a value of  $p < 0.05$  was regarded as significant. The

primers used for RT-qPCR are shown in Table 3.1 Three independent experiments were performed and analyzed for each gene expression study.

***Alkaline phosphatase (ALP) activity:*** After 7 days of induction in the osteogenic media, the BMSCs seeded on PDL and virus coated substrates were determined number of cells on each substrate by CellTiter Blue<sup>®</sup> assay. Then the cells were fixed with 4% paraformaldehyde for 15 min at room temperature prior to analyze ALP activity by incubating the briefly fixed cells with 1-Step p-nitrophenylphosphate solution (Thermo Scientific) for 15 min at room temperature. The solution was transferred to a new microfuge tube contained 250  $\mu$ L of 2 N NaOH and the absorbance at 405 nm was measured. The measure ALP activity from each sample was normalized to the corresponding cell number. Three independent experiments were performed and analyzed for ALP activity.

***Alizarin red staining and quantification:*** Calcium deposition on each substrate was visualized and quantified to confirm and compare osteogenic differentiation by Alizarin red staining. Fixed cell on day 7 were stained with 0.1% Alizarin red solution (Sigma-Aldrich) pH 4.1-4.5 for 30 min in the dark. The samples were washed with water (18.2 M $\Omega$ ) prior to imaging. To quantify the amount of dye on each substrate, 300  $\mu$ L of 0.1 N NaOH was added to each sample to extract the dye from the sample. The extracted dye solution was measured the absorbance at 548 nm wavelength. The measure absorbance from each sample was normalized to the corresponding cell number from CellTiter Blue<sup>®</sup> assay. Three independent experiments were performed and analyzed for Alizarin red staining and quantification.

Table 3.1 Primers used for RT-qPCR to measure gene expression levels. BGLAP: bone-gamma-carboxyglutamate protein; BMP2: bone morphogenetic protein 2

Gene	Sequence (5'-3')
BGLAP	Forward: AAAGCCCAGCGACTCT
	Reverse: CTAAACGGTGGTGCCATAGAT
BMP2	Forward: ACCAACCATGGGTTTGTGGTGGAAGT
	Reverse: TCCGCTGTTTGTGTTTGGCTTGACG

***Immunofluorescence assays and image analysis:*** For immunofluorescence assays and image analysis, the substrates were seeded with  $4.0 \times 10^5$  cells per sample. The cultures were terminated at 8 hours after osteoinduction for BMP2 immunostaining analysis. After termination, cells were fixed in 4% paraformaldehyde at room temperature for 30 min. Each of the samples was then permeabilized for 20 min by 0.1% Triton-X 100 for 15 min and blocked in 1.5% bovine serum albumin (BSA, Sigma Aldrich) in PBS for 1 hour at room temperature. After the blocking, the cells were incubated overnight with mouse monoclonal antibody targeting BMP2 (R&D Systems) at 1:100 dilution in blocking buffer (Santa Cruz Biotechnology). After overnight incubation, secondary goat anti-mouse antibody conjugated with fluorescein (Chemicon) was used at 1:400 dilution for 2 hours at room temperature. Rhodamin phalloidin (1:100 in PBS) was used to stain filamentous actin. Nuclei were stained with DAPI (4,6-diamidino-2-phenylindole, 100 ng/mL). The sample were then mounted and sealed with clear nail polish before imaging. Images of the stained substrates were taken on an Olympus IX81 fluorescent microscope.

### 3.5 REFERENCES

- [1] Lee LA, Nguyen QL, Wu L, Horvath G, Nelson RS, Wang Q. Mutant plant viruses with cell binding motifs provide differential adhesion strengths and morphologies. *Biomacromolecules*. 2012;13:422-31.
- [2] Pokorski JK, Steinmetz NF. The art of engineering viral nanoparticles. *Mol Pharm*. 2011;8:29-43.

- [3] Chung W-J, Merzlyak A, Lee S-W. Fabrication of engineered M13 bacteriophages into liquid crystalline films and fibers for directional growth and encapsulation of fibroblasts. *Soft Matter*. 2010;6:4454-9.
- [4] Wang J, Wang L, Li X, Mao C. Virus activated artificial ECM induces the osteoblastic differentiation of mesenchymal stem cells without osteogenic supplements. *Sci Rep*. 2013;3:1242.
- [5] Merzlyak A, Indrakanti S, Lee SW. Genetically engineered nanofiber-like viruses for tissue regenerating materials. *Nano Lett*. 2009;9:846-52.
- [6] Zhu H, Cao B, Zhen Z, Laxmi AA, Li D, Liu S, et al. Controlled growth and differentiation of MSCs on grooved films assembled from monodisperse biological nanofibers with genetically tunable surface chemistries. *Biomaterials*. 2011;32:4744-52.
- [7] Wang Q, Lin T, Tang L, Johnson JE, Finn MG. Icosahedral Virus Particles as Addressable Nanoscale Building Blocks. *Angewandte Chemie International Edition*. 2002;41:459-62.
- [8] Destito G, Schneemann A, Manchester M. Biomedical Nanotechnology Using Virus-Based Nanoparticles. In: Manchester M, Steinmetz N, editors. *Viruses and Nanotechnology*: Springer Berlin Heidelberg; 2009. p. 95-122.
- [9] Nemerow GR, Pache L, Reddy V, Stewart PL. Insights into adenovirus host cell interactions from structural studies. *Virology*. 2009;384:380-8.
- [10] Dicara D, Burman A, Clark S, Berryman S, Howard MJ, Hart IR, et al. Foot-and-mouth disease virus forms a highly stable, EDTA-resistant complex with its principal receptor, integrin  $\alpha 5 \beta 1$ : implications for infectiousness. *J Virol*. 2008;82:1537-46.

- [11] Kiessling LL, Gestwicki JE, Strong LE. Synthetic multivalent ligands as probes of signal transduction. *Angew Chem Int Ed Engl.* 2006;45:2348-68.
- [12] Petrie TA, Raynor JE, Dumbauld DW, Lee TT, Jagtap S, Templeman KL, et al. Multivalent integrin-specific ligands enhance tissue healing and biomaterial integration. *Sci Transl Med.* 2010;2:45ra60.
- [13] Hynes RO. The extracellular matrix: not just pretty fibrils. *Science.* 2009;326:1216-9.
- [14] Danen EH, Yamada KM. Fibronectin, integrins, and growth control. *J Cell Physiol.* 2001;189:1-13.
- [15] Kaur G, Valarmathi MT, Potts JD, Wang Q. The promotion of osteoblastic differentiation of rat bone marrow stromal cells by a polyvalent plant mosaic virus. *Biomaterials.* 2008;29:4074-81.
- [16] Kaur G, Valarmathi MT, Potts JD, Jabbari E, Sabo-Attwood T, Wang Q. Regulation of osteogenic differentiation of rat bone marrow stromal cells on 2D nanorod substrates. *Biomaterials.* 2010;31:1732-41.
- [17] Kaur G, Wang C, Sun J, Wang Q. The synergistic effects of multivalent ligand display and nanotopography on osteogenic differentiation of rat bone marrow stem cells. *Biomaterials.* 2010;31:5813-24.
- [18] Sitasuwan P, Andrew Lee L, Bo P, Davis EN, Lin Y, Wang Q. A plant virus substrate induces early upregulation of BMP2 for rapid bone formation. *Integr Biol (Camb).* 2012;4:651-60.

- [19] Sitasuwan P, Lee LA, Li K, Nguyen HG, Wang Q. RGD-conjugated rod-like viral nanoparticles on 2D scaffold improve bone differentiation of mesenchymal stem cells. *Front Chem.* 2014;2:31.
- [20] Metavarayuth K, Sitasuwan P, Luckanagul JA, Feng S, Wang Q. Virus Nanoparticles Mediated Osteogenic Differentiation of Bone Derived Mesenchymal Stem Cells. *Advanced Science.* 2015;2:150026-34.
- [21] Yim EK, Leong KW. Significance of synthetic nanostructures in dictating cellular response. *Nanomedicine.* 2005;1:10-21.
- [22] Flemming RG, Murphy CJ, Abrams GA, Goodman SL, Nealey PF. Effects of synthetic micro- and nano-structured surfaces on cell behavior. *Biomaterials.* 1999;20:573-88.
- [23] Nalwa HS. *Handbook of Nanostructured Biomaterials and Their Applications in Nanobiotechnology: Biomaterials. 1: American Scientific Publishers; 2005.*
- [24] McKay WF, Peckham SM, Badura JM. A comprehensive clinical review of recombinant human bone morphogenetic protein-2 (INFUSE Bone Graft). *Int Orthop.* 2007;31:729-34.
- [25] Carragee EJ, Hurwitz EL, Weiner BK. A critical review of recombinant human bone morphogenetic protein-2 trials in spinal surgery: emerging safety concerns and lessons learned. *Spine J.* 2011;11:471-91.
- [26] Fraenkel-Conrat H. Degradation of tobacco mosaic virus with acetic acid. *Virology.* 1957;4:1-4.
- [27] Lees WJ, Spaltenstein A, Kingery-Wood JE, Whitesides GM. Polyacrylamides bearing pendant alpha-sialoside groups strongly inhibit agglutination of erythrocytes by

influenza A virus: multivalency and steric stabilization of particulate biological systems.

J Med Chem. 1994;37:3419-33.

[28] Mammen M, Dahmann G, Whitesides GM. Effective inhibitors of hemagglutination by influenza virus synthesized from polymers having active ester groups. Insight into mechanism of inhibition. J Med Chem. 1995;38:4179-90.

[29] Gole A, Murphy CJ. Polyelectrolyte-Coated Gold Nanorods: Synthesis, Characterization and Immobilization. Chemistry of Materials. 2005;17:1325-30.

[30] Busbee BD, Obare SO, Murphy CJ. An Improved Synthesis of High-Aspect-Ratio Gold Nanorods. Advanced Materials. 2003;15:414-6.

[31] Goh D, Gong T, Dinish US, Maiti KK, Fu CY, Yong K-T, et al. Pluronic Triblock Copolymer Encapsulated Gold Nanorods as Biocompatible Localized Plasmon Resonance-Enhanced Scattering Probes for Dark-Field Imaging of Cancer Cells. Plasmonics. 2012;7:595-601.

[32] Liu Z, Gu J, Wu M, Jiang S, Wu D, Wang Q, et al. Nonionic block copolymers assemble on the surface of protein bionanoparticle. Langmuir. 2012;28:11957-61.

[33] Baik KY, Park SY, Heo K, Lee KB, Hong S. Carbon nanotube monolayer cues for osteogenesis of mesenchymal stem cells. Small. 2011;7:741-5.

## CHAPTER 4

### POSSIBLE SIGNALING PATHWAY INVOLVED IN VIRUS SUBSTRATE-MEDIATED BONE DIFFERENTIATION OF MESENCHYMAL STEM CELL

#### 4.1 INTRODUCTION

Stem cells can sense and response to surrounding stimuli, including both soluble and insoluble factors. The mechanism stem cells use to probe different nanoscale cues on biomaterials has been extensively studied for tissue engineering and regenerative medicine applications.[1-4] Several studies have demonstrated that stem cell differentiation can be dictated at the nanometer level.[5-14] Bone marrow derived mesenchymal stem cells (BMSCs) are from the non-hematopoietic sub-population of bone marrow stroma,[15-17] which have the ability to self-renew and differentiate to various lineages, such as adipocytes, osteocytes, chondrocytes, hepatocytes, neurons, muscle cells, and epithelial cells.[17-22] The pluripotent potential of BMSCs, ease of isolation, rapid expansion,[23] and less controversial use than embryonic stem cells make this cell type an ideal source of adult stem cells to study material-mediated differentiation.

Plant viruses have recently been utilized as multifacet nanosized building blocks for directing cell growth and differentiation.[24-28] Plant viruses can be constantly isolated in high purity with batch to batch consistencies at low costs. The chemical and

genetic modifications of virus surfaces to incorporate new functional groups has been extensively studied, which provides a library of viruses with different surface properties.[24-26, 29-31] In addition, the symmetrical arrangement of the viral proteins makes it an attractive scaffold for displaying identical copies of the functional groups for applications in electronics, catalysis, drug/gene delivery, imaging, and immunotherapy.

BMP2 is a member of bone morphogenetic protein subgroup within the transforming growth factor  $\beta$  (TGF- $\beta$ ) super family. Among the bone morphogenetic proteins (BMPs), BMP2 has been extensively documented to play major role in osteoblast differentiation and bone formation during embryonic skeletal development and postnatal bone remodeling.[32-36] Genetic transfection to overexpress BMP2 has proven to increase bone regeneration,[37-41], however the regulation of endogenous BMP2 expression is still unclear. Recent evidences have reported that external mechanical stress can induce the upregulation of endogenous BMP2 expression, leading to a long term osteogenesis [42-44] Kearney *et al.* suggested that stress and strain induced osteogenesis through 46 mitogen-activated protein kinases (MAPKs), such as extracellular regulated kinase (ERK), phosphatidylinositol 3-kinase (PI3K), and p38 MAPK.[43] In this chapter, we attempted to verify whether BMP2 is a specific mediator of virus substrates stimulate osteogenesis of MSCs or not. In addition, we further investigated the signaling cascade associate with BMP2 for a better understanding of the discovery. Noggin is a BMP2 inhibitor that competitively binds to BMP2 receptor.[45] Therefore investigating osteogenic differentiation of MSCs treated with Noggin may confirm the significance of BMP2 in the virus substrates enhance osteogenesis.

Besides chemical cues, bone mass and strength can be regulated by mechanical cues as well.[46, 47] Frost *et al.* hypothesized in bone (re)modelling that the biological response of cell to mechanical cues is through a complex mechanotransduction process in order to accommodate the new loading environment within the limits of normal daily stress stimuli.[48] Indeed, many studies have shown that bone cells (osteoblasts and osteocytes) are sensitive to physical stimuli,[49, 50] and that this sensitivity seems to be greatly relied on the differentiation state.[51, 52] Mechanical forces have also been shown *in vivo* to play an important role in bone formation by inducing osteoprogenitor cells of the marrow stroma to differentiate into osteoblasts.[53, 54] Accordingly, there is a growing interest in manipulating mechanical stress to regulate the differentiation of bone progenitor cells. With mechanical stimulation, the time in culture required to predifferentiate cells may be greatly reduced.

Cells sense the changes in their environment through integrins, a group of transmembrane proteins that bind to ECM proteins including collagen, fibronectin, laminin, and vitronectin. They confer information about the cellular microenvironment and initiate signaling cascades such as the MAPK/ERK pathway. In addition, a member of the larger Rho-family of GTPases, RhoA, has been widely implicated in integrin-mediated signaling [55-57] to control cell migration.[58-60] RhoA plays a critical role in the assembly of actin stress fibers in response to various stimuli,[61-63] mediated in part by one of its downstream effectors, the Rho-associated protein kinase, or ROCK. RhoA has also been demonstrated to associate with the cellular response to mechanical stress and the maintenance of tensional homeostasis.[64-69] Other studies have shown that RhoA regulates the switch between adipogenesis and myogenesis[70] and that osteogenic

commitment also relies on RhoA-ROCK signaling.[71] In this chapter, we attempted to examine the engagement of RhoA/ROCK pathway in our phenomenon by exploring the effect of a specific ROCK inhibitor, Y27632 on osteogenesis of MSCs cultured on virus substrates. Y27632 inhibits ROCK by binding to the kinase catalytic site, thus interferes cell adhesion and migration. Attenuation of virus substrates osteogenic mediation ability by Y27632 would insist the contribution of RhoA/ROCK pathway in virus substrates stimulated osteogenesis of MSCs.

## 4.2 RESULTS AND DISCUSSION

### ***4.2.1 BMP2 inhibitor attenuates virus scaffold mediated osteogenesis of mesenchymal stem cells***

To verify BMP2 as the key modulator of this phenomenon, BMP2 inhibitor, Noggin, was added into cell culture media to interfere the binding of BMP2 with its receptor. This would result in diminished cell osteogenic differentiation. As expected, BMP2 protein level gradually decreased with the increasing concentration of noggin to treated cells on TMV substrate as shown by immunohistochemical staining of BMP2 (Figure 4.1a). Furthermore, the differentiation of BMSCs on TMV substrate correlates to Noggin treatment in a concentration dependent manner, as probed by decreasing alkaline phosphatase activity and calcium mineralization of cells on TMV substrates compared to no change in cells on PDL substrates (Figure 4.1c, d). Surprisingly, Cells slightly increase BMP2 gene expression with the addition of noggin at different concentration. This might due to the negative feedback from the reduction of free BMP2 protein availability for BMP2 receptor (Figure 4.1b).

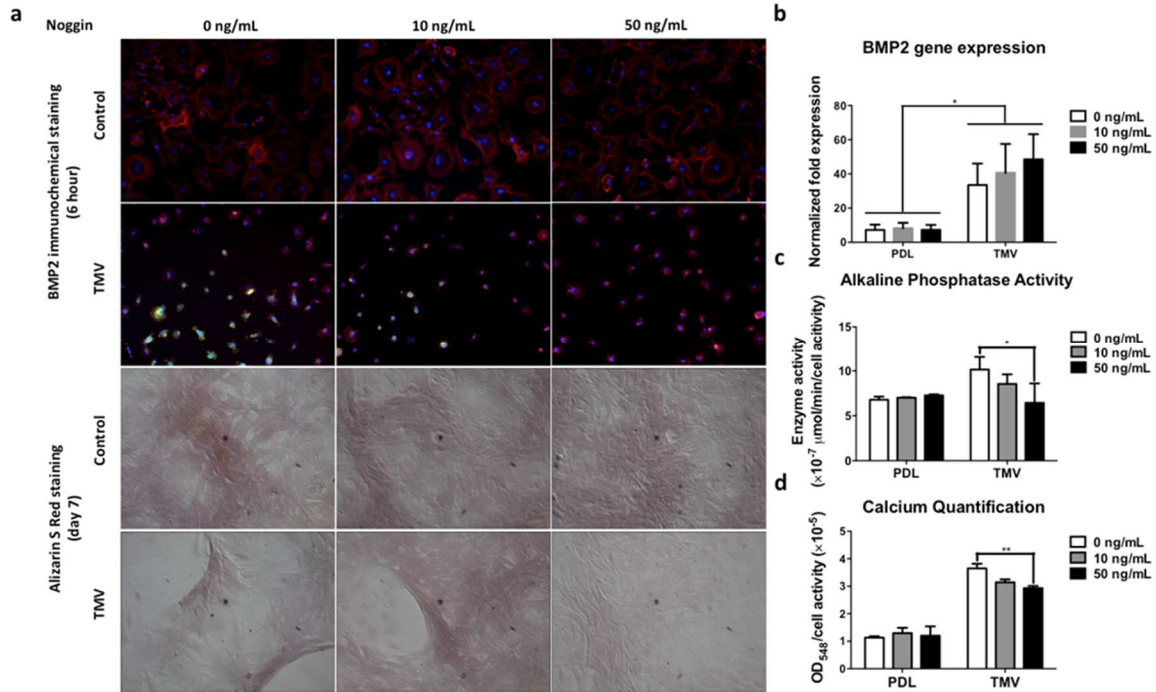


Figure 4.1 BMP2 inhibitor (Noggin) inhibits TMV induced osteogenesis of stem cells. (a) Immunofluorescence images of cells on PDL and TMV substrates incubated with Noggin at different concentration ( 0 ng/mL – 50 ng/mL) for 6 h (top panel). Color representation: nucleus (blue), actin (red), and BMP2 (green). Cells on TMV substrate have higher BMP2 expression compared to cells on PDL substrates and BMP2 protein level decreases at higher Noggin concentration. The bottom panel shows calcium staining of each sample at day 7. Treatment of Noggin reduces calcium mineralization in cells culture on TMV substrates. (b) The expression of BMP2 in cells on PDL and TMV substrates treated with Noggin at different concentration for 6 h. Cells slightly increase BMP2 gene expression when incubated with Noggin. This might due to the negative feedback from the reduction of free BMP2 protein availability for BMP2 receptor. (c) Alkaline phosphatase activity of cells treated with Noggin when cultured on PDL and TMV substrates 7 days after osteoinduction. The enzyme activity reduces as Noggin concentration is increased. (d) Calcium mineralization is also reduced with increasing concentration of Noggin treatment. The data were expressed as mean  $\pm$  s.d. (n = 3, \*  $p \leq 0.05$ , \*\*  $p \leq 0.01$  based on ANOVA)

#### ***4.2.2 ROCK inhibitor and actin depolymerization inducer affect virus substrate mediate osteogenesis of mesenchymal stem cells***

To investigate the involvement of RhoA/ROCK pathway and cytoskeleton tension in virus substrate mediate osteogenesis, we treated BMSC on TMV substrate with ROCK inhibitor, Y27632 and actin polymerization inhibitor, cytochalasin D and studied the osteoblastic differentiation. BMSCs were isolated and cultured as reported in literature. [13] The purity of the stem cells populations has been previously verified with several stem cells markers such as CD73 and CD90. [13] The difference in the expression of BMP2 gene, an early osteogenic marker, [12b] among BMSCs cultured on PDL and TMV substrates with or without Cytochalasin D and Y27632 treatment were recorded at 8 hours after osteoinduction (Figure 4.2a). Moreover, after 7 days of induction, ALP activity and calcium mineralization supported the osteogenic differentiation of cells on TMV substrates. ALP is an early marker of osteogenesis and its activity mediates matrix mineralization.[72] Calcium mineralization was analyzed by Alizarin S Red staining, which was positive as shown by deep red color in big cells nodules on TMV substrate without Y27632 treatment and small nodules when treated with Y27632. BMP2 expression, ALP activity, and calcium mineralization were dramatically declined when cells on TMV substrates were treated with cytochalasin D. This indicates by the intervention of actin polymerization process interfered cell cytoskeleton system therefore obstructed the cell differentiation. Surprisingly, BMP2 gene expression was stabled when Y27632 was administered to the cells while ALP activity and calcium mineralization were reduced. Since Y27632 is a ROCK inhibitor, it is possible that BMP2 is an upstream modulator of RhoA/ROCK

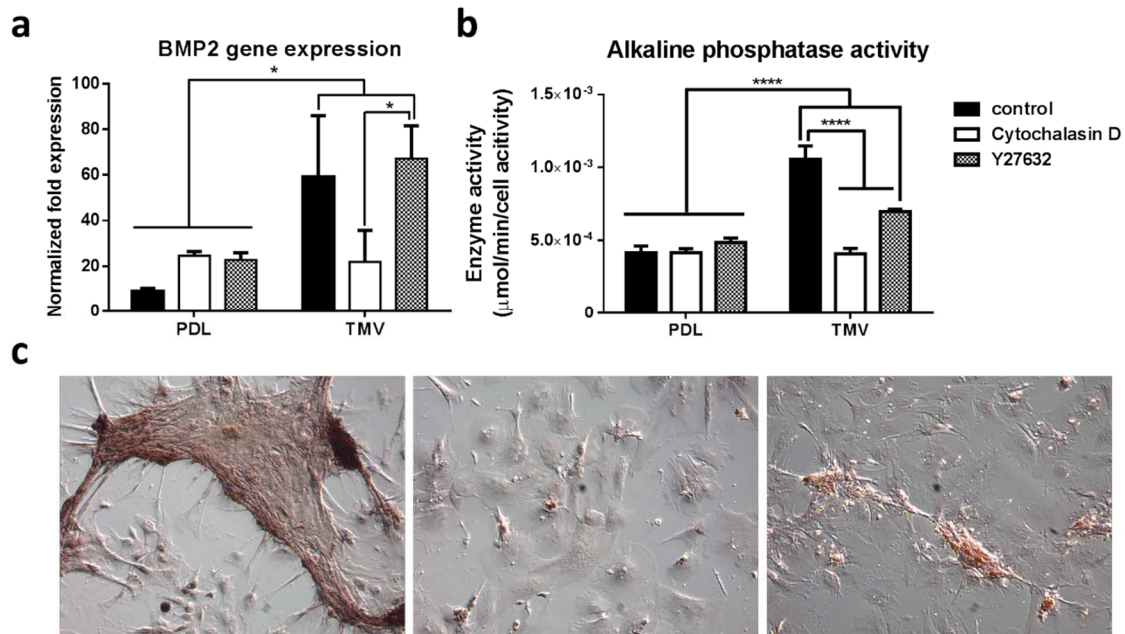


Figure 4.2 RhoA/ROCK pathway involves in TMV substrates mediated osteogenesis of stem cells. (a) The expression of BMP2 in cells on PDL and TMV substrates treated with Cytochalasin D and Y27632 at 8 h after osteoinduction. BMP2 was upregulated in cells on TMV substrate without any inhibitors administration as expected. Cytochalasin D abolished the effect of TMV substrate on osteogenic mediation as shown by comparable level of BMP2 expression in cells treated with the compound on both PDL and TMV substrates. Y27632 did not alter BMP2 mRNA level. This result may show that BMP2 is an upstream signaling molecule of ROCK therefore inhibition of ROCK did not affect BMP2 expression level. (b) Alkaline phosphatase activity of cells treated with Cytochalasin D and Y27632 when cultured on PDL and TMV substrates 7 days after osteoinduction. The enzyme activity decreased when either of the inhibitors was applied. (c) Calcium staining of cells on TMV substrates without inhibitor (left), with Cytochalasin D (middle), and with Y27632 (right) at day 7 after osteoinduction. Cells on TMV substrate without inhibitor exhibited positive stained as shown by deep red color staining of extracellular calcium in cell aggregates and cells also form big nodules, which is one of the characteristics of osteogenic differentiation of MSCs. The absence of cell nodules as well as positive staining for calcium mineralization were noticed when cells were treated with Cytochalasin D. When we treated cells with Y27632, nodule size was reduced and cells were less aggregated compared to non-treated cells. The data were expressed as mean  $\pm$  s.d. (n = 3, \*  $p \leq 0.05$ , \*\*\*\*  $p \leq 0.0001$  based on ANOVA)

pathway therefore its expression level was not disturbed by the application of the inhibitor. Conclusively, inhibition of ROCK was demonstrated to impede the osteogenic mediation property of TMV substrate, which indicates the involvement of RhoA/ROCK pathway in TMV substrate mediates bone formation of MSCs.

#### ***4.2.3 Virus substrates mediated endogenous BMP2 expression enhanced osteogenesis via RhoA/ROCK pathway***

In the previous section, we have confirmed the significant of native BMP2 upregulation in virus substrate mediated osteogenesis of MSCs. While, most of the other studies done on BMP2 are on the inductive effect of recombinants BMP2 and downstream osteogenic and protein expression,[73-79] there were some reports on the overexpression of BMP2 to improve bone healing process.[37-41] Although, little has been published on the native regulation of BMP2, there were recent evidences that showed external mechanical stress could induce the upregulation of endogenous BMP2 expression, leading to long term osteogenesis.[42-44] Liu *et al* suggested that fluid shear stress promotes osteogenic differentiation through two novel signaling pathways besides the classical MAPK/ERK1 pathway.[80] These signaling cascades start at the important mechanoreceptors, integrins, which sense the stimulation from the virus substrate and in turn activate ERK1/2 by activating FAK. The activated ERK1/2 leads to the expression of BMP2 via activating NF-kB, the increased BMP2 results in the activation of BMPs/Smad pathway and finally leads to the expression of Runx2 and other osteospecific genes. Recently, RhoA and ROCK have been stated as key signals during mechanotransduction and differentiation. Results from our study also indicate RhoA/ROCK pathway as the downstream cascade of the centralized BMP2 modulator, which correspond to a study by Wang *et al.*,[81] which

demonstrated that BMP2-induced osteogenesis is regulated by RhoA/ROCK, cell shape, and cytoskeleton tension. In addition, previous PCR array screening for genes involved in the movement of cells confirms the association of cell adhesion and migration processes to the osteogenic differentiation phenomenon.[82] Specifically, many genes that were significantly changed in expression level were associated with RhoA/ROCK pathway. For example the highest upregulated gene, ARHGEF7 (1766.22-fold) directly activates RhoA, which trigger RhoA/ROCK pathway and leads to myosin contraction, formation of actin stress fiber, and ultimately cell migration. Therefore the remarkable restricted cell morphology and the presence of actin stress fibres observed in cells on TMV substrate could also be another evidence of RhoA/ROCK activation. Furthermore, the extreme activation activity of RhoA by ARHGEF7 may result in downregulation of other signaling molecules involved in RhoA/ROCK pathway such as RhoA itself (-2.49-fold), ROCK (-2.29-fold), MYLK (-47.22-fold), Actr2 (-33.97-fold), and Cfl1 (-27.3-fold).[82] More importantly, the treatment of cells on TMV substrate with ROCK inhibitor, Y27632 intensely attenuated osteoblastic differentiation of cells as reported in section 4.2.2.

(Figure 4.3)

Collectively, these results suggest that structural changes to the cytoskeleton play key roles in determining MSC differentiation. Although it is well established that RhoA affects focal adhesions and stress fibres, and plays a key role in determining osteogenic–adipogenic fate decisions,[71] the downstream effects of such factors on other MSC differentiation pathways are less clear.

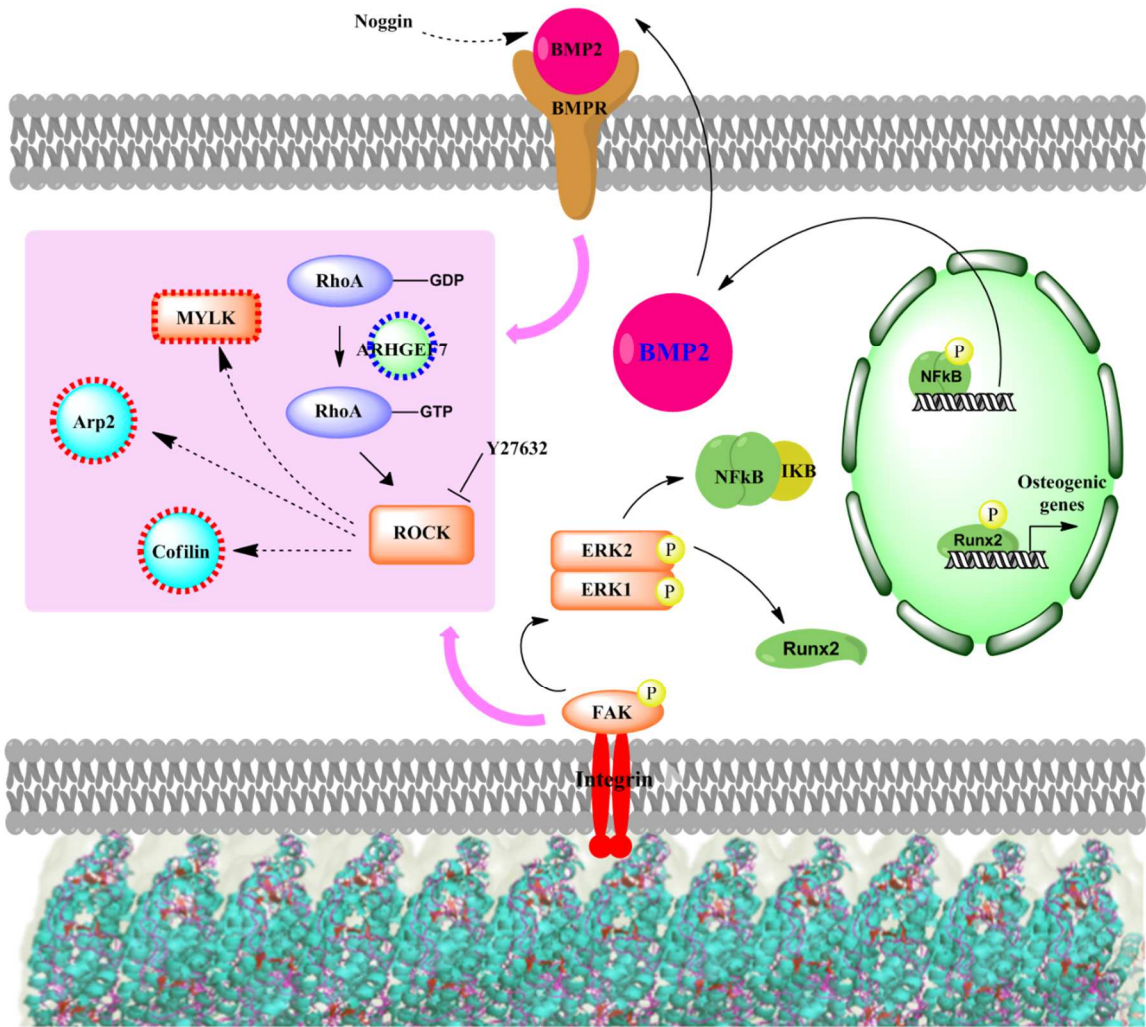


Figure 4.3 Proposed signaling cascade of virus substrates mediated osteogenesis of MSCs.

Further investigation on expression level of potential protein kinases such as FAK, ERK1/2, and PI3K may confirm the contribution of these kinases in the osteogenic process. It may also be insightful to inspect NF- $\kappa$ B expression levels to explore another possible upstream pathway regulated BMP2 expression. Regarding the commitment of RhoA/ROCK pathway in virus substrates mediated osteogenesis of MSCs, RhoA GTPase assay could be performed to analyze the amount of active RhoA in the system and ROCK activity can be probed by immunoprecipitation to isolate ROCK from cell lysates or knock down ROCK by using siRNA method.

#### 4.3 CONCLUSIONS

Early BMP2 upregulation was detected in cells cultured on TMV substrates and osteogenesis of cells was diminished upon treatment with a BMP2 inhibitor, Noggin. This confirms the significance of BMP2 in virus substrates mediated osteogenesis of MSCs. Previous result from PCR arrays points toward RhoA/ROCK pathway, which responsible for cell cytoskeleton tension and cell migration, guides to another experiment focusing on RhoA/ROCK pathway. By applying a ROCK inhibitor, Y27632 osteogenesis of cells was declined while BMP2 mRNA level was not altered. This may approve the involvement of the myosin-targeted pathway as a downstream signaling pathway of BMP2 in this situation. Cell cytoskeleton system has strong relationship to the differentiation of cells by virus substrates, as shown by Cytochalasin D: an actin depolymerization compound withdrew the osteogenic mediation property of virus substrates.

Regarding upstream cascade of BMP2, further investigation on expression level of potential protein kinases such as FAK and ERK1/2 that are common signaling network of integrins may reveal the connection between the cell mechanoreceptor and native BMP2 expression. Another pathway that could not be ruled out is the NF- $\kappa$ B pathway, which was reported to activate BMP2 expression leads to osteoblastic differentiation of MSCs by fluid shear stress induction.[80]

#### 4.4 EXPERIMENTAL SECTION

***TMV purification:*** Infected leaves were blended with 3 volumes of 0.1 M potassium phosphate buffer pH 7.0 and 0.1%  $\beta$ -mercaptoethanol. The mixture was filtered, and the filtrate was subjected to centrifugation to remove bulk plant material. The supernatant was collected and clarified by adding an equal volume of  $\text{CHCl}_3$ /1-butanol (v/v = 1:1). The aqueous layer was then collected followed by precipitation of virus with 4% PEG 8K and 0.2 M NaCl. The pellet was centrifuged and resuspended in buffer before it was subjected to low speed centrifuge to remove PEG. The virus in supernatant was final pelleted by ultracentrifugation and resuspended in buffer.

***Fabrication of virus based scaffolds:*** 1 mg/mL TMV in aqueous solution 0.7 mL were dropped into 12 well plates that were coated with Poly-d-Lysine using protocol suggested by Corning<sup>®</sup>. The virus solutions were incubated with the PDL coated plate under sterile cells culture hood for overnight. Then the bottoms of each well were rinsed briefly with 18.2 m $\Omega$  water before used for BMSCs culture.

***Surface characterization of virus based scaffolds by AFM:*** The surface morphology of virus based scaffolds was observed by AFM (Nanoscope IIIA MultiMode

AFM (Veeco)). The bottoms of each 12 well plate were cut out after virus coating and rinsed with 18.2 mΩ water then dried with a stream of nitrogen gas before mounted onto AFM sample holder for imaging in the tapping mode.

***BMSC isolation and expansion:*** Primary BMSCs were isolated from the bone marrow of young adult 80 g male Wister rats (Harlan Sprague-Dawley Inc.). The procedures were performed in accordance with the guideline for animal experimentation by the Institutional Animal Care and Use committee, School of Medicine, University of South Carolina. Cells were maintained in primary media (Dulbecco's Modified Eagle's Medium (DMEM) supplemented with 10% fetal bovine serum (FBS), penicillin (100 U/mL), streptomycin (100 µg/mL), and amphotericin B (250 ng/mL)), kept at 37 °C in a CO<sub>2</sub> incubator with 95% air/5% CO<sub>2</sub> and passaged no more than seven times after isolation. To induce osteogenesis, primary media were replaced with osteogenic media consisting of DMEM supplemented with 10% FBS, penicillin (100 U/mL), streptomycin (100 µg/mL), and amphotericin B (250 ng/mL), 10 mM sodium β-glycerolphosphate, L-ascorbic acid 2-phosphate (50 µg/mL), and 10<sup>-8</sup> M dexamethasone. Media were replenished every 3-4 days. To inhibit BMP2, either 10 µg/mL or 50 µg/mL of noggin was added to the osteogenic media in the first induction state and every replenishments. Likewise, inhibition of ROCK and actin polymerization were experimented by adding 10 µM Y27632 and 1 µM Cytochalasin D, respectively to the induction media.

***Quantitative real-time RT-PCR analysis (RT-qPCR):*** PDL and virus coated substrates were seeded with  $4.0 \times 10^4$  cells per well in primary media and allowed to attach overnight. The unseeded cells were used as a control to normalize the change in gene expression. The media were replaced to osteogenic media and cultured for 6 hours,

4 days, 7 days, and 14 days. The cell cultures were terminated at these time points and total RNA was subsequently extracted using E.Z.N.A<sup>®</sup> RNA Isolation Kit, OMEGA. At least two separate experiments were conducted with each type of sample. The purity and quantity of the extracted RNA were analyzed using Thermo Scientific Nanodrop 2000c spectrophotometer and was reverse transcribed by qScript<sup>™</sup> cDNA Supermix (Quanta Biosciences). RT-qPCR (iQ5 real-time PCR detection system Bio-Rad Laboratories) was done by the method described as: 60 cycles of PCR (95 °C for 20 s, 58 °C for 15 s, and 72 °C for 15 s), after initial denaturation step of 5 min at 95 °C, by using 12.5 µL of iQ5 SYBR Green I Supermix, 2 pmol/µL of each forward and reverse primers and 0.5 µL cDNA templates in a final reaction volume of 25 µL. Glyceraldehyde 3-phosphate dehydrogenase (GAPDH) was used as the house keeping gene. Data collection was enabled at 72 °C in each cycle and CT (threshold cycle) values were calculated using the iQ5 optical system software version 2.1. The expression levels of differentiated genes and undifferentiated genes were calculated using Pfaffl's method (M. W. Pfaffl, G. W. Horgan and L. Dempfle, Relative expression software tool) for group-wise comparison and statistical analysis of relative expression results in real-time PCR, using GAPDH as the reference gene. Quantification of gene expression was based on the CT value of each sample which was calculated as the average of at least two replicate measurements for each sample analyzed. "Pair Wise Fixed Reallocation Randomization Test" was performed on each sample and a value of  $p < 0.05$  was regarded as significant. The primers used for RT-qPCR are shown in Table 4.1. Three independent experiments were performed and analyzed for each gene expression study.

Table 4.1 Primers used for RT-qPCR to measure gene expression levels. BGLAP: bone-gamma-carboxyglutamate protein; BMP2: bone morphogenetic protein 2

Gene	Sequence (5'-3')
BGLAP	Forward: AAAGCCCAGCGACTCT
	Reverse: CTAAACGGTGGTGCCATAGAT
BMP2	Forward: ACCAACCATGGGTTTGTGGTGGAAGT
	Reverse: TCCGCTGTTTGTGTTTGGCTTGACG

***Alkaline phosphatase (ALP) activity:*** After 4 and 7 days of induction in the osteogenic media, the BMSCs seeded on PDL and virus coated substrates were determined number of cells on each substrate by CellTiter Blue<sup>®</sup> assay. Then the cells were fixed with 4% paraformaldehyde for 15 min at room temperature prior to analyze ALP activity by incubating the briefly fixed cells with 1-Step p-nitrophenylphosphate solution (Thermo Scientific) for 15 min at room temperature. The solution was transferred to a new microfuge tube contained 250  $\mu$ L of 2 N NaOH and the absorbance at 405 nm was measured. The measure ALP activity from each sample was normalized to the corresponding cell number. Three independent experiments were performed and analyzed for ALP activity.

***Alizarin red staining and quantification:*** Calcium deposition on each substrate was visualized and quantified to confirm and compare osteogenic differentiation by Alizarin red staining. Fixed cell on day 7 were stained with 0.1% Alizarin red solution (Sigma-Aldrich) pH 4.1-4.5 for 30 min in the dark. The samples were washed with water (18.2 M $\Omega$ ) prior to imaging. To quantify the amount of dye on each substrate, 300  $\mu$ L of 0.1 N NaOH was added to each sample to extract the dye from the sample. The extracted dye solution was measured the absorbance at 548 nm wavelength. The measure absorbance from each sample was normalized to the corresponding cell number from CellTiter Blue<sup>®</sup> assay. Three independent experiments were performed and analyzed for Alizarin red staining and quantification.

***Immunofluorescence assays and image analysis:*** For immunofluorescence assays and image analysis, the substrates were seeded with  $4.0 \times 10^5$  cells per sample. The cultures were terminated at 8 hours after osteoinduction for BMP2 immunostaining

analysis. After termination, cells were fixed in 4% paraformaldehyde at room temperature for 30 min. Each of the samples was then permeabilized for 20 min by 0.1% Triton-X 100 for 15 min and blocked in 1.5% bovine serum albumin (BSA, Sigma Aldrich) in PBS for 1 hour at room temperature. After the blocking, the cells were incubated overnight with mouse monoclonal antibody targeting BMP2 (R&D Systems) at 1:100 dilution in blocking buffer (Santa Cruz Biotechnology). After overnight incubation, secondary goat anti-mouse antibody conjugated with fluorescein (Chemicon) was used at 1:400 dilution for 2 hours at room temperature. Rhodamin phalloidin (1:100 in PBS) was used to stain filamentous actin. Nuclei were stained with DAPI (4,6-diamidino-2-phenylindole, 100 ng/mL). The sample were then mounted and sealed with clear nail polish before imaging. Images of the stained substrates were taken on an Olympus IX81 fluorescent microscope.

#### 4.5 REFERENCES

- [1] Ayres CE, Jha BS, Sell SA, Bowlin GL, Simpson DG. Nanotechnology in the design of soft tissue scaffolds: innovations in structure and function. Wiley Interdiscip Rev Nanomed Nanobiotechnol. 2010;2:20-34.
- [2] Discher DE, Mooney DJ, Zandstra PW. Growth factors, matrices, and forces combine and control stem cells. Science. 2009;324:1673-7.
- [3] Dvir T, Timko BP, Kohane DS, Langer R. Nanotechnological strategies for engineering complex tissues. Nature nanotechnology. 2011;6:13-22.
- [4] Hynes RO. The extracellular matrix: not just pretty fibrils. Science. 2009;326:1216-9.
- [5] Biggs MJ, Richards RG, McFarlane S, Wilkinson CD, Oreffo RO, Dalby MJ. Adhesion formation of primary human osteoblasts and the functional response of

mesenchymal stem cells to 330nm deep microgrooves. *Journal of the Royal Society, Interface / the Royal Society*. 2008;5:1231-42.

[6] Biggs MJ, Richards RG, Gadegaard N, McMurray RJ, Affrossman S, Wilkinson CD, et al. Interactions with nanoscale topography: adhesion quantification and signal transduction in cells of osteogenic and multipotent lineage. *J Biomed Mater Res A*. 2009;91:195-208.

[7] Lipski AM, Jaquiere C, Choi H, Eberli D, Stevens M, Martin I, et al. Nanoscale Engineering of Biomaterial Surfaces. *Advanced Materials*. 2007;19:553-7.

[8] Lohmann CH, Sagun R, Jr., Sylvia VL, Cochran DL, Dean DD, Boyan BD, et al. Surface roughness modulates the response of MG63 osteoblast-like cells to 1,25-(OH)<sub>2</sub>D<sub>3</sub> through regulation of phospholipase A<sub>2</sub> activity and activation of protein kinase A. *J Biomed Mater Res*. 1999;47:139-51.

[9] Lovmand J, Justesen J, Foss M, Lauridsen RH, Lovmand M, Modin C, et al. The use of combinatorial topographical libraries for the screening of enhanced osteogenic expression and mineralization. *Biomaterials*. 2009;30:2015-22.

[10] Martin JY, Schwartz Z, Hummert TW, Schraub DM, Simpson J, Lankford J, Jr., et al. Effect of titanium surface roughness on proliferation, differentiation, and protein synthesis of human osteoblast-like cells (MG63). *J Biomed Mater Res*. 1995;29:389-401.

[11] McNamara LE, McMurray RJ, Biggs MJ, Kantawong F, Oreffo RO, Dalby MJ. Nanotopographical control of stem cell differentiation. *J Tissue Eng*. 2010;2010:120623.

[12] Park J, Bauer S, Schlegel KA, Neukam FW, von der Mark K, Schmuki P. TiO<sub>2</sub> nanotube surfaces: 15 nm--an optimal length scale of surface topography for cell adhesion and differentiation. *Small*. 2009;5:666-71.

- [13] Park J, Bauer S, von der Mark K, Schmuki P. Nanosize and vitality: TiO<sub>2</sub> nanotube diameter directs cell fate. *Nano letters*. 2007;7:1686-91.
- [14] Schwartz Z, Martin JY, Dean DD, Simpson J, Cochran DL, Boyan BD. Effect of titanium surface roughness on chondrocyte proliferation, matrix production, and differentiation depends on the state of cell maturation. *J Biomed Mater Res*. 1996;30:145-55.
- [15] Jiang Y, Jahagirdar BN, Reinhardt RL, Schwartz RE, Keene CD, Ortiz-Gonzalez XR, et al. Pluripotency of mesenchymal stem cells derived from adult marrow. *Nature*. 2002;418:41-9.
- [16] Minguell JJ, Erices A, Conget P. Mesenchymal stem cells. *Exp Biol Med* (Maywood). 2001;226:507-20.
- [17] Pittenger MF, Mackay AM, Beck SC, Jaiswal RK, Douglas R, Mosca JD, et al. Multilineage potential of adult human mesenchymal stem cells. *Science*. 1999;284:143-7.
- [18] Si YL, Zhao YL, Hao HJ, Fu XB, Han WD. MSCs: Biological characteristics, clinical applications and their outstanding concerns. *Ageing Res Rev*. 2011;10:93-103.
- [19] Mackay AM, Beck SC, Murphy JM, Barry FP, Chichester CO, Pittenger MF. Chondrogenic differentiation of cultured human mesenchymal stem cells from marrow. *Tissue engineering*. 1998;4:415-28.
- [20] Drost AC, Weng S, Feil G, Schafer J, Baumann S, Kanz L, et al. In vitro myogenic differentiation of human bone marrow-derived mesenchymal stem cells as a potential treatment for urethral sphincter muscle repair. *Ann N Y Acad Sci*. 2009;1176:135-43.

- [21] Oswald J, Boxberger S, Jorgensen B, Feldmann S, Ehninger G, Bornhauser M, et al. Mesenchymal stem cells can be differentiated into endothelial cells in vitro. *Stem Cells*. 2004;22:377-84.
- [22] Gong Z, Calkins G, Cheng EC, Krause D, Niklason LE. Influence of culture medium on smooth muscle cell differentiation from human bone marrow-derived mesenchymal stem cells. *Tissue Eng Part A*. 2009;15:319-30.
- [23] Porada CD, Almeida-Porada G. Mesenchymal stem cells as therapeutics and vehicles for gene and drug delivery. *Adv Drug Deliv Rev*. 2010;62:1156-66.
- [24] Lee LA, Nguyen QL, Wu L, Horvath G, Nelson RS, Wang Q. Mutant plant viruses with cell binding motifs provide differential adhesion strengths and morphologies. *Biomacromolecules*. 2012;13:422-31.
- [25] Pokorski JK, Steinmetz NF. The art of engineering viral nanoparticles. *Mol Pharm*. 2011;8:29-43.
- [26] Chung W-J, Merzlyak A, Lee S-W. Fabrication of engineered M13 bacteriophages into liquid crystalline films and fibers for directional growth and encapsulation of fibroblasts. *Soft Matter*. 2010;6:4454-9.
- [27] Wang J, Wang L, Li X, Mao C. Virus activated artificial ECM induces the osteoblastic differentiation of mesenchymal stem cells without osteogenic supplements. *Sci Rep*. 2013;3:1242.
- [28] Merzlyak A, Indrakanti S, Lee SW. Genetically engineered nanofiber-like viruses for tissue regenerating materials. *Nano Lett*. 2009;9:846-52.

- [29] Zhu H, Cao B, Zhen Z, Laxmi AA, Li D, Liu S, et al. Controlled growth and differentiation of MSCs on grooved films assembled from monodisperse biological nanofibers with genetically tunable surface chemistries. *Biomaterials*. 2011;32:4744-52.
- [30] Wang Q, Lin T, Tang L, Johnson JE, Finn MG. Icosahedral Virus Particles as Addressable Nanoscale Building Blocks. *Angewandte Chemie International Edition*. 2002;41:459-62.
- [31] Destito G, Schneemann A, Manchester M. Biomedical Nanotechnology Using Virus-Based Nanoparticles. In: Manchester M, Steinmetz N, editors. *Viruses and Nanotechnology*: Springer Berlin Heidelberg; 2009. p. 95-122.
- [32] Rosen V. BMP2 signaling in bone development and repair. *Cytokine & Growth Factor Reviews*. 2009;20:475-80.
- [33] Ishibashi O, Ikegame M, Takizawa F, Yoshizawa T, Moksed MA, Iizawa F, et al. Endoglin is involved in BMP-2-induced osteogenic differentiation of periodontal ligament cells through a pathway independent of Smad-1/5/8 phosphorylation. *J Cell Physiol*. 2010;222:465-73.
- [34] Kawasaki T, Niki Y, Miyamoto T, Horiuchi K, Matsumoto M, Aizawa M, et al. The effect of timing in the administration of hepatocyte growth factor to modulate BMP-2-induced osteoblast differentiation. *Biomaterials*. 2010;31:1191-8.
- [35] Lee JH, Kim CS, Choi KH, Jung UW, Yun JH, Choi SH, et al. The induction of bone formation in rat calvarial defects and subcutaneous tissues by recombinant human BMP-2, produced in *Escherichia coli*. *Biomaterials*. 2010;31:3512-9.

- [36] Wang L, Huang Y, Pan K, Jiang X, Liu C. Osteogenic responses to different concentrations/ratios of BMP-2 and bFGF in bone formation. *Ann Biomed Eng.* 2010;38:77-87.
- [37] Ahrens M, Ankenbauer T, Schroder D, Hollnagel A, Mayer H, Gross G. Expression of human bone morphogenetic proteins-2 or -4 in murine mesenchymal progenitor C3H10T1/2 cells induces differentiation into distinct mesenchymal cell lineages. *DNA Cell Biol.* 1993;12:871-80.
- [38] Baltzer AW, Lattermann C, Whalen JD, Wooley P, Weiss K, Grimm M, et al. Genetic enhancement of fracture repair: healing of an experimental segmental defect by adenoviral transfer of the BMP-2 gene. *Gene Ther.* 2000;7:734-9.
- [39] Betz OB, Betz VM, Nazarian A, Egermann M, Gerstenfeld LC, Einhorn TA, et al. Delayed administration of adenoviral BMP-2 vector improves the formation of bone in osseous defects. *Gene Ther.* 2007;14:1039-44.
- [40] Betz OB, Betz VM, Nazarian A, Pilapil CG, Vrahas MS, Boussein ML, et al. Direct percutaneous gene delivery to enhance healing of segmental bone defects. *J Bone Joint Surg Am.* 2006;88:355-65.
- [41] Egermann M, Baltzer AW, Adamaszek S, Evans C, Robbins P, Schneider E, et al. Direct adenoviral transfer of bone morphogenetic protein-2 cDNA enhances fracture healing in osteoporotic sheep. *Hum Gene Ther.* 2006;17:507-17.
- [42] Mai Z, Peng Z, Wu S, Zhang J, Chen L, Liang H, et al. Single bout short duration fluid shear stress induces osteogenic differentiation of MC3T3-E1 cells via integrin beta1 and BMP2 signaling cross-talk. *PLoS One.* 2013;8:e61600.

- [43] Kearney EM, Farrell E, Prendergast PJ, Campbell VA. Tensile strain as a regulator of mesenchymal stem cell osteogenesis. *Ann Biomed Eng.* 2010;38:1767-79.
- [44] Sumanasinghe RD, Bernacki SH, Lobo EG. Osteogenic differentiation of human mesenchymal stem cells in collagen matrices: effect of uniaxial cyclic tensile strain on bone morphogenetic protein (BMP-2) mRNA expression. *Tissue Eng.* 2006;12:3459-65.
- [45] Groppe J, Greenwald J, Wiater E, Rodriguez-Leon J, Economides AN, Kwiatkowski W, et al. Structural basis of BMP signaling inhibition by Noggin, a novel twelve-membered cystine knot protein. *J Bone Joint Surg Am.* 2003;85-A Suppl 3:52-8.
- [46] Batson EL, Reilly GC, Currey JD, Balderson DS. Postexercise and positional variation in mechanical properties of the radius in young horses. *Equine Vet J.* 2000;32:95-100.
- [47] Kopher RA, Mao JJ. Suture growth modulated by the oscillatory component of micromechanical strain. *J Bone Miner Res.* 2003;18:521-8.
- [48] Jee WS, Frost HM. Skeletal adaptations during growth. *Triangle.* 1992;31:77-88.
- [49] Duncan RL, Turner CH. Mechanotransduction and the functional response of bone to mechanical strain. *Calcif Tissue Int.* 1995;57:344-58.
- [50] Kapur S, Baylink DJ, Lau KH. Fluid flow shear stress stimulates human osteoblast proliferation and differentiation through multiple interacting and competing signal transduction pathways. *Bone.* 2003;32:241-51.
- [51] Mikuni-Takagaki Y, Suzuki Y, Kawase T, Saito S. Distinct responses of different populations of bone cells to mechanical stress. *Endocrinology.* 1996;137:2028-35.

- [52] Jansen JH, Weyts FA, Westbroek I, Jahr H, Chiba H, Pols HA, et al. Stretch-induced phosphorylation of ERK1/2 depends on differentiation stage of osteoblasts. *J Cell Biochem.* 2004;93:542-51.
- [53] Turner CH, Owan I, Alvey T, Hulman J, Hock JM. Recruitment and proliferative responses of osteoblasts after mechanical loading in vivo determined using sustained-release bromodeoxyuridine. *Bone.* 1998;22:463-9.
- [54] Holtorf HL, Jansen JA, Mikos AG. Flow perfusion culture induces the osteoblastic differentiation of marrow stroma cell-scaffold constructs in the absence of dexamethasone. *J Biomed Mater Res A.* 2005;72:326-34.
- [55] Ren XD, Kiosses WB, Schwartz MA. Regulation of the small GTP-binding protein Rho by cell adhesion and the cytoskeleton. *EMBO J.* 1999;18:578-85.
- [56] Schoenwaelder SM, Burridge K. Bidirectional signaling between the cytoskeleton and integrins. *Curr Opin Cell Biol.* 1999;11:274-86.
- [57] Clark EA, King WG, Brugge JS, Symons M, Hynes RO. Integrin-mediated signals regulated by members of the rho family of GTPases. *J Cell Biol.* 1998;142:573-86.
- [58] Etienne-Manneville S, Hall A. Rho GTPases in cell biology. *Nature.* 2002;420:629-35.
- [59] Hall A. Rho GTPases and the actin cytoskeleton. *Science.* 1998;279:509-14.
- [60] Wittmann T, Waterman-Storer CM. Cell motility: can Rho GTPases and microtubules point the way? *J Cell Sci.* 2001;114:3795-803.
- [61] Chong LD, Traynor-Kaplan A, Bokoch GM, Schwartz MA. The small GTP-binding protein Rho regulates a phosphatidylinositol 4-phosphate 5-kinase in mammalian cells. *Cell.* 1994;79:507-13.

- [62] Chrzanowska-Wodnicka M, Burridge K. Rho-stimulated contractility drives the formation of stress fibers and focal adhesions. *J Cell Biol.* 1996;133:1403-15.
- [63] Nobes CD, Hall A. Rho, rac, and cdc42 GTPases regulate the assembly of multimolecular focal complexes associated with actin stress fibers, lamellipodia, and filopodia. *Cell.* 1995;81:53-62.
- [64] Putnam AJ, Cunningham JJ, Pillemer BB, Mooney DJ. External mechanical strain regulates membrane targeting of Rho GTPases by controlling microtubule assembly. *Am J Physiol Cell Physiol.* 2003;284:C627-39.
- [65] Matthews BD, Overby DR, Mannix R, Ingber DE. Cellular adaptation to mechanical stress: role of integrins, Rho, cytoskeletal tension and mechanosensitive ion channels. *J Cell Sci.* 2006;119:508-18.
- [66] Aikawa R, Komuro I, Yamazaki T, Zou Y, Kudoh S, Zhu W, et al. Rho family small G proteins play critical roles in mechanical stress-induced hypertrophic responses in cardiac myocytes. *Circ Res.* 1999;84:458-66.
- [67] Aoki H, Izumo S, Sadoshima J. Angiotensin II activates RhoA in cardiac myocytes: a critical role of RhoA in angiotensin II-induced premyofibril formation. *Circ Res.* 1998;82:666-76.
- [68] Katsumi A, Milanini J, Kiosses WB, del Pozo MA, Kaunas R, Chien S, et al. Effects of cell tension on the small GTPase Rac. *J Cell Biol.* 2002;158:153-64.
- [69] Numaguchi K, Eguchi S, Yamakawa T, Motley ED, Inagami T. Mechanotransduction of rat aortic vascular smooth muscle cells requires RhoA and intact actin filaments. *Circ Res.* 1999;85:5-11.

- [70] Sordella R, Jiang W, Chen GC, Curto M, Settleman J. Modulation of Rho GTPase signaling regulates a switch between adipogenesis and myogenesis. *Cell*. 2003;113:147-58.
- [71] McBeath R, Pirone DM, Nelson CM, Bhadriraju K, Chen CS. Cell shape, cytoskeletal tension, and RhoA regulate stem cell lineage commitment. *Dev Cell*. 2004;6:483-95.
- [72] Vunjak-Novakovic G. Tissue Engineering: Basic Considerations. In: Freshney RI, editor. *Culture of Cells for Tissue Engineering*. Hoboken, New Jersey: John Wiley & Sons, Inc.; 2006. p. 129-55.
- [73] Boyne PJ, Lilly LC, Marx RE, Moy PK, Nevins M, Spagnoli DB, et al. De novo bone induction by recombinant human bone morphogenetic protein-2 (rhBMP-2) in maxillary sinus floor augmentation. *J Oral Maxillofac Surg*. 2005;63:1693-707.
- [74] Burkus JK, Gornet MF, Dickman CA, Zdeblick TA. Anterior lumbar interbody fusion using rhBMP-2 with tapered interbody cages. *J Spinal Disord Tech*. 2002;15:337-49.
- [75] Carragee EJ, Hurwitz EL, Weiner BK. A critical review of recombinant human bone morphogenetic protein-2 trials in spinal surgery: emerging safety concerns and lessons learned. *Spine J*. 2011;11:471-91.
- [76] Carreon LY, Glassman SD, Brock DC, Dimar JR, Puno RM, Campbell MJ. Adverse events in patients re-exposed to bone morphogenetic protein for spine surgery. *Spine (Phila Pa 1976)*. 2008;33:391-3.

- [77] Fiorellini JP, Howell TH, Cochran D, Malmquist J, Lilly LC, Spagnoli D, et al. Randomized study evaluating recombinant human bone morphogenetic protein-2 for extraction socket augmentation. *J Periodontol.* 2005;76:605-13.
- [78] McKay WF, Peckham SM, Badura JM. A comprehensive clinical review of recombinant human bone morphogenetic protein-2 (INFUSE Bone Graft). *Int Orthop.* 2007;31:729-34.
- [79] Shields LB, Raque GH, Glassman SD, Campbell M, Vitaz T, Harpring J, et al. Adverse effects associated with high-dose recombinant human bone morphogenetic protein-2 use in anterior cervical spine fusion. *Spine (Phila Pa 1976).* 2006;31:542-7.
- [80] Liu L, Shao L, Li B, Zong C, Li J, Zheng Q, et al. Extracellular signal-regulated kinase1/2 activated by fluid shear stress promotes osteogenic differentiation of human bone marrow-derived mesenchymal stem cells through novel signaling pathways. *Int J Biochem Cell Biol.* 2011;43:1591-601.
- [81] Wang YK, Yu X, Cohen DM, Wozniak MA, Yang MT, Gao L, et al. Bone morphogenetic protein-2-induced signaling and osteogenesis is regulated by cell shape, RhoA/ROCK, and cytoskeletal tension. *Stem Cells Dev.* 2012;21:1176-86.
- [82] Sitasuwan P. Biomaterial-Induced Osteogenesis of Mesenchymal Stem Cells by Surface Roughness and Functionalization. Columbia, SC: University of South Carolina; 2013.

## APPENDIX A – REPRINT PERMISSION FOR CHAPTER 1



RightsLink®

Home

Account  
Info

Help



ACS Publications  
Most Trusted. Most Cited. Most Read.

**Title:** Influence of Surface Topographical Cues on the Differentiation of Mesenchymal Stem Cells in Vitro  
**Author:** Kamolrat Metavarayuth, Pongkwan Sitasuwan, Xia Zhao, et al  
**Publication:** ACS Biomaterials Science & Engineering  
**Publisher:** American Chemical Society  
**Date:** Feb 1, 2016  
Copyright © 2016, American Chemical Society

Logged in as:  
Kamolrat Metavarayuth  
Account #:  
3000954143

LOGOUT

### PERMISSION/LICENSE IS GRANTED FOR YOUR ORDER AT NO CHARGE

This type of permission/license, instead of the standard Terms & Conditions, is sent to you because no fee is being charged for your order. Please note the following:

- Permission is granted for your request in both print and electronic formats, and translations.
- If figures and/or tables were requested, they may be adapted or used in part.
- Please print this page for your records and send a copy of it to your publisher/graduate school.
- Appropriate credit for the requested material should be given as follows: "Reprinted (adapted) with permission from (COMPLETE REFERENCE CITATION). Copyright (YEAR) American Chemical Society." Insert appropriate information in place of the capitalized words.
- One-time permission is granted only for the use specified in your request. No additional uses are granted (such as derivative works or other editions). For any other uses, please submit a new request.

BACK

CLOSE WINDOW

## APPENDIX B – REPRINT PERMISSION FOR CHAPTER 2

### AW: NON-RIGHTSLINK

Rights DE <RIGHTS-and-LICENCES@wiley-vch.de>

Fri 4/1/2016 2:49 AM

To: METAVARAYUTH, KAMOLRAT <metavara@email.sc.edu>;

Dear Kamolrat Metavarayuth,

About the Wiley-VCH Journal	
Journal Title	Advanced Science
Year of Publication	2015
Volume and Issue Number	Volume 2 Issue 10
Article Title (please include page numbers)	Virus Nanoparticles Mediated Osteogenic Differentiation of Bone Derived Mesenchymal Stem Cells (page 1500026)
Author	Kamolrat Metavarayuth
Figure and Page Reference	Page 1500026-1500033 (Full article)
Do you or your institute hold a current subscription to this journal?	yes
Are you the original author of the requested material?	yes

Where would you like to include our material?

About Your Publication	
Author / Editor	Kamolrat Metavarayuth
Title of Publication	VIRUS PARTICLES PROVIDE NANOTOPOGRAPHICAL CUES FOR OSTEOGENIC
Rights Required (eg. Print/ Electronic/ Translation, etc.)	Print and electronic
Publisher	ProQuest LLC
Publication Date	15. Apr 16
Medium (e.g. Book/Journal, Handout, CD Rom, Internet, etc.)	Dissertation and internet
Print Run (hard back / paper back)	hard back
If Making Copies Please include the Number of Copies You Wish to Make	5
Retail Price	0
Web address material will be posted on	15. Apr 16
Is the website password-protected?	no

Tell us how to get in touch with you (Please note that this will be where your invoice and/or permission will be addressed to. We are unable to send documents to more than one address):

Please provide your full address details:

Name	Kamolrat Metavarayuth
Salutation	Miss
Department	Department of Chemistry and Biochemistry
Job title	Graduate student
Organisation	University of South Carolina
Street	631 Sumter St.
Town	Columbia
State / Province	S.C.
Zip / Postal Code	29208
Country	USA
Telephone	8037775264
Fax	8037779521
Email	metavara@email.sc.edu

This is an open access article under the terms of the [Creative Commons Attribution License](#), which permits use, distribution and reproduction in any medium, provided the original work is properly cited: Author(s) Name(s); Title of the Article. Name of the Journal. Publication year. Volume. Page(s). © 2015 The Authors. Published by WILEY-VCH Verlag GmbH & Co. KGaA, Weinheim.

You may therefore use the article as requested.

Kind regards

Bettina Loyoke  
Senior Rights Manager  
Rights & Licenses

Wiley-VCH Verlag GmbH & Co. KGaA